Targeting Tumor Hypoxia
to Overcome Radioresistance

Dissertation

zur

Erlangung der naturwissenschaftlichen Doktorwürde
(Dr. sc. nat.)

vorgelegt der

Mathematisch-naturwissenschaftlichen Fakultät

der

Universität Zürich

von

Ivo Grgic

von Leuggern/AG

Promotionskommission

Prof. Dr. Martin Pruschy (Vorsitz)

Prof. Dr. Lubor Borsig

Prof. Dr. Rolf Graf

Prof. Dr. Roger Schibli

Prof. Dr. med. Matthias Guckenberger

Zürich, 2018

Abstract

When proliferating mutated cells lead to the formation of a solid tumor, they will reach a point where part of the cancer cells outgrow their blood supply. These cells will be deprived of oxygen and are designated as "hypoxic". Since oxygen plays a crucial role in the cytotoxicity of ionizing radiation (IR), hypoxic cells are associated with resistance to radiotherapy. Current radiotherapy protocols to partly overcome tumor hypoxia utilize fractionated irradiation, where a dose of IR will preferentially kill the normoxic cell population and the remaining cell population with a higher relative proportion of hypoxic cells will become reoxygenated by the microenvironment thereafter. As part of a repetitive process, reoxygenated cells will subsequently be killed by the next dose of a fractionated treatment schedule. Driven by technological progress and novel insights in radiobiology, clinicians increasingly use stereotactic body radiotherapy (SBRT), where one or a few high-dose fractions of IR are precisely delivered to the tumor without overly co-irradiating the healthy surrounding tissue. However, single or a few high dose fractions do not exploit the process of tumor reoxygenation. Therefore, reoxygenation or a reduction of the hypoxic tumor fraction by a combined treatment modality with a pharmaceutical agent is of high interest to reduce the required dose of IR and thereby further minimizing normal tissue toxicity.

In this PhD project, we investigated two distinct hypoxia-modulating pharmaceutical compounds and their relevance for radiotherapy in extensive preclinical tumor animal studies. The hypoxia-activated prodrug evofosfamide is bioreductively activated in tumor regions with a low oxygen concentration whereupon it acts as a DNA-alkylating cytotoxic agent. Thereby it specifically kills hypoxic tumor cells without considerably damaging healthy tissue. We demonstrated a synergistic effect of evofosfamide and IR in A549 non-small cell lung cancer (NSCLC) xenografts, whereas it remained completely ineffective in UT-SCC-14 head and neck squamous cell carcinoma (HNSCC), both *in vitro* and *in vivo*. Retrospective analysis revealed a lack of the cytochrome P450 oxidoreductase (POR) in the irresponsive HNSCC cells. We and other groups identified that in addition to low oxygen concentrations, evofosfamide requires POR for its activation. SiRNA-mediated knockdown of POR in evofosfamide-sensitive A549 cells rendered this cell line irresponsive to evofosfamide treatment. Based on these insights we recommend to investigate the therapeutic efficacy of combined evofosfamide and IR treatment for cancer patients with hypoxic solid tumors that are tested positive for POR expression.

An alternative approach for pharmacological radiosensitization was evaluated with the hemoglobin-effector myo-inositol trispyrophosphate (ITPP). Systemic ITPP administration leads to a decreased hemoglobin-oxygen binding affinity and results in enhanced oxygenation of hypoxic tissue. By using a non-invasive luciferase-based *in vivo* hypoxia reporter assay, we demonstrated increased tumor oxygenation already two hours after ITPP administration. Tumor irradiation two hours upon ITPP injection resulted in significantly delayed tumor growth when compared to radiotherapy alone. Immunohistochemical analysis of γH2AX foci demonstrated increased IR-induced DNA damage within initially hypoxic tumor regions after combined treatment with ITPP as compared to IR alone. Furthermore, we observed a direct relation between initial tumor hypoxia and ITPP-mediated radiosensitization. A549 NSCLC xenografts with high hypoxic fractions responded better to combined ITPP and IR treatment as compared to FaDu HNSCC with an initially low hypoxic fraction. SBRT leads to endothelial cell death and results in a depletion of the tumor vasculature. Interestingly, neoadjuvant ITPP treatment completely prevented the disruption of tumor blood vessels as determined by immunohistochemistry four days after irradiation. The pericyte coverage and absolute perfusion rate was higher after combined ITPP and IR treatment when compared to irradiated tumors without previous ITPP treatment. Consequently, ITPP-mediated vascular protection prevented radiotherapy-induced tumor hypoxia.

Supplementary experiments in MC-38 syngeneic colorectal carcinoma (CRC) indicate an involvement of the adaptive immune system to the response to combined ITPP and IR treatment. Within all tested tumor entities, we identified the strongest ITPP-mediated radiosensitization in MC-38 cells, even though these allografts are only intermediately hypoxic. Extensive exploration of the tumor microenvironment (TME) by immunohistochemistry (IHC) seven days after irradiation confirmed ITPP-mediated vascular protection. Preserved integrity of the tumor vasculature after combined ITPP and IR treatment was associated with an elevated infiltration of CD4+ T cells that might positively contribute to tumor control. Further experiments will be required to unravel the mechanistic implications of vascular protection and subsequent increase in immune-cell trafficking.

As part of my PhD project, we implemented an image-guided small animal radiotherapy platform in our group. CT-based treatment planning with Monte Carlo dose calculation, followed by static or dynamic irradiation enables to precisely treat very small structures in animal models and is an attempt to increase the translational relevance of preclinical radiotherapy research. To further develop our promising results obtained with ITPP treatment of subcutaneous tumors, we generated an orthotopic colorectal liver metastases (CLM) model. CLMs manifest in a high unmet need for novel treatment strategies, as the golden standard - surgical resection - is not always applicable. We demonstrated that selective intraportal injection of CRC cells yields a high rate in liver metastasis formation. Highly selective irradiation of the right liver lobe is technically feasible and can be delivered with acceptable healthy tissue involvement. We identified significant animal weight loss and an impairment of liver performance biomarkers at single doses of 20 Gy and higher. On the other hand, CLM irradiation with single doses of 15 Gy and lower was well tolerated and resulted in dose-dependent tumor growth delay kinetics. Preliminary combined treatment with ITPP indicated a radioprotective effect on the healthy liver that might underlie the same mechanism as observed in the protection of the tumor vasculature. Cumulatively these findings demonstrate that small animal image-guided radiotherapy of CLMs is feasible, accurate and effective. Based on these results, we will further investigate the multimodal combination of ITPP and SBRT in CLMs.

In summary, my PhD work demonstrates that modulation of tumor hypoxia is an attractive and potent approach to increase the efficacy of radiotherapy. While evofosfamide requires the abundance of oxidoreductases for its activation, ITPP acts independently of the molecular and genetic background of a solid tumor. Overall, our results support the strong rationale to combine ITPP with SBRT for clinical investigation in patients suffering from hypoxic solid tumors.

List of Abbreviations

ABC	ATP-binding cassette transporter
APC	Antigen presenting cell
ARCON	Accelerated radiotherapy with carbogen and nicotinamide
BMDC	Bone-marrow derived cell
BOLD-MRI	Blood oxygen level MRI
CAF	Cancer-associated fibroblast
CAIX	Carbonic anhydrase 9
CAR	Chimeric antigen receptor
CLM	Colorectal liver metastases
CRC	Colorectal carcinoma
CSC	Cancer stem cell
CT	Computed tomography
CTC	Circulating tumor cell
CYP	Cytochrome P450
DCE-MRI	Dynamic contrast-enhanced MRI
DNA DSB	DNA double strand break
DWI-MRI	Diffusion-weighted imaging MRI
ECM	Extracellular matrix
EGFR	Epidermal growth factor receptor
EMT	Epithelial to mesenchymal transition
EPR-MRI	Electron paramagnetic resonance MRI
FAZA	Fluoroazomycin arabinoside
FDA	Food and Drug Administration
FDG	Fluorodeoxyglucose
FMISO	Fluoromisonidazole
fMRI	functional MRI
GLUT-1	Glucose transporter 1
HAP	Hypoxia activated prodrug
HIF	Hypoxia-inducible factor
HNSCC	Head and neck squamous cell carcinoma
HRR	Homologous recombination repair Immunohistochemistry
IHC	Ionizing radiation
IR	myo-Inositol trispyrophosphate
ITPP	Linear accelerator
LINAC	Lysyl oxidase
LOX	Multidrug resistance
MDR	Mesenchymal to epithelial transition
MET	Matrix metalloproteinase
MMP	Magnetic resonance imaging
MRI	Microtubule-stabilizing agent
MSA	Maximally tolerated dose
MTD	Non-homologous recombination
NHEJ	Non-small-cell lung cancer
NSCLC	Positron emission tomography
PET	Permeability-glycoprotein
P-gp	

PoC	Proof of Concept
POR	P450 oxidoreductase
PTEN	Phosphatase and tensin homologue
PWI-MRI	Perfusion-weighted imaging MRI
ROS	Reactive oxygen species
SBRT	Stereotactic body radiotherapy
SPECT	Single photon emission computed tomography
TGF-β	Tumor growth factor β
TKI	Tyrosine kinase inhibitor
TME	Tumor microenvironment
VEGF	Vascular endothelial growth factor

Table of contents

1. Introduction 8
1.1 Cancer overview 8
1.1.1 Cancer and carcinogenesis 8
1.1.2 Hallmarks of cancer 8
1.1.3 The tumor microenvironment 10
1.1.3.1 Cytokines and Chemokines 10
1.1.3.2 Cancer-associated fibroblasts 10
1.1.3.3 Immune cells 10
1.1.3.4 Vasculature 11
1.1.3.5 Hypoxia 12
1.1.4 Metastases 13
1.2 Cancer diagnosis and imaging 16
1.2.1 General aspects of cancer diagnosis 16
1.2.2 Computed tomography 16
1.2.3 Magnetic resonance imaging 16
1.2.4 PET and SPECT 17
1.2.5 Methods to detect tumor hypoxia 17
1.3 Cancer treatment 18
1.3.1 General aspects of cancer therapy 18
1.3.2 Surgery and Chemotherapy 18
1.3.3 Molecularly targeted therapy 19
1.3.4 Immunotherapy 20
1.3.5 Radiotherapy 21
1.3.5.1 The 5 R's 21
1.3.5.2 Brachytherapy 22
1.3.5.3 Radiation physics and LINAC technology 22
1.3.5.4 Fractionation and treatment scheduling 22
1.3.5.5 Small animal radiotherapy 23
1.3.6 Combined treatment modalities 23
1.4 Treatment resistance 23
1.4.1 Chemoresistance 24
1.4.2 Radioresistance 24
1.4.2.1 Cell cycle control and DNA damage 24
1.4.2.2 TME-driven radioresistance 25
1.5 Combined treatment modalities to overcome radioresistance 27
1.5.1 Targeting intracellular signalling pathways 27
1.5.2 Targeting DNA damage and cell cycle control pathways 27
1.5.3 Targeting the tumor vasculature 27

1.5.4 Targeting immune cells....27
1.5.5 Targeting tumor hypoxia....28
2. Aims of the study....30
3. Results....31
3.1 The hypoxia-activated prodrug evofosfamide in combination with multiple regimens of radiotherapy....31
3.2 Neoadjuvant tumor reoxygenation with myo-inositol trispyrophosphate increases the radiosensitivity of hypoxic tumors....50
3.3 Image-guided radiotherapy of murine colorectal liver metastases....84
4. Discussion....102
4.1 Current status of hypoxia modulation for radiotherapy....102
4.2 Hypoxia activated prodrugs and their implications in clinical oncology....103
4.3 Overcoming radioresistance by tumor reoxygenation with myo-inositol trispyrophosphate....104
4.4 Implementation of image-guided small animal radiotherapy in Zurich....106
4.5 Translational relevance....107
4.6 Design of multimodal treatment strategies to overcome radioresistance....108

1. Introduction

1.1 Cancer overview

1.1.1 Cancer and carcinogenesis

The human body is a complex organism consisting of approximately 4×10^{13} cells [1]. These cells harbour and constantly reproduce an individual's genetic information (genotype). In a multistep process described as carcinogenesis, minimal molecular changes in the genetic information occur and may lead to cancer if they remain unrepaired. As such, cancer can be defined as an accumulation of genetic alterations that change the cellular fate and lead to uncontrolled cell division and proliferation [2]. Typically, simultaneous mutations of several genes in one cell are required to achieve neoplastic tissue growth [3]. Amongst the most frequently mutated gene categories involved in cancer formation are gain of function mutations in oncogenes and loss of function mutations in tumor suppressor genes. Oncogenes promote proliferation and survival of cells, whereas tumor suppressor genes dampen cell proliferation and promote apoptosis, a form of programmed cell death. [4-6]. In 90 – 95% of the cases environmental and lifestyle factors, e.g. cigarette smoking, sun exposure or environmental pollutants are responsible for the genetic mutations that lead to cancer [7].
Cancer can either affect the blood system or form a tumor in solid tissue, i.e. in organs, muscles or bones. Depending on the site of origin, tumors are further subclassified: carcinomas are tumors formed by epithelial cells, whereas sarcomas affect the connective tissue, i.e. muscles and fibrous tissue. If a tumor remains encapsulated in the tissue of origin it is defined as benign, whereas invasive and metastatic tumors are described as malignant neoplasms. The concept of metastases will be discussed later in this dissertation.
Behind cardiovascular disorders, cancer is the second most frequent cause of death with 14.1 million new cancer cases and 8.2 million cancer-related deaths worldwide in 2012. Incidence and morbidity depend on the gender and countries development. Worldwide, the five most common sites of cancer diagnosed in men are lung, prostate, colon & rectum, stomach and liver, whereas the female population most frequently suffers from breast, lung, colon & rectum, cervix and stomach cancer [8, 9].

1.1.2 Hallmarks of cancer

Even though cancer is a highly versatile disease, Hanahan and Weinberg described the cancer cell genotypes as a manifestation of six underlying alterations in cell physiology that determine malignant growth and named them as "The Hallmarks of Cancer" [10]. Eleven years later and after tremendous progress in cancer research, the same authors complemented the list with four additional hallmarks [11]. Since then, these pivotal publications have been cited and discussed more than 15'000 times and serve as a general reference and inspiration for basic and applied cancer research. I briefly summarized the 10 Hallmarks of Cancer and potential therapeutic strategies to target the individual Hallmarks in Figure 1:

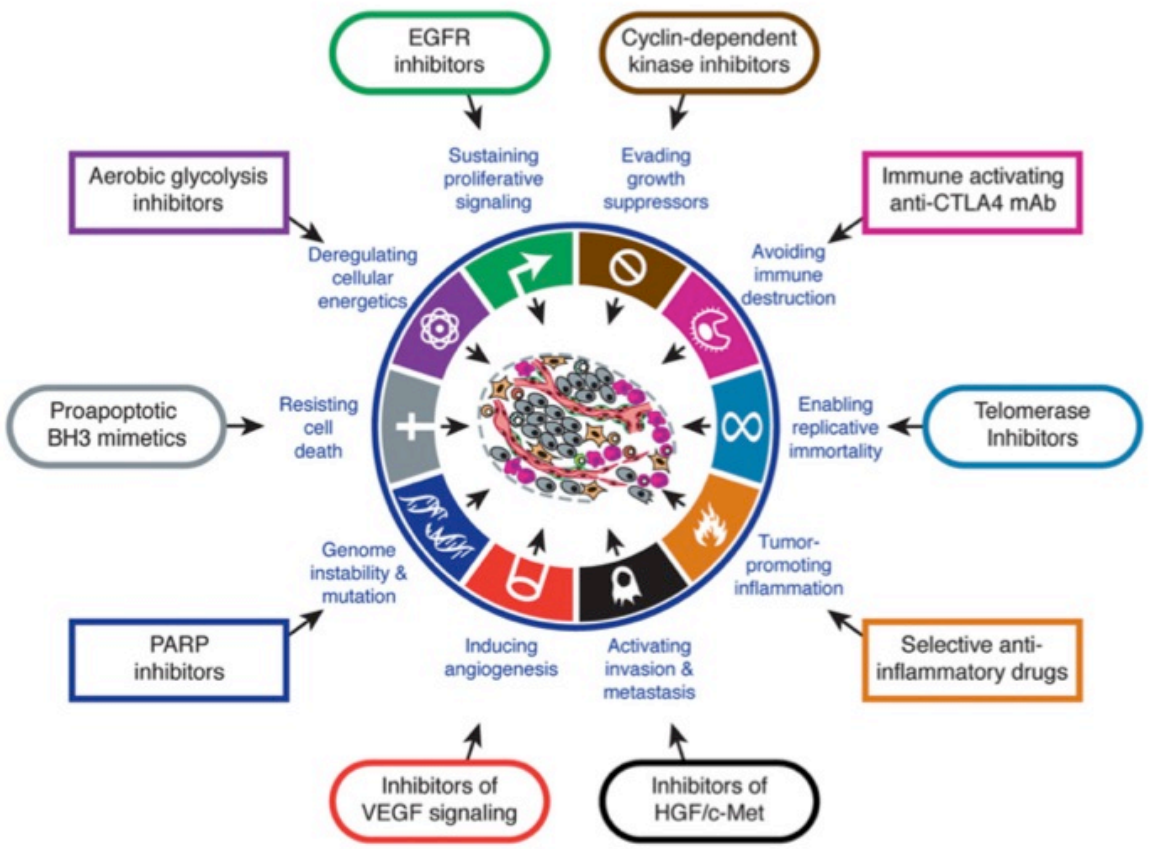

Figure 1 Schematic representation of the hallmarks of cancer and therapeutic strategies to tackle the individual hallmarks. **Sustaining proliferative signalling** is associated with enhanced production and release of growth-promoting signals in cancer cells, acquired by a number of alternative pathways. Autocrine proliferative stimulation, interaction with tumor-associated stroma and deregulated intracellular signalling are only some of the ways that cancer cells sustain proliferation. Cancer cells **evade growth suppressors** by acquired mutations in key tumor suppressor genes like TP53, which negatively regulate cell proliferation in the case of excessive genome damage or other intracellular stress. Cancer cells evolve numerous strategies to limit or **resist cell death** mainly by misbalancing pro- and anti-apoptotic signals. **Enabling replicative immortality** is another hallmark of cancer. Cells in healthy tissue usually pass through only a limited number of cell cycles, resulting in progressive telomere shortening and eventually senescence or apoptosis. On the contrary, cancer cells upregulate the expression of telomerase that maintains telomere length avoiding cell death. In order to sustain their neoplastic growth with nutrients and oxygen, cancer cells **induce angiogenesis** by increased expression of pro-angiogenic genes like vascular endothelial growth factor (VEGF) or fibroblast growth factor (FGF). This in turn causes normally quiescent vasculature to continuously develop new vessels. Cancer cells **activate invasion and metastasis** pathways mainly by alternating cell-to-cell and cell-to-ECM adhesion molecules. Certain mutations confer a selective growth advantage in cell subclones. Defects in so-called caretaker genes that detect, repair or inactivate damaged DNA lead to **genome instability**. Immune cells infiltrate almost every tumor and paradoxically some cell subsets enhance tumorigenesis and progression. **Tumor-promoting inflammation** is associated with attraction of pro-tumorigenic molecules, e.g. growth factors or pro-angiogenic factors to the tumor microenvironment. To fuel their increased proliferation rates, cancer cells can **reprogram their energy metabolism** from oxidative phosphorylation to anaerobic glycolysis and continue growing also under low oxygen concentrations. Tumors can **evade immune destruction** by recruiting immunosuppressive cells, such as regulatory T cells and myeloid-derived suppressor cells (MDSCs).

1.1.3 The tumor microenvironment

The tumor microenvironment (TME) is a collective term for the cells and molecules surrounding a tumor, including the stroma, ECM, vasculature, immune cells and their respective physicochemical milieu. The heterogeneous composition of the tumor microenvironment is continuously adapting to evolving environmental conditions and oncogenic signals coming from the tumor [12]. Based on the composition and activation state of the individual components, the TME can either promote or restrict tumor growth [13]. In order to predict the fate of tumor progression, it is important to understand the components of the TME and their influence on the tumor. In the following paragraphs, I will summarize the fundamental components of the TME and their major characteristics.

1.1.3.1 Cytokines and Chemokines

Cytokines are small proteins released by cancer cells, immune cells or stromal cells. The molecular group of cytokines includes chemokines, interferons, interleukins and tumor necrosis factors. Their expression and secretion is regulated by tumor microenvironmental factors and genetic and epigenetic mechanisms [14]. Chemokines orchestrate the trafficking of immune cells and vascular endothelial cells in the TME and thereby affect tumor immunity, cell migration, cell survival and cancer progression [15]. Depending on the secreted chemokine signature, the infiltrating immune cells can be of pro- or anti-tumorigenic subtype [16, 17]. Likewise, chemokines can also directly affect cancer cells and either promote or limit their survival [18, 19].

1.1.3.2 Cancer-associated fibroblasts

A major component of the tumor stroma is represented by cancer-associated fibroblasts (CAFs). Their morphology is similar to myofibroblasts with large spindle-shaped mesenchymal cells but as opposed to normal fibroblasts CAFs are constantly activated and neither revert to a normal phenotype nor undergo apoptosis and elimination [20]. The transformation of normal fibroblasts into CAFs is caused either by direct mutations or upon secretion of growth factors, miRNAs or reactive oxygen species (ROS). Once activated, CAFs promote cancer progression and invasion through the induction of angiogenesis, inflammation and ECM-remodeling [21-24]. Furthermore, genetic and epigenetic changes in CAFs are evidently contributing to cancer progression and resistance to current therapies [25]. Even though current biomarkers are not fully satisfactory, CAFs were found to be present in most solid tumors, in particular in breast, prostate and pancreatic carcinoma [26]. Different studies indicate the potential of CAFs as predictive biomarkers for cancer therapy across different cancer types [27].

1.1.3.3 Immune cells

Solid tumors are co-colonized by a plethora of immune cells with distinct functions. An extensive immunogenomic analysis of more than 10’000 tumors across 33 different cancer types revealed that the leukocyte fraction within the TME ranges between <10% and >90%. The same investigators identified six different clusters of immune signatures, aiming to summarize and simplify the complex interplay of tumor-infiltrating lymphocytes and their effect on tumor progression (*Figure 2*) [28].

	Macrophage: lymphocyte	Th1:Th2	Proliferation	Intratumoral heterogeneity	Other
Wound healing	Balanced	Low	High	High	
IFN-γ dominant	Lowest	Lowest	High	Highest	Highest M1 and highest CD8 T cells
Inflammatory	Balanced	High	Low	Lowest	Highest Th17
Lymphocyte depleted	High	Minimal Th	Moderate	Moderate	
Immunologically quiet	Highest	Minimal Th	Low	Low	Highest M2
TGF-β dominant	High	Balanced	Moderate	Moderate	Highest TGF-β signature

Figure 2 Solid tumors are characterized by immune subtype into six different classes termed wound healing, IFN-γ dominant, inflammatory, lymphocyte depleted, immunologically quiet and TGF-β dominant. Classification of the tumor immune landscape serves as a resource for future targeted therapies against solid tumors [28].

1.1.3.4 Vasculature

To maintain the nutrient and oxygen supply, cancer cells release pro-angiogenic factors that subsequently vascularize the tumor [29, 30]. In general, there are two subtypes of tumor vascularisation. Angiogenesis is the formation of new blood vessels from existing ones and vasculogenesis is the formation of new blood vessels after recruitment of endothelial cells from the bone marrow [31]. Depending on the released growth factors, angiogenesis can be further subdivided into sprouting angiogenesis, where new vessels are formed from pre-existing blood vessels and intussusceptive angiogenesis, where existing blood vessels split into two new blood vessels [32]. Chronic secretion of pro-angiogenic factors from solid tumors leads to an uncontrolled overproduction of new blood vessels and results in a structurally and functionally abnormal tumor vasculature. Tumor blood vessels are often leaky, dilated and interconnected with loosely attached or absent pericytes and basement membranes. Consequently, blood flow is spatially and temporally heterogeneous leading to interstitial hypertension, acidosis and hypoxia in the tumor microenvironment [33]. Hypoxia and acidosis in turn stimulate the secretion of pro-angiogenic factors and further aggravate angiogenesis [34]. Vessel leakiness results in swelling and oedema in the TME and facilitates metastatic tumor dissemination [35]. Furthermore, the abnormal tumor vasculature negatively affects tumor treatment by different means. An inefficient blood supply impedes the delivery of chemotherapeutic agents to the cancer cells and in response to tumor hypoxia, cancer cells respond less to radiotherapy [33].
In summary, a multitude of reasons highlights the importance of vascular deregulation for malignant progression of solid tumors. Based on that, academic researchers and pharmaceutical companies gained interest in developing cancer therapies that target the tumor vasculature. Whether tumor vessels should be destroyed to starve the tumor and induce its shrinkage or whether tumor vessels should be normalized to reduce metastatic spread and improve the delivery of cytotoxic drugs is still under debate [36]. So far, approved anti-angiogenic therapy for cancer mainly attempts to neutralize VEGF, which is the most important pro-angiogenic molecule that is

overexpressed in the majority of solid tumors [37]. VEGF-targeting drugs, including the antibody bevacizumab and the tyrosine kinase inhibitor sorafenib have been approved for several cancer-related indications but failed to show satisfactory results in overall patient survival [38, 39]. The paradigm is now shifting towards the preclinical evaluation of vasculature-normalizing agents, including chloroquine and ITPP [40, 41].

1.1.3.5 Hypoxia

A tumor area is defined as hypoxic when its partial oxygen pressure (pO_2) is lower than the pO_2 in the surrounding healthy tissue. Theoretically, an exact pO_2 threshold level that divides tumors into hypoxic or normoxic should not exist, because the oxygen demand in the human body is tissue-dependent [42]. Nevertheless, the scientific community generally accepts oxygen levels below 2% (pO_2= 15 mmHg) as hypoxic [43]. The oxygenation status of most solid tumors manifests in an extremely heterogeneous pattern of normoxic, mildly hypoxic and severely hypoxic areas. Tumor hypoxia can be further subdivided in acute (ischemic) and chronic (diffusion-limited) hypoxia. Acute hypoxia is a result of temporary obstruction or reduction of the blood low, whereas chronic hypoxia appears in tumor areas whose distance to the closest blood vessel is further than the maximal oxygen diffusion distance (100 – 200 µm) [44, 45]. To explain this heterogeneity it is important to understand how tumor hypoxia is induced.

When proliferating mutated cells lead to the formation of a neoplastic tumor, they will reach a point where part of the cancer cells outgrow their blood supply. The decreased oxygen concentration in these cells will trigger signalling pathways to restore oxygenation. A family of heterodimeric transcription factors named hypoxia inducible factors (HIFs) plays a central role in cellular oxygen homeostasis. They consist of an oxygen-dependent alpha domain (HIF1α, HIF2α, and HIF3α) and a constitutively expressed beta domain (HIF1β) [46]. The activities of the alpha-subunits are primarily regulated by post-translational hydroxylation of a proline residue in the oxygen-dependent degradation domain by prolyl hydroxylase domain proteins (PHDs). Proline hydroxylation targets the alpha subunits for proteasomal degradation by promoting their interaction to von Hippel-Lindau (VHL), a tumor suppressor with ubiquitin ligase activity [47]. At cellular oxygen concentrations below 1%, PHDs become inactive and HIF1α is consequently stabilized [48, 49]. A nuclear localization signal (NLS) in its C-terminal region enables rapid translocation of HIF1α into the nucleus, where it dimerizes with HIF1β and induces the expression of downstream target genes [50]. More than 60 HIF1 target genes, mainly affecting cell metabolism, cell survival and angiogenesis have been identified, including VEGF-A, the key regulator of tumor angiogenesis [51]. As discussed previously, constant secretion of VEGF by hypoxic tumors leads to the formation of a leaky and dysfunctional vasculature. The resulting irregularities in blood flow create hypoxic regions, which further aggravate VEGF secretion, leading to a vicious cycle of hypoxia and angiogenesis.

Tumor hypoxia results in numerous pro-tumorigenic transformations, such as repression of DNA damage repair and genomic instability [52-54]. Moreover, hypoxia promotes a stem-like phenotype in the tumor cell population by maintaining cancer stem cells (CSCs) in an undifferentiated stem cell state, which enables self-renewal and continuous accumulation of genetic and epigenetic alterations [55, 56]. The selection and maintenance of CSC in the hypoxic TME further promotes malignant progression and therapy resistance [57]. An important aftermath of tumor hypoxia and increased HIF-signalling is the promotion of metastatic spread. Owing to the leaky and dilated tumor vasculature induced by hypoxia, escape of cancer cells from the primary tumor appears logical. Irrespective of the abnormal vasculature, hypoxia-mediated expression of HIF target genes that control immune suppression, invasion and migration further support early stages of metastases [58]. Tumor hypoxia is associated with increased secretion of

the matrix metalloproteinase MMP-1, an ECM-modifying protein that facilitates the extravasation of cancer cells from the primary tumor into the blood and lymphatic system [59]. Another HIF target gene involved in metastatic progression is lysyl oxidase (LOX), which was shown to post-translationally modify the ECM in distant tissues to establish a microenvironment that enables the growth and survival of metastasized cancer cells [60]. High LOX-expression in primary tumors is associated with poor metastasis-free and overall survival in cancer patients [61].
Tumor hypoxia not only leads to malignant transformation and progression of cancer cells but also is responsible for treatment resistance, especially in combination with radiotherapy. These important aspects will be addressed later in my thesis.

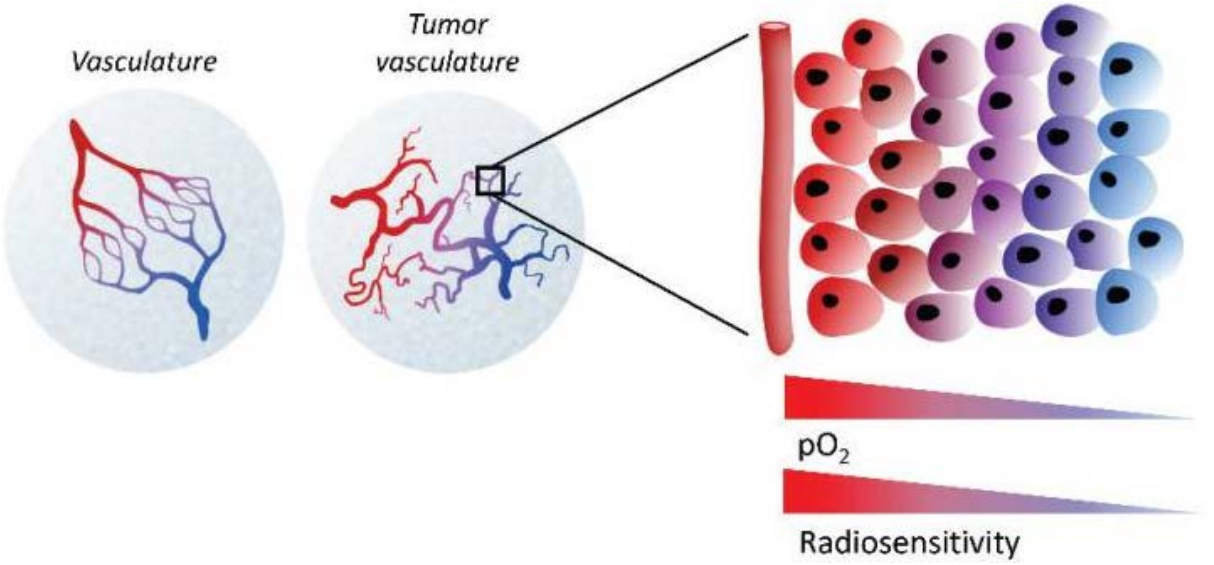

Figure 3 Most solid tumors are associated with a chaotic and unfunctional vasculature driven by constant release of VEGF as a result of tumor hypoxia. Vascular malfunction limits the oxygen deliver to cancer cells and thereby decreases their radiosensitivity [62].

1.1.4 Metastases

Representing one of the hallmarks of cancer, metastases are the result of a biological multi-step process that triggers the dissemination of primary tumors to anatomically distant organs. Although the exact trigger that drives a cancer cell to become metastatic is still under debate, a multitude of factors have been shown to influence this malignant process. As mentioned above, tumor hypoxia is one of the key-drivers of metastatic spread. Nevertheless, other causative mechanisms must be accountable for metastases deriving from normoxic cancer cells. It is hypothesized that oncogenic mutations play an essential role for the initiation of the metastatic process [63]. Tumor hypoxia or mutations leading to deregulated TGF-β signalling are considered the most relevant metastatic triggers [64]. TGF-β induces epithelial-mesenchymal transition, in which epithelial cells acquire a mesenchymal phenotype, resulting in enhanced motility and invasion [65, 66]. Driven by transcription factors, including SNAIL, TWIST and ZEB, epithelial cells lose their cell junction proteins and reprogram their gene expression towards an invasive, mesenchymal phenotype [67]. Subsequent secretion of proteolytic matrix-metalloproteases (MMPs) degrades the extracellular matrix (ECM) and creates a path for metastatic cells to reach the systemic circulation. The accompanying abundance of growth factors and cytokines sustains the proliferation and survival of liberated primary tumor cells [68]. The leaky and chaotic tumor microvasculature described in

previous paragraphs, facilitates the lymphatic or blood vessels invasion. Consequently, circulating tumor cells (CTCs) face an inhospitable environment in the vascular circulation, caused by hemodynamic shear forces and the abundance of anti-tumorigenic innate immune cells [69]. It is estimated that less than 0.01 % of all CTCs survive in the circulation and successfully disseminate to distant organs [70]. The survival of CTCs is supported by blood platelets, which form platelet-cancer cell clusters and thereby prevent immune cell recognition and further aid in attaching to endothelial cells and extravasating to distant tissues [71, 72]. The "seed and soil" hypothesis proposed by Stephen Paget in 1889, claiming that the distribution of metastases is not random, resulted in the pre-metastatic niche model. This is characterized by a plethora of bone marrow derived cells (BMDCs) that render the microenvironment of distant organ sites receptive to tumor growth by secreting bioactive molecules that remodel the ECM to accelerate cancer cell adhesion and invasion [61, 73, 74]. By inducing VEGF signalling, the BMDCs further help in overcoming angiogenic dormancy, an inability of metastasized cancer cells to proliferate due to insufficient vascularization [75-77]. Finally, by reprograming their gene expression, metastasized cells commit to mesenchymal-epithelial transition (MET) and continue to proliferate in the distant tissue [78].
While primary tumors are often curable by surgical resection and adjuvant therapy, metastatic lesions are usually incurable as a result of systemic spread [69]. As metastases have comparably low proliferation rates, they are relatively resistant to cytotoxic drugs targeting cell growth and division [77]. Moreover, metastatic lesions often acquire mutations that are molecularly distinct from the primary tumor and thereby do not respond to targeted therapy against the primary tumor lesion [79]. Based on the lack of curative treatment options, metastatic disease accounts for approximately 90 % of cancer-related deaths [80]. To overcome this dramatic fact, novel treatment strategies simultaneously targeting the tumor microenvironment and intracellular signalling pathways have to be investigated and implemented in current treatment protocols.

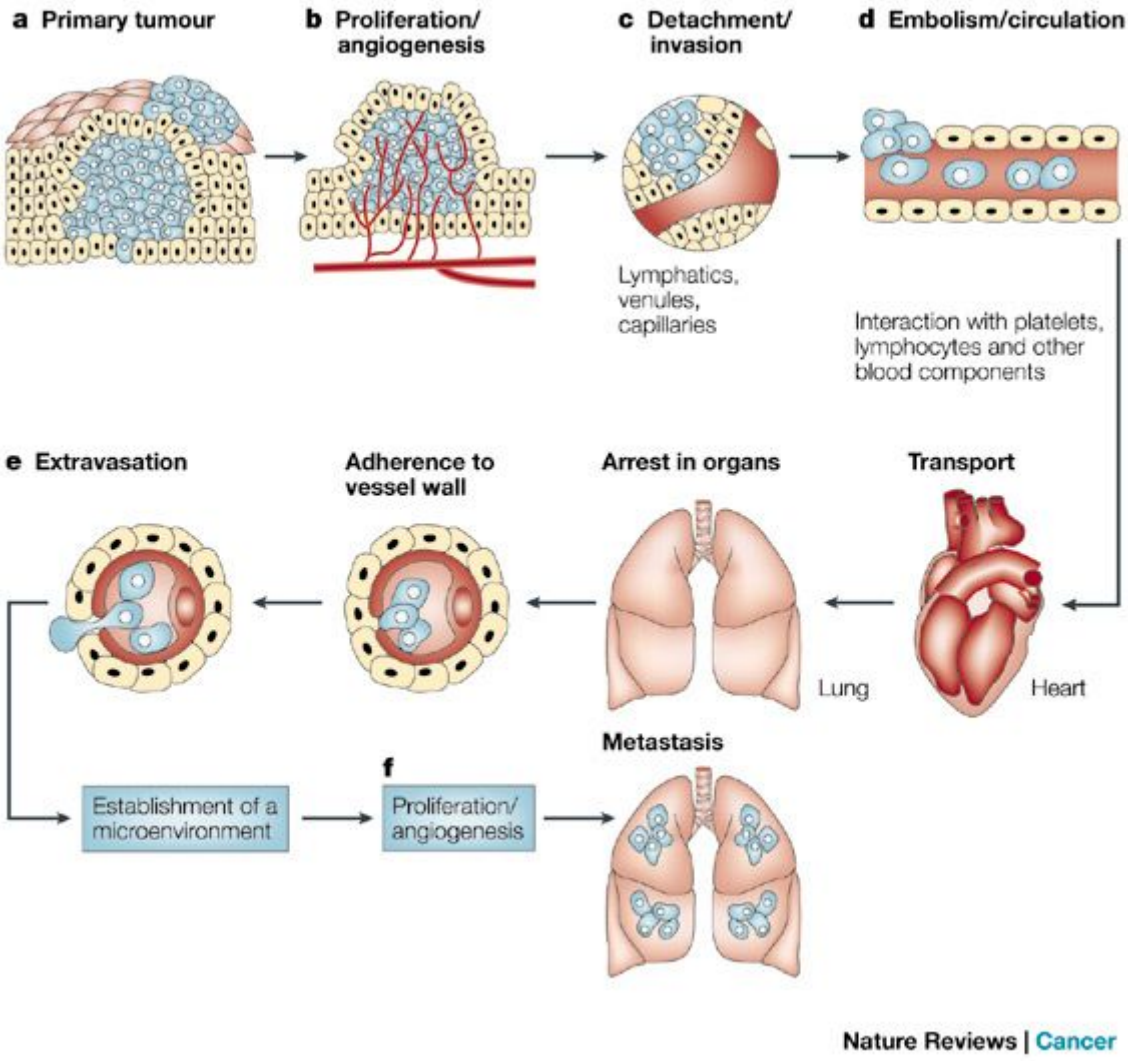

Figure 4 The main steps in the formation of a metastasis include **a)** progressive cellular transformation **b)** extensive vascularization to permit primary tumor growth **c)** local invasion of the tumor stroma **d)** detachment from the primary tumor, transport through vascular or lymphatic system and adharence in vessel walls **e)** extravasation to a secondary tissue, followed by **f)** proliferation in the metastatic site [81].

1.2 Cancer diagnosis and imaging

1.2.1 General aspects of cancer diagnosis

In 2012, 14.1 million new cancer cases have been diagnosed worldwide. The incidence of newly diagnosed cancer patients is estimated to further increase due to population growth and aging [9]. In order to diagnose cancer, a plethora of invasive and non-invasive methods has been developed over the past centuries. Early diagnosis of malignant transformation is key for successful cancer therapy, because treatment of tumors that have not yet metastasized is more promising. Screening programs for supposedly healthy individuals with a specific risk for cancer development based on age, gender, lifestyle or genetic predisposition have evolved and play a vital role in early diagnosis. Depending on the surveyed tissue, diagnostic methods range from physical examination (breast, testis and skin), invasive imaging (colon and stomach), non-invasive imaging (breast, lung and ovaries) to specific biomarker detection (prostate, cervix and ovaries) [82]. Upon detection of a tumor, clinicians have to determine the malignancy of the neoplastic lesion. Apart from TNM-staging that describes tumor size, lymph node involvement and metastatic spread, the malignancy is further examined by invasively collecting tumor biopsies and analyzing their genetic or proteomic signatures. The detection of cancer-specific biomarkers in liquid biopsies is an emerging and non-invasive approach to diagnose cancer or assess molecular changes of cancer cells during therapy. Extensive research is ongoing to reliably interpret the limited amount of tumor material in liquid biopsies [83].
In the following paragraphs, I will summarize some of the most relevant non-invasive tumor imaging modalities and specifically address the diagnostic tools to measure tumor hypoxia.

1.2.2 Computed tomography

In 1895 Wilhelm Conrad Röntgen discovered X-rays, a form of electromagnetic radiation with wavelengths between 0.01 and 10 nm. Only a few months after his discovery, the medical use of X-rays was probed to scan the wrist of a patient [84]. The interactions of X-rays with the human body are nowadays well known. As X-rays pass through the body, different organs and structures absorb them before they reach the detecting film. The absorption rate is tissue-dependent, i.e. bones with a high atomic density absorb more X-rays than soft tissue organs or the lungs. A conventional X-ray scan (radiograph) accordingly depicts the different tissues within a human body in two dimensions. Röntgen's discovery was further developed and translated into computed tomography (CT), where rotating X-ray beams together with a digital detector generate cross-sectional images that can be stacked together to provide a three-dimensional representation of the structures in the human body. CT scans are extensively used in clinical practice for cancer diagnosis and monitoring, as a prerequisite for treatment planning in radiotherapy and as a basis for functional imaging modalities (PET/SPECT). As tumors usually have a similar tissue density to that of the surrounding healthy organs, CT scans are often acquired after systemic injection of a contrast-enhancing agent to increase the visibility of tumors [85]. In the relatively novel field of image-guided small-animal radiotherapy researchers utilize cone-beam CT (CBCT) scanners, where the emitted X-rays form a cone-shape. This increases the scan area and enables to acquire volumetric images without a full gantry cycle.

1.2.3 Magnetic resonance imaging

Magnetic resonance imaging (MRI) is another frequently used medical imaging technique in the field of oncology. As opposed to CT imaging, MRI does not utilize ionizing radiation to generate a patient scan. Instead, the patient is exposed to strong, oscillating magnetic fields, which excite hydrogen atoms of water molecules in the human body. The rate at which excited hydrogen atoms

return to the equilibrium state determines the contrast between different tissues [86]. The return to the equilibrium state consists of longitudinal relaxation (T1) and transverse magnetization (T2). Depending on the tissue of interest, radiologists can acquire T1-weighted or T2-weighted scans by adjusting the scanning parameters [87]. As for CT imaging, contrast agents are an important measure to increase the visibility of neoplastic lesions in MRI scans. These contrast agents are usually based on paramagnetic gadolinium or superparamagnetic iron molecules that based on their structure and route of administration accumulate in specific tissues where they influence T1 or T2 relaxation times and thereby enhance the tissue visibility [88]. In contrast to CT imaging, MRI scans can reveal additional physiological information. Advanced MRI techniques can for example monitor the circulation of body fluids by diffusion-weighted imaging (DWI) or perfusion-weighted imaging (PWI). Furthermore, functional MRI (fMRI) measures oxygen concentrations by a method that I will describe in the paragraph "Methods to detect tumor hypoxia" [89].

1.2.4 PET and SPECT

The information acquired from CT or MRI scans is sometimes not sufficient to detect or quantify a tumor. In this case, radiopharmaceutical agents specifically targeting the desired tissue can facilitate tumor diagnosis. Depending on the physical decay properties of the radionuclide it is either traced by positron emission tomography (PET) or single photon computed tomography (SPECT) and co-registered with a CT or MRI scan to obtain anatomical information. For PET-imaging, patients are intravenously injected with a PET tracer containing a radionuclide that decays to a positively charged positron that thereupon annihilates with an electron in close proximity. Annihilation generates two opposing gamma rays that can be detected and processed by a circular PET detector. Subsequently the annihilation position can be reconstructed and overlaid with the anatomical scan. Finally, a three-dimensional scan showing the accumulation of the radiotracer gives detailed information about the location and size of the primary tumor and eventual metastases. The most widely used PET tracer in oncology is based on glucose (^{18}F-FDG) and is taken up to a higher extent by cancer cells [90]. In SPECT-imaging, patients receive radiotracers that directly decay by gamma ray emission. Similar to PET scanners, SPECT-imaging detects, processes and reconstructs the gamma rays to pinpoint the localization of radiotracer accumulation. The most frequently used tracers in SPECT-imaging contain the metastable ^{99m}Tc radionuclide [91].
The main advantage of functional and metabolic imaging by PET or SPECT is the potential to detect small lesions and metastases that are usually not visible by conventional CT or MR imaging [92]. Furthermore, target-specific radiotracers can depict certain microenvironments (e.g. hypoxia) or extracellular receptors indicative of a malignant prognosis and progression [93, 94].

1.2.5 Methods to detect tumor hypoxia

Tumor hypoxia is one of the major factors limiting the success of cancer therapy [95]. To improve clinical treatment strategies and provide measures for patient stratification a variety of invasive and non-invasive methods to detect and quantify tumor hypoxia were developed over the past decades.
An invasive approach that measures tumor hypoxia are polarographic oxygen microelectrodes where thin needle sensors are directly inserted into the tumor and quantitatively determine the pO_2 in real time. As these measurements depict spatial pO_2 information, repeated measures in different tumor areas have to be performed in order to get an overview of the whole tumor. The invasiveness of this approach together with technical long-term instability and the development of non-invasive imaging methods have led to the discontinuation of oxygen microelectrodes in clinical practice [96, 97]. Another invasive method to detect tumor hypoxia is histological staining

of tumor biopsies. Excised tissues are either stained for endogenous hypoxia-specific biomarkers (e.g. HIF-1α and carbonic anhydrase IX (CAIX)) or for exogenously injected nitroimidazole compounds [98]. Nitroimidazoles, including its most prominent substance pimonidazole are a group of related compounds that are chemically reduced in areas of pO_2 < 10mmHg and subsequently form irreversible adducts with unspecific proteins [99]. The disadvantages of histological hypoxia detection are invasiveness, spatial restriction and the relatively long processing time. As such, hypoxia characterization by histology is nowadays primarily used in preclinical or retrospective investigations. In clinical trials, tumor biopsies are also used for correlation of tumor hypoxia with a specific genetic landscape. Investigators could identify a 26-gene signature that predicts the benefit from hypoxia-modifying therapy in a specific type of cancer [100, 101].
Since all of the methods described above are invasive and relatively time consuming, the scientific and clinical community tends to favor non-invasive hypoxia detection methods. A frequently used approach are PET/CT scans with radiopharmaceuticals specifically targeting hypoxic tissues. Most tracers are derived from the nitroimidazole family of compounds and are radiolabelled with ^{18}F (e.g. ^{18}F-fluoromisonidazole (^{18}F-FMISO) or ^{18}F-fluoroazomycin-arabinofuranoside (^{18}F-FAZA)) [102]. The radioactive PET tracers represent an additional burden of ionizing radiation for cancer patients, which emphasizes the importance of alternative non-invasive methods to detect hypoxia.
A variety of functional MRI methods is suitable to non-invasively detect tumor hypoxia without the aid of radioactive tracers. Blood oxygen level-dependent (BOLD) MRI measures blood oxygenation on the basis of changes in the paramagnetic deoxyhemoglobin molecule. The BOLD effect is not strictly oxygen-dependent and also influenced by blood flow, hemoglobin levels and the state of the vasculature, a quantitative relationship to pO_2 could not be proven [102, 103]. However, BOLD measurements showed significantly increased signals after carbogen treatment in patients [104]. Other fMRI methods that indirectly reflect tumor oxygenation on the clinical and preclinical level are dynamic contrast-enhanced (DCE)-MRI, diffusion weighted imaging (DWI)-MRI and electron paramagnetic resonance (EPR)-MRI [105-107].

1.3 Cancer treatment

1.3.1 General aspects of cancer therapy

The incidence of cancer patients is increasing worldwide and is projected to reach 19.3 million new cancer cases per year by 2025 [108]. The vast heterogeneity in cancer genetics, epigenetics, location, malignancy and stage requires a broad spectrum of independent or synergistic treatment approaches to cover the unique molecular features of each cancer patient. Depending on the individual diagnosis and regional healthcare guidelines, cancer patients are treated by surgery, chemotherapy, targeted therapy, immunotherapy, radiotherapy or a combination of different approaches. In the following paragraphs, I will summarize the rationale and application of the various cancer treatment modalities.

1.3.2 Surgery and Chemotherapy

Surgical resection of tumors is the oldest oncological discipline and is currently regarded as the only curative treatment strategy available. Driven by technical innovation and combinations with neoadjuvant or adjuvant therapies cancer surgery has reached a level of optimal local control and minimal surgical morbidity and mortality in almost all types of solid tumors [109].
Chemotherapy is a cancer treatment that uses pharmacological compounds to target rapidly dividing cells with a curative or palliative intent. Since some healthy cells in the human body also have high proliferation rates (e.g cells lining the mucosal tissues), chemotherapy is often accompanied with side effects like nausea and diarrhea. Chemotherapeutic agents are often

combined with surgery or radiotherapy and based on their mode of action classified in different subgroups:

Alkylating agents are electrophilic compounds that react with DNA or proteins to form irreversible covalent bonds, which subsequently impair DNA replication and transcription. DNA alkylating agents exert their effect independently of the cell cycle phase. Some of the most frequently used alkylating agents in oncology are cyclophosphamide, cisplatin and temozolomide [110].

Antimetabolites interfere with DNA synthesis by either inhibiting the biosynthesis of deoxyribonucleotides for DNA replication (e.g. 5-fluorouracil) or by becoming fraudulent substrates for DNA polymerases (e.g. gemcitabine) [111]. Antimetabolites usually affect cells in the S phase of the cell cycle. Other frequently used antimetabolites for cancer therapy are methotrexate, doxorubicin or bleomycin.

Microtubule-interfering agents, also called microtubule-targeting agents or spindle poisons act on the cell spindle during mitosis by either stabilizing microtubule polymers (taxane class, e.g. paclitaxel) or by disrupting microtubule polymerization (vinca alkaloids class, e.g. vincristine) [112]. Dysregulated microtubule function results in cell cycle arrest and subsequent apoptosis.

Topoisomerase inhibitors interfere with topoisomerases, which are enzymes that prevent DNA supercoiling and entanglements during DNA replication and transcription. Lack of topoisomerase activity results in stalled polymerases or formation of abnormal nucleic acid structures that eventually induce cell cycle arrest in the G2 phase [113]. Some of the most frequently used topoisomerase inhibitors for cancer therapy are irinotecan or etoposide.

1.3.3 Molecularly targeted therapy

Unlike in chemotherapy where all rapidly dividing cells are affected, targeted therapy limits the growth of cancer cells by specifically interacting with molecules or pathways required for carcinogenesis, by inducing apoptosis or by modifying the function of proteins that regulate gene expression. The rationale of personalized medicine is to identify patients that could benefit from a specific targeted therapy based on the expression of molecular markers [114]. At the same time, patients unresponsive to a specific treatment can be given different treatment modalities. Based on that, molecularly targeted therapy is associated with improved efficacy and decreased toxicity in cancer patients. Numerous molecularly targeting drugs with different modes of action are approved for the treatment of cancer patients. So far, they mostly consist of small molecules like the tyrosine kinase inhibitors (e.g. imatinib) and monoclonal antibodies like anti-angiogenic drugs (e.g. bevacizumab).

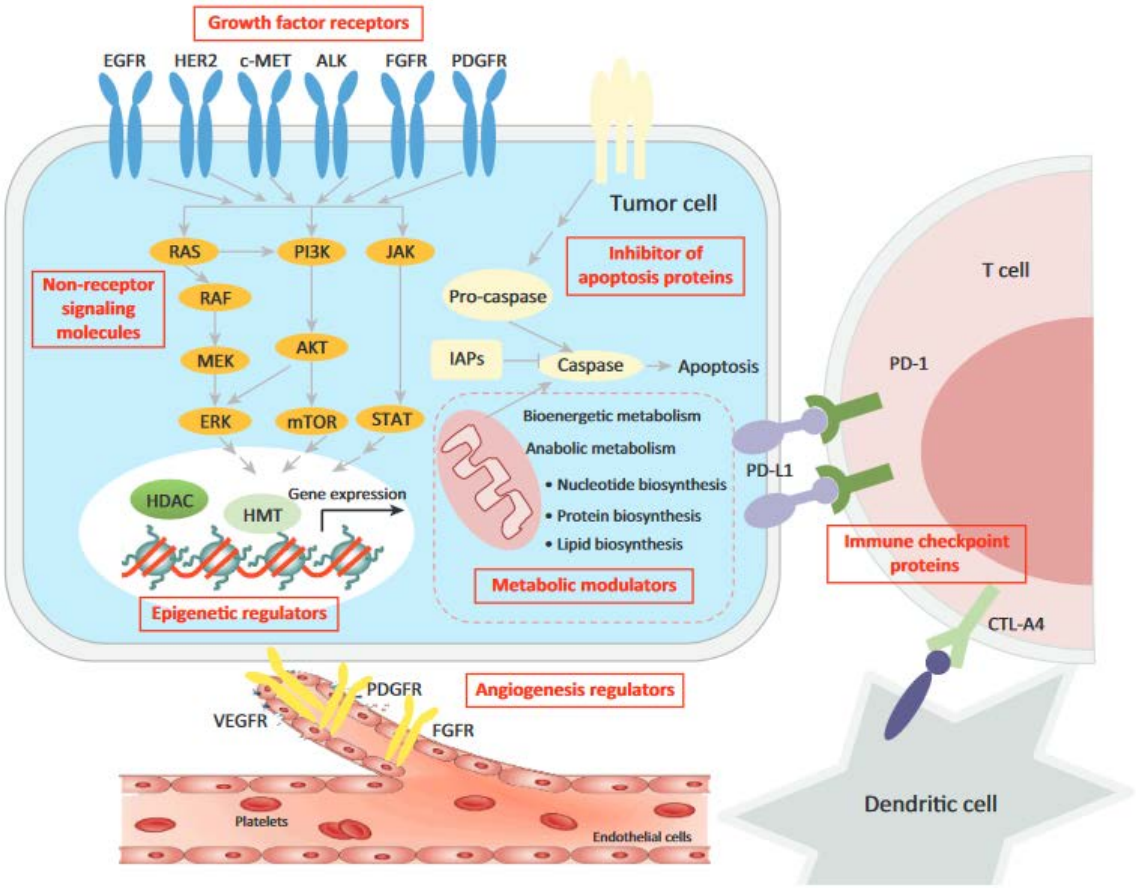

Figure 5 Schematic representation of cellular targets for molecularly targeted therapies. Potential targets and currently approved drugs include growth factor receptors (e.g. gefitinib), non-receptor signalling molecules (e.g. everolimus), inhibitors of apoptosis proteins (e.g. bortezomib), epigenetic regulators (e.g. vorinostat), metabolic modulators (no drugs on the market), angiogenesis regulators (e.g. bevacizumab) and immune checkpoint proteins (e.g. nivolumab). Figure adapted from Huang M et al [115].

1.3.4 Immunotherapy

The immune system not only recognizes and eliminates malignant cancer cells, but also plays a critical role in promoting tumor progression. The dual role by which the immune system can limit or stimulate cancer growth is called cancer immunoediting [116]. The concept of immunoediting consists of three sequential phases: elimination, equilibrium and escape. In the elimination phase, cancer cells are destroyed before they become clinically apparent. If a cancer cell remains unrecognized and survives the elimination phase it may reach the equilibrium phase, where further outgrowth is prevented by several adaptive immunity mechanisms. Constant immune selection pressure placed on genetically unstable cancer cells may induce their escape from the immune system and cause clinically apparent disease [117]. The understanding of cancer immune evasion provided new ideas for the development of cancer therapeutics. The cytotoxic T-lymphocyte associated immune checkpoint inhibitors CTLA4 and PD-1/PD-L1 have been identified as the most relevant targets [118]. CTLA-4 is expressed exclusively on T cells and functions as a co-receptor for antigen presenting cells (APCs). Unlike the other T cell co-receptor CD28, CTLA-4 does not induce an anti-tumorigenic response [119]. The CTLA-4-targeting antibody ipilimumab improves survival of metastatic melanoma patients and has been approved by the US Food and Drug Administration (FDA) for this indication [120]. PD-1 is another costimulatory molecule expressed on the T cell surface that interacts with PD-L1 on APCs. Similar to CTLA-4, PD-1 binding prevents

T cell proliferation and secretion of anti-tumorigenic factors. Inhibition of PD-1 (e.g. with nivolumab) or PD-L1 (e.g. with pembrolizumab) improved the survival of cancer patients in clinical trials [121, 122]. Another class of immunotherapeutic agents are chimeric antigen receptor (CAR) T cells. In a procedure termed adoptive T cell therapy, T cells are isolated from cancer patients and are genetically modified with antigen-binding domains recognizing tumor antigens (e.g. CD19). The engineered CAR T cells are then reinfused into the patient where they can target tumor cells and activate anti-tumorigenic T cell responses [123, 124]. The FDA approved the first CAR T cell therapy (Kymriah) for the treatment of acute lymphoblastic leukemia.

1.3.5 Radiotherapy

Radiotherapy is the treatment of cancer patients by ionizing radiation (IR), which induces DNA double strand breaks that result in growth arrest and cell death. IR can either directly ionize and thereby damage DNA molecules or indirectly induce the production of free radicals from water and oxygen molecules within the tumor. For X-rays, approximately 60% of the cellular damage is triggered by free radicals that attack DNA molecules [125, 126]. IR does not discriminate between healthy and cancerous cells, which emphasizes the importance of accurate treatment planning and delivery. Owing to tremendous progress in the development of linear accelerators, it is now feasible to use imaging modalities and planning software to precisely deliver conformal high doses of IR to the tumor without overly co-irradiating the healthy surrounding tissue [127]. Radiation can be delivered either by linear accelerators (external beam radiotherapy) or by decaying radionuclides (brachytherapy). Based on the tumor entity and the hospital equipment, external beam radiotherapy can be applied by different physical moieties including photons, protons, electrons or carbon ions [128]. Typically, radiotherapy is combined with chemotherapy, immunotherapy or surgery. Radiotherapy is not only used for curative intent, but also to palliate advanced cancer patients and improve their quality of life [129].

1.3.5.1 The 5 R's

In order to exploit the full potential of radiotherapy it is important to understand how radiation influences the biology and microenvironment of cancer cells and to apply these insights in translational studies [130]. Based on this notion, Steel et al. suggested the 5Rs that influence the outcome of radiotherapy and how their optimization may improve tumor control and reduce normal-tissue toxicity [131]. In the following lines, I will briefly describe the 5Rs, which will be discussed in more detail in section 1.4 Treatment resistance:

Repair is induced by the DNA damage response machinery after radiation-induced double strand breaks in the DNA.

Repopulation is caused by the enhanced proliferation rate of surviving cells that continue to grow and replace the cells killed by IR.

Reassortment or Redistribution exploits the differential radiation sensitivity of cancer cells depending on the cell cycle phase.

Reoxygenation of the TME after a dose fraction enhances the radiosensitivity of the following dose fractions.

Radiosensitivity of cancer cells depends primarily on their proliferative rate, i.e. rapidly dividing cells are more radiosensitive than slowly proliferating cells.

1.3.5.2 Brachytherapy

Brachytherapy is a treatment for cancer patients in which radionuclides are placed in close proximity to the lesion that should be irradiated. As such, it can be described as an invasive radiotherapy approach. Brachytherapy is used either as a single treatment or in combination with surgery or external beam radiotherapy. Moreover, it is used as a salvage therapy for local recurrence. Gynaecological tumors are the most common application for brachytherapy [132]. Other tumor entities include prostate, breast, eye, oesophagus and head & neck [133]. Typical radionuclides used in brachytherapy are ^{60}Co, ^{192}Ir and ^{125}I [134].

1.3.5.3 Radiation physics and LINAC technology

A linear accelerator (LINAC) generates X-rays by accelerating electrons and striking them on a high atomic number target (e.g. tungsten). When the electrons strike the target, electromagnetic radiation in form of photons are generated by an effect termed "Bremsstrahlung". A contoured flattening filter subsequently shapes the photons (X-rays) to a uniform energy of typically 4 MeV to 10 MeV. The patient lies on a couch that can rotate and move in all three translational directions, while the LINAC gantry can rotate 360° around the patient and deliver the X-rays statically or dynamically.
Photons are uncharged packets of energy that travel at the speed of light and exert forces to atoms in the human body. There are three main interactions that can occur. In photoelectric interactions, the photon collides with an electron that is repelled, leaving behind an ionized atom. Unlike in photoelectric interactions, where the entire kinetic photon energy is transferred to the escaping electron, in Compton interactions only a fraction of the kinetic photon energy is transferred to the escaping electrons while the initial photons are scattered and continue to travel with a lower kinetic energy. The third interaction is pair production, where photons interact with the atomic nucleus and create an electron and a positron. Compton interactions are the most important interactions of therapeutic photon beams. Once an atom has been ionized, some of the chemical bonds within the molecule will be disrupted leading to irreversible biological damage. The radiation dose is a measure of the amount of energy deposited at a point of interest and expressed in units of Gray (Gy), where 1 Gy = 1 J/kg [135].

1.3.5.4 Fractionation and treatment scheduling

The 5R's are the best approach to describe the rationale of fractionated radiotherapy. One goal is to increase the damage to the tumor by reoxygenation of hypoxic cells and redistribution of cells along the cell cycle. At the same time, healthy tissue is spared by repair of sublethal damage and repopulation from surviving cells. The main variables influencing the design of a fractionated treatment schedule are overall dose, number of fractions, dose per fraction and the time interval between fractions [136]. A conventional treatment schedule consists of 30 fractions with 2 Gy. Altered fractionation schedules have shown to be beneficial for cancer patients. One example is the improved survival in patients with head & neck cancer that were treated with hyperfractionated radiotherapy where IR-fractions are given more than once daily [137].
The other extreme is hypofractionated radiotherapy that delivers high doses of IR in a limited number of fractions. Hypofractionated radiotherapy, also termed as stereotactic body radiotherapy (SBRT) has emerged over the past decades due to remarkable technical progress. Numerous clinical investigations have demonstrated improved efficacy of SBRT as compared to conventional radiotherapy in cancer patients [138]. The underlying radiobiological mechanisms cannot be explained with the 5R's of radiotherapy, therefore it is assumed that mechanisms other than direct cell killing of cancer cells through DNA DSBs are responsible for the improved efficacy

of SBRT. Secondary cell death by damaging the tumor vasculature and inducing an anti-tumor immune response are hypothesized as the main reasons for the success of SBRT. It was shown that IR-fractions above 10 Gy cause endothelial cell death and vascular disruption resulting in ischemic cancer cell death within a few days after irradiation. Vascular disruption and extensive cancer cell death further increase the release of tumor-associated antigens, thereby triggering an anti-tumorigenic immune response [139].
Sporadic clinical case reports have described a remission of non-irradiated cancer lesions after radiotherapy of primary tumors. This phenomenon was described as the "abscopal effect" and is associated with immunogenic responses after high-dose radiotherapy. The release of tumor antigens from the primary tumor improves antigen presentation to cytotoxic T cells, which in turn are activated and kill cancer cells at distant sites [140, 141].

1.3.5.5 Small animal radiotherapy

Basic and applied research in the field of radiobiology helped to reveal the biological relation of ionizing radiation and cytotoxicity. Many lessons learned in preclinical trials were successfully translated into treatment options for cancer patients. However, the physical and technical aspects in preclinical research were historically always a few steps behind the corresponding developments in the clinical field. In contrast, innovations in clinical radiotherapy are primarily attributed to technological progress rather than a more comprehensive understanding of the underlying radiobiological mechanisms.
With the development of small animal radiotherapy platforms, preclinical researchers aim to bridge the technological gap in radiation oncology. Cone beam CT (CBCT) based treatment planning with Monte Carlo dose calculation, followed by static or dynamic irradiation with millimeter-sized collimators enable to precisely deliver high conformal doses of IR to very small structures in animal models. Further development in the small animal radiotherapy field is leading towards the integration of functional imaging modalities like PET. As such, preclinical radiobiological studies can be performed in high accordance to clinical practice and investigate previously not applicable aspects including dose painting or spatiotemporal fractionation [142].

1.3.6 Combined treatment modalities

As previously mentioned, most cancer patients are treated with a combination of different treatment options in order to improve therapeutic success. Surgical tumor resections often go along with neoadjuvant chemo- or radiotherapy in order to reduce the extents of the tumor and permit surgery in previously inoperable disease. Likewise, adjuvant radiotherapy kills macroscopically invisible tumor cells remaining along the surgery margin and thereby further improves tumor control [109]. Other combined treatment modalities are often prescribed to prevent treatment resistance or to modulate cancer cells and their TME in a manner that enables synergistic therapy effects. The underlying mechanisms and rationales for combined treatment will be discussed in the following sections.

1.4 Treatment resistance

Treatment resistance is one of the major factors contributing to disease progression leading to treatment failure. The high adaptability of tumors can induce treatment resistance by distinct mechanisms. The genomic landscape of a tumor is highly heterogeneous among patients suffering from the same type of cancer, rendering targeted therapy ineffective in some cases. This is further complicated by intra-patient heterogeneity. Distinct mutational profiles within a tumor result in unequal therapeutic response to any anti-proliferative treatment options, which increases the probability that a subpopulation of cancer cells does not respond to a given cancer therapy [143].

Functional genomic techniques are then employed to identify novel genes and signalling networks involved in treatment resistance [144].
Treatment resistance can be categorized into acquired resistance and intrinsic resistance. Intrinsic or innate resistance is the pre-existence of cancer cell properties that prevent the effectiveness of a certain treatment, e.g. by compensatory signalling pathways. Acquired resistance on the other hand develops over the course of the treatment, e.g. by mutational changes in a signalling network. Acquisition of treatment resistance is not exclusively driven by mutational changes on the cellular level but to a considerable extent also by alterations in the TME. Furthermore, it is important to understand the conceptual differences of chemoresistance and radioresistance. These key aspects will be discussed in the following sections.

1.4.1 Chemoresistance

Chemoresistance is a result of intrinsic or acquired resistance of cancer cells to chemotherapeutic or targeted agents. The list of causes for chemoresistance includes alterations of drug uptake, efflux and metabolization as well as alterations and decreased expression of drug targets, increased repair capacity and limited perfusion [145]. Specific DNA-mutations in cancer cells can lead to pseudo-resistance, whereupon molecularly targeted drugs become ineffective. A prominent example is the activation of alternative signalling pathways (e.g. c-Met) upon treatment with EGFR-tyrosine kinase inhibitors (TKIs) (e.g. erlotinib or gefitinib) [146]. A large number of patients acquire resistance to functionally and structurally unrelated drugs, a phenomenon termed as multidrug resistance (MDR). ATP-binding cassette (ABC) efflux transporters including P-glycoprotein (P-gp) play an important role in MDR. These transmembrane proteins actively pump drugs out of the cell and thereby reduce intracellular drug concentrations [147]. Overexpression of P-gp is associated with drug resistance and has been reported in numerous tumor entities [148]. Drug-metabolizing enzymes of the cytochrome P450 (CYP) family mediate another important mechanism for chemoresistance. These enzymes are primarily expressed in the liver and metabolize drugs by the addition of a hydroxyl moiety that renders the xenobiotic compound more hydrophilic, which improves its secretion and thereby reduces intracellular drug concentrations. Approximately 70-80% of all drugs in clinical use are metabolized by CYPs [149].

1.4.2 Radioresistance

The resistance of cancer cells to radiotherapy is determined by intrinsic cellular factors and by the surrounding TME. Adaptive changes of intracellular signalling pathways, primarily involved in DNA repair and replication, cell cycle arrest and apoptosis are some of the intrinsic factors leading to radioresistance.
The most extensively involved pathways are the p53, phosphatidylinositol-3-kinases (PI3K) and epidermal growth factor receptor (EGFR) signalling cascades. IR has been shown to induce autophosphorylation of EGFR intracellular domains resulting in the activation of the PI3K/AKT signalling cascade. Hyperactivation of PI3K/AKT signalling results in enhanced proliferative activity and inhibition of apoptosis [150, 151]. Based on these features, EGFR overexpression is associated with poor prognosis, especially in glioblastoma and head & neck cancer patients [152, 153]. Another key regulator of intrinsic radioresistance is the tumor suppressor p53 that is strongly involved in the DNA damage response induced by IR [154].

1.4.2.1 Cell cycle control and DNA damage

IR leads to the formation of DNA DSBs as previously described. The irradiated cells continue to grow until they arrive at the next cell cycle checkpoint, where different mechanisms assess whether the cell is fit for division or whether the DNA is damaged and needs to be repaired. The

cells pass the checkpoint in case of successful DNA repair. If the induced damage cannot be repaired, the cell will undergo apoptosis. If a cancer cell evades the apoptotic process it will likely continue to proliferate and eventually develop new mutations [155]. Mammalian cells have two cell cycle checkpoints that are involved in DNA damage repair induction. The G1/S checkpoint is regulated by Cdk4/6 kinases and Cyclin D in a p53-dependent manner and commonly defective in cancer cells due to mutations in p53 or Cyclin D [156]. On the other hand, the G2/M checkpoint is primarily regulated via p53-independent mechanisms [157, 158]. Consequently, abrogation of the G2/M checkpoint sensitizes cancer cells to radiotherapy [159].
The key regulators of the DNA damage repair response are ataxia telangiectasia and Rad3-related protein (ATR) and ataxia telangiectasia mutated (ATM). In presence of DNA DSBs ATR and ATM are activated and in turn phosphorylate downstream targets including Chk1/Chk2, BRCA1 and p53, which eventually leads to cell cycle arrest [160]. During cell cycle arrest, IR-induced DNA DSBs can be repaired by two independent repair pathways termed homologous recombination (HR) and nonhomologous endjoining (NHEJ). In HR, the correct sequence is derived from an intact DNA strand, whereas in NHEJ damaged bases are digested, repolymerized and ligated [155]. Repair of DNA DSBs by HR is more precise than by NHEJ but limited to the S and G2 phases of the cell cycle [161].

1.4.2.2 TME-driven radioresistance

Historically, radiation biologists have primarily paid attention to intrinsic radioresistance. Basic research and clinical evidence over the past century yet revealed that radioresistance driven by the tumor microenvironment also negatively influences the outcome of radiotherapy.
It was shown that upon irradiation CAFs release TGF-β, which mediates ECM remodelling in irradiated tissues and results in tumor progression, fibrosis and metastases [162, 163]. Furthermore, it leads to the activation of DNA damage-associated factors including p53 and to enhanced expression of p21, which triggers cell cycle arrest [164, 165]. Bone marrow derived cells (BMDCs) mainly consisting of tumor-associated macrophages (TAMs), mononuclear cells and myeloid derived immune suppressive cells are recruited to the TME following irradiation. They are involved in the restoration of the IR-induced vascular damage through vasculogenesis and thereby drive tumor regrowth and metastatic spread [166, 167]. Cancer stem cells (CSCs) are another factor contributing to radioresistance. Owing to their enhanced DNA-repair capacity, self-renewal potential and defense mechanisms against reactive oxygen species (ROS), they are intrinsically more resistant to IR. By resisting IR-induced cell death, CSCs further contribute to adaptive radioresistance via their selective repopulation [168].
Tumor hypoxia is one of the major limiting factors for successful radiotherapy. X-ray mediated ionization results in the formation of radicals within the DNA structure (DNA·). In the presence of molecular oxygen DNA radicals can be irreversibly fixed with ROS, including hydroxyl (HO·), peroxyl (ROO·) and superoxide ($O^{\cdot -}_2$) radicals [169]. ROS-mediated radical fixation is followed by DNA DSBs and cell death. Under hypoxic conditions, ROS are not sufficiently aberrant to fix IR-induced DNA radicals and are outperformed by thiol-containing compounds that reduce the DNA-radical to its native form. Consequently, IR-induced DNA damage and cell death are reduced in hypoxic regions of the tumor. This phenomenon was termed "Sauerstoffeffekt" and it can be roughly estimated that hypoxic cells are up to three times more radioresistant than their normoxic counterparts [170]. Numerous clinical trials have demonstrated that patients with a lower hypoxic tumor fraction have an improved overall survival after radiotherapy [95, 171].
Besides the physicochemical aspects for hypoxia-mediated radioresistance described above, the concurrent activation of HIF-signalling also gives rise to radioresistance on a more biological level. For example, HIF-1 signalling leads to the activation of MDM2, which negatively regulates p53

and thereby renders hypoxic cells resistant to apoptosis and promotes cell survival after radiotherapy [172]. Moreover, HIF-1 can negatively affect the radiosensitivity of tumors by altering their cellular metabolism. In a process named the Warburg effect, cancer cells switch their energy metabolism in favour of aerobic glycolysis over oxidative phosphorylation. It was shown that the Warburg effect negatively influences the outcome of radiotherapy by enhancing the DNA damage repair of cancer cells [173, 174].

The vicious cycle of hypoxia and angiogenesis is further promoted by radiotherapy. Endothelial cells within the TME are relatively radiosensitive due to their rapid proliferation rates [175]. Especially high dose fractions of IR have been shown to induce endothelial cell apoptosis, resulting in post-radiation hypoxia that in turn may lead to metastatic spread [176].

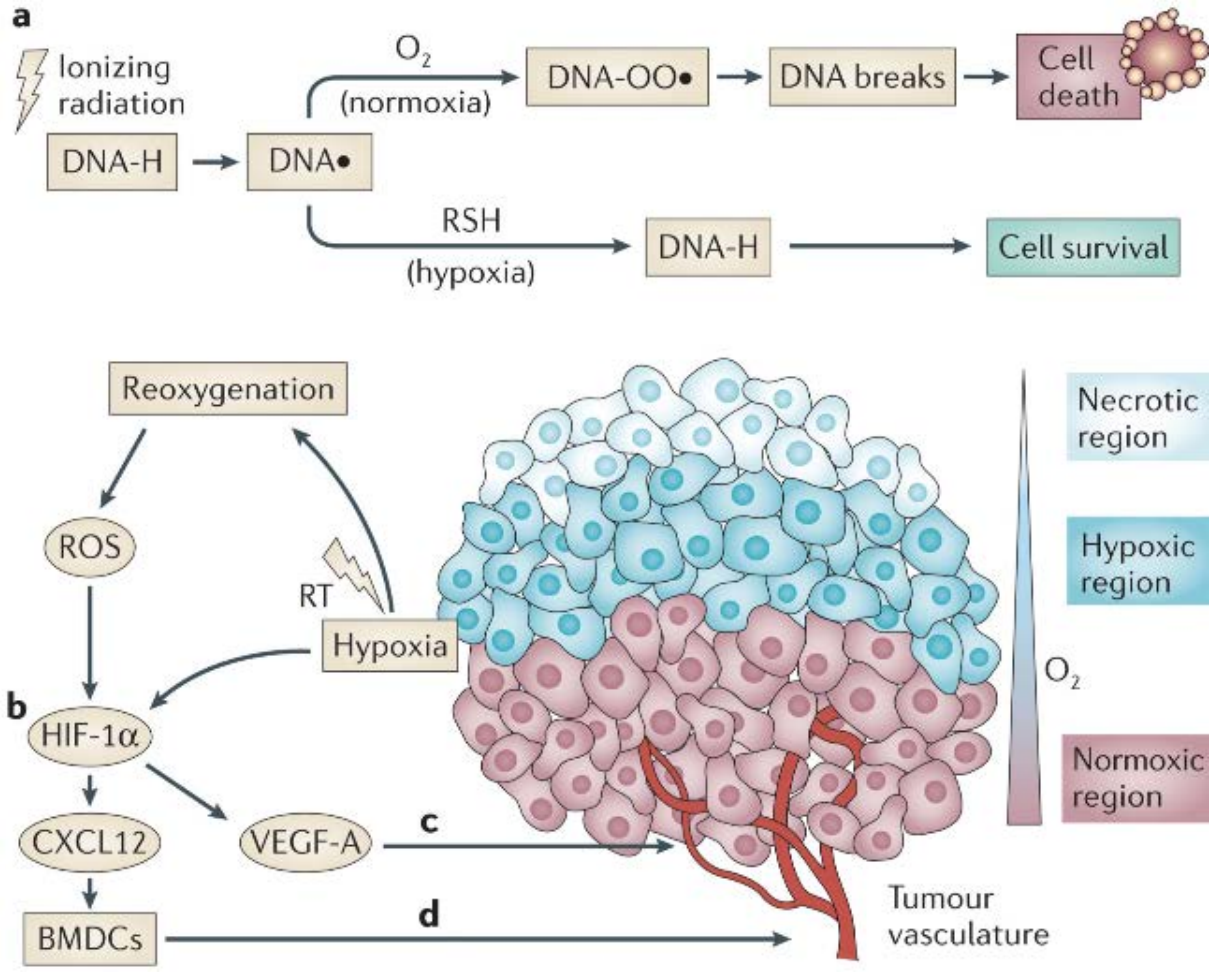

Figure 6 a) Ionizing radiation produces DNA radicals that can be fixed by molecular oxygen, thereby generating irreversible DNA double strand breaks followed by cell death. Under hypoxic conditions, glutathione-like molecules reduce DNA radicals to its native form, thus preventing cell death. **b)** In response to low intracellular oxygen concentrations, cancer cells release HIF-1α. At the same time, RT-mediated tumor reoxygenation leads to increased ROS levels further stabilizing HIF-1α, which induces the expression of target genes inclusing VEGF and CXCL12. **c & d)** Increased influx of BMDCs together with VEGF aid tumor recurrence after radiotherapy [176].

1.5 Combined treatment modalities to overcome radioresistance

A multitude of intrinsic and adaptive factors contributes to the radioresistance of cancer cells. Targeted therapies to overcome some of these restrictive factors have been developed over the past decades. Current clinical radiotherapy protocols typically involve at least one additional treatment regimen to improve the success of radiotherapy. Based on their mode of action, combined treatment agents are either administered before (neoadjuvant), during (concomitant) or after (adjuvant) radiotherapy. In the following paragraphs, some of the most relevant combination treatment strategies to overcome radioresistance will be discussed.

1.5.1 Targeting intracellular signalling pathways

Attempts to target increased EGFR expression and the corresponding activation of the PI3K/AKT pathway have led to the evaluation and implementation of different pharmaceutical agents. The most important development was the EGFR-targeting antibody Cetuximab, which in combination with radiotherapy was used for the treatment of HNSCC where it successfully improved patient overall survival [177, 178]. However, clinical evidence showed that cancer cells became resistant to EGFR inhibitors due to activation of the MET pathway as a compensatory mechanisms [179]. To overcome EGFR-blockade resistance, drugs targeting the downstream PI3K/AKT pathway are being investigated and show preliminary anti-tumor activity and acceptable safety profiles in early clinical trials [180].

1.5.2 Targeting DNA damage and cell cycle control pathways

Another strategy to improve the efficacy of radiotherapy is to target proteins involved in the DNA damage response. One example is the poly (ADP-ribose) polymerase (PARP) inhibitor olaparib, which is used for the treatment of tumors with mutations in BRCA1 or BRCA2 and corresponding defects in HRR [181]. On the preclinical level, PARP inhibition in combination with radiotherapy was shown to increase the incidence of collapsed replication forks resulting in persistent DNA DSBs [182]. Olaparib is approved as single treatment for BRCA-mutated breast and ovarian cancer but latest preclinical results and hypotheses are pointing towards a radiosensitizing effect, especially in combination with proton radiotherapy [183, 184].
Microtubule-stabilizing agents (MSA) induce cells to arrest at the G2/M checkpoint, which was identified as the most radiosensitive phase of the cell cycle [185]. Combined treatment of IR and MSAs is therefore a promising approach to overcome radioresistance. Our preclinical research with novel MSAs has led to clinical trials that investigate the combined effect of IR and MSAs [186].

1.5.3 Targeting the tumor vasculature

VEGF overexpression in solid tumors drives the vicious cycle of angiogenesis and hypoxia, resulting in decreased radiosensitivity of the cancer cells. Phase III clinical trials investigating the combined treatment of radiotherapy and bevacizumab in glioblastoma patients failed to improve overall survival. However, there was a modest increase in progression-free survival and quality of life [187]. Early clinical trials with the newer-generation VEGF inhibitors sorafenib and sunitinib also failed to show increased overall survival and were accompanied with severe toxicity [188, 189]. Based on these findings and current understanding it can be concluded that the tumor vasculature is not an attractive target to increase the efficacy of radiotherapy.

1.5.4 Targeting immune cells

Immune checkpoint inhibitors have recently shown promising results in improving the overall survival of melanoma and lung cancer patients [120-122]. Since radiotherapy increases antigen

presentation and immune cell infiltration in the tumor it is believed to be a potent sensitizer for immune checkpoint therapy. First clinical trials showed only modest improvements in overall patient survival after combined radioimmunotherapy with ipilimumab in prostate cancer [190]. Numerous clinical trials with distinct immune checkpoint inhibitors for various indications are currently ongoing [191, 192]. Immune checkpoint blockade is presently the most extensively studied combination approach in the field of radiotherapy.

1.5.5 Targeting tumor hypoxia

The key aim of my doctoral thesis has been to target tumor hypoxia in order to overcome radioresistance. Tumor hypoxia is an interesting target for radiosensitization, since all solid tumors irrespective of their site and genetic background develop hypoxic tumor regions. Hypoxia can be modulated on the biological level by targeting deregulated signalling molecules, such as HIF-1α and CAIX, or on the physiological level by specifically targeting or reoxygenating hypoxic cancer cells.

The development of HIF-inhibitors interfering with HIF mRNA expression, protein synthesis, protein degradation, DNA binding or transcriptional activity were approved for treating cancer patients. Promising compounds like acriflavine or YC-1 failed to show therapeutic efficacy or were associated with treatment-induced toxicity [193].

Oxygen mimetic drugs belonging to the group of nitroimidazoles were investigated extensively. Clinical trials combining misonidazole with radiotherapy did not improve the outcome. Moreover, a substantial amount of patients developed peripheral neuropathy upon misonidazole treatment [194]. Although the next generation therapeutic nimorazole had fewer side effects, it only showed modest benefits in efficacy [195].

Hypoxia-activated prodrugs (HAPs) are compounds that get bioreductively activated in areas of low oxygen concentrations where they subsequently exert cytotoxic functions by DNA alkylation. Tirapazamine and evofosfamide as shown by our own laboratory and several others demonstrated a promising radiosensitizing potential in preclinical tumor animal models [196, 197]. A phase I clinical trial investigating the combined treatment modality of radiotherapy and evofosfamide was discontinued, since evofosfamide alone failed to improve overall patient survival in phase II & III clinical trials [198-200].

An alternative to radiosensitization is to reoxygenate the hypoxic tumor fraction prior to irradiation. Since compounds that directly increase tumor oxygenation are rare, there have been attempts to indirectly increase the oxygen concentration within the tumor with the use of erythropoietin (EPO), a cytokine that is endogenously secreted by the kidneys in response to hypoxia. Clinical administration of recombinant EPO failed to improve the outcome of radiotherapy and the possibility of a detrimental effect could not be excluded [201]. ARCON treatment combines accelerated radiotherapy (multiple IR fractions per day) with inhalation of carbogen (98% O_2 + 2% CO_2) and the vasodilator nicotinamide to decrease tumor hypoxia. ARCON treatment in patients with laryngeal cancer improved the regional control in comparison to accelerated radiotherapy alone, but failed to significantly improve local control and overall survival [202].

As part of my doctoral thesis, we investigate the novel tumor reoxygenting agent myo-inositol trispyrophosphate (ITPP). It is actively taken up by red blood cells whereupon it triggers a decrease of the oxygen/hemoglobin binding affinity, resulting in enhanced oxygen release and reoxygenation of hypoxic tissues [203, 204]. Besides this rapidly induced physicochemical effect, ITPP further normalizes tumor hypoxia by downregulating pro-angiogenic factors like HIF-1α and VEGF leading to a long lasting normalization of the TME [41].

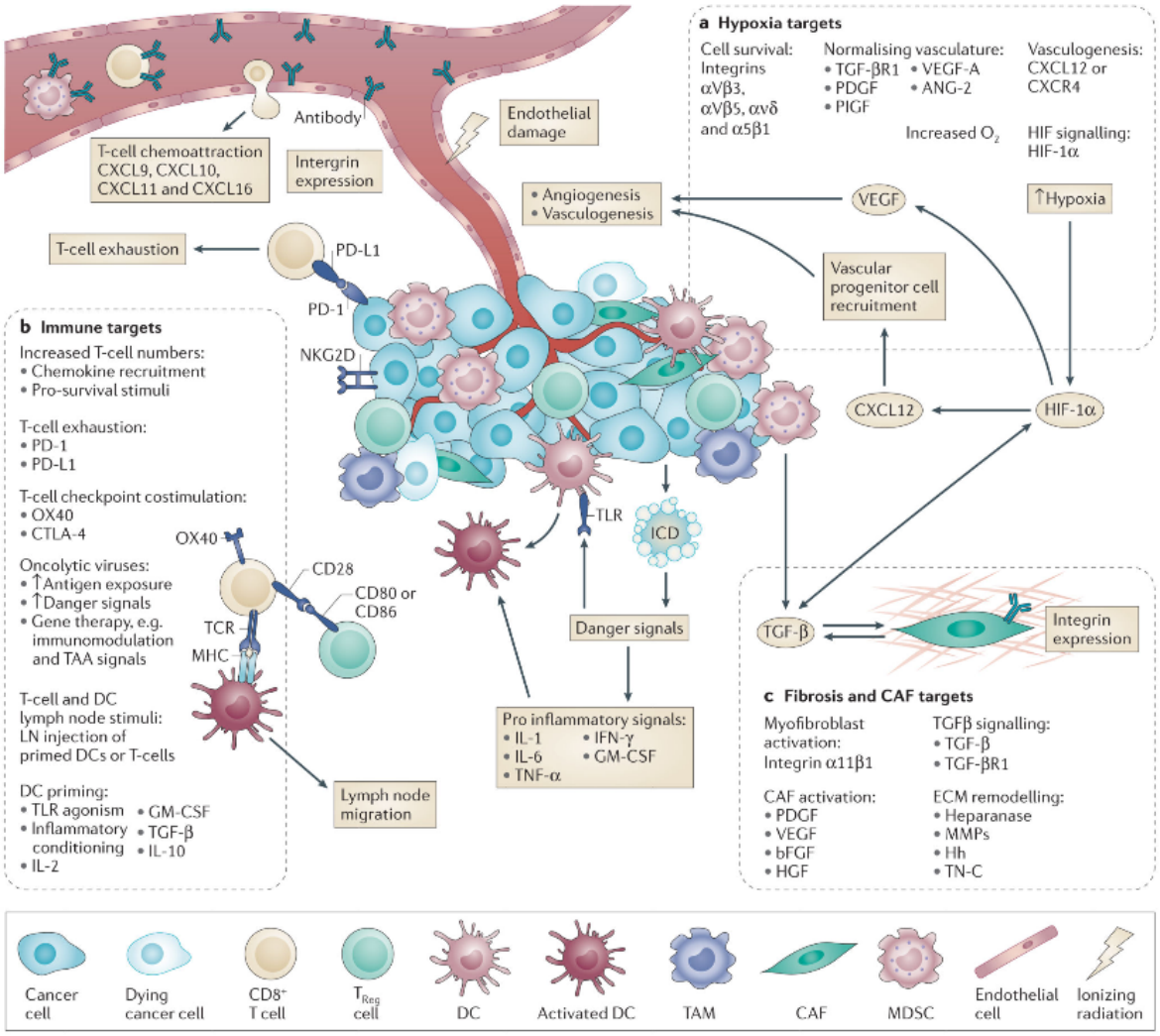

Figure 7 Radioresistance can be reduced by targeting different compartments of the TME. **a)** Targeting of tumor hypoxia and vasculature aims to increase the oxygen delivery to cancer cells before or during irradiation. **b)** Increased immune-cell infiltration and tumor antigen presentation after radiotherapy can be achieved by targeting immune cells. **c)** Targeting of fibrosis aids in preventing ECM remodeling or TGF-β singalling associated with radioresistance and recurrence [176].

2. Aims of the study

Tumor hypoxia is associated with resistance to radiotherapy, an increased risk of tumor dissemination and poor clinical prognosis. Reactive oxygen species induced by ionizing radiation generate irreversible DNA double-strand breaks followed by chromosomal aberrations and cell death. This radiation-induced cytotoxic effect is less abundant under hypoxia and thus hypoxic cells are more resistant to radiotherapy.
In this PhD project, we aim to modulate tumor hypoxia with pharmaceutical agents as part of combined treatment modalities with hypofractionated radiotherapy. The rationale is to develop novel combination therapies that aid to overcome hypoxia-mediated radioresistance of solid tumors. The ultimate goal is to apply the gained knowledge into treatment protocols for cancer patients undergoing radiotherapy. Our specific aims are:

1. We investigate the combined treatment of the hypoxia-activated prodrug evofosfamide and radiotherapy *in vitro*. To reveal the underlying mechanism of differential response to evofosfamide treatment in different cell lines, proliferative activity, clonogenic cell survival and pattern of DNA damage upon combined treatment are examined. Furthermore, the involvement of drug-metabolizing enzymes for prodrug activation is studied across responding and non-responding cell lines.
2. In the second project, we investigate the potential of the anti-hypoxia compound myo-inositol trispyrophosphate (ITPP) to overcome radioresistance. The radiosensitizing effect is tested by tumor growth delay studies *in vivo,* using different tumor entities with varying tumor hypoxic fractions. The contribution of the immune system is determined by performing experiments in both, immunodeficient and immunocompetent mice. Additional functional endpoints including differential progression of the TME upon combined treatment are investigated by exhaustive immunohistochemical stainings. Kinetics of tumor reoxygenation by non-invasive hypoxia-imaging and characterization of treatment-induced DNA damage complete the extensive exploration.
   Finally, an orthotopic colorectal liver metastases model was developed and investigated to study multimodal treatments in a tumor model that is representing clinical radiotherapy in a more concise manner.

3. Results

3.1 The hypoxia-activated prodrug evofosfamide in combination with multiple regimens of radiotherapy

Nytko KJ[1,2], Grgic I[1,2], Bender S[1], Ott J[1], Guckenberger M[3], Riesterer O[2,3], Pruschy M[1,2]

[1]Laboratory for Applied Radiobiology, Department of Radiation Oncology, University Hospital Zurich, Zurich, Switzerland

[2]Clinical Research Priority Program "Tumor Oxygenation", Zurich, Switzerland

[3]Department of Radiation Oncology, University Hospital Zurich, Zurich, Switzerland

Status of the manuscript: Published in Oncotarget 2017

Author contribution I. Grgic:

- *In vitro* characterization of proliferative activity and clonogenic cell survival (Fig. 4)
- Characterization of treatment-induced DNA damage (Fig. 5a)
- Differential sensitivity towards evofosfamide across different cell lines (Suppl. Fig. 2)
- Impact of POR on cellular sensitivity towards evofosfamide (Suppl. Fig. 3)
- Data acquisition, data analysis and interpretation, proofreading and major revisions of the manuscript

www.impactjournals.com/oncotarget/ Oncotarget, 2017, Vol. 8, (No. 14), pp: 23702-23712

Research Paper

The hypoxia-activated prodrug evofosfamide in combination with multiple regimens of radiotherapy

Katarzyna J. Nytko[1,2], Ivo Grgic[1,2], Sabine Bender[1], Janosch Ott[1], Matthias Guckenberger[3], Oliver Riesterer[2,3], Martin Pruschy[1,2]

[1]Laboratory for Applied Radiobiology, Department of Radiation Oncology, University Hospital Zurich, Zurich, Switzerland

[2]Clinical Research Priority Program "Tumor Oxygenation", Zurich, Switzerland

[3]Department of Radiation Oncology, University Hospital Zurich, Zurich, Switzerland

Correspondence to: *Martin Pruschy,* ***email:*** *martin.pruschy@usz.ch*

Keywords: *evofosfamide, TH-302, hypoxia-activated prodrug, ionizing radiation, P450 oxidoreductase*

Received: *June 29, 2016* ***Accepted:*** *February 06, 2017* ***Published:*** *February 28, 2017*

ABSTRACT

The promising treatment combination of ionizing radiation (IR) with a hypoxia-activated prodrug (HAP) is based on biological cooperation. Here we investigated the hypoxia-activated prodrug evofosfamide in combination with different treatment regimens of IR against lung A549- and head&neck UT-SCC-14-derived tumor xenografts. DNA damage-related endpoints and clonogenic cell survival of A549 and UT-SCC-14 carcinoma cells were probed under normoxia and hypoxia.

Evofosfamide (TH-302) induced DNA-damage and a dose-dependent antiproliferative response in A549 cells on cellular pretreatment under hypoxia, and supra-additively reduced clonogenic survival in combination with IR. Concomitant treatment of A549-derived tumor xenografts with evofosfamide and fractionated irradiation induced the strongest treatment response in comparison to the corresponding neoadjuvant and adjuvant regimens. Adjuvant evofosfamide was more potent than concomitant and neoadjuvant evofosfamide when combined with a single high dose of IR. Hypoxic UT-SCC-14 cells and tumor xenografts thereof were resistant to evofosfamide alone and in combination with IR, most probably due to reduced P450 oxidoreductase expression, which might act as major predictive determinant of sensitivity to HAPs.

In conclusion, evofosfamide with IR is a potent combined treatment modality against hypoxic tumors. However, the efficacy and the therapeutic outcome of this combined treatment modality is, as indicated here in preclinical tumor models, dependent on scheduling parameters and tumor type, which is most probably related to the status of respective HAP-activating oxidoreductases. Further biomarker development is necessary for the launch of successful clinical trials.

INTRODUCTION

Radiotherapy, along with surgery and chemotherapy is one of the major treatment options for solid tumors. However, solid tumors are often radiation resistant due to tumor hypoxia, which thereby represents a major clinical challenge. Several strategies have been developped during the last decades to overcome the hurdle of tumor hypoxia for successful radiotherapy [1–4]. One of these concepts is based on biological cooperation, which refers to strategies that target distinct cell populations, or employ different mechanisms for cell killing. The combination of ionizing radiation (IR) with a Hypoxia-Activated Prodrug (HAP), targeting hypoxic tumor cells and thereby complementing the effect of IR in well-oxygenated cells, nicely represents the concept of biological cooperation [5]. Originally, nitrobenzenes, followed by the nitroimidazoles (misonidazole, etanidazole, pimonidazole) [6], were proposed to act as oxygen mimetic agents and to generate together with short-lived IR-induced free DNA radicals cytotoxic DNA strand breaks [7, 8]. Unfortunately, and despite the clarity of the concept, severe toxicities of these

early generation compounds have contributed that these hypoxic radiosensitizers did not find their recognition in the clinical routine. Nevertheless these findings paved the way for the generation of hypoxia-selective bioreductive prodrugs, which are activated by enzymatic reduction in hypoxic tissues [9].

This risk of severe side-effects is reduced with HAPs that are less toxic and especially with compounds that are only activated under severe hypoxia. At the same time such prodrugs should release a diffusible, active cytotoxic agent, not only to kill the most hypoxic tumor cells, but also to induce a bystander effect thereby killing tumor cells of intermediate levels of tumor hypoxia. The 2-nitroimidazole-conjugated bromo-isophosphoramide mustard (Br-IPM) evofosfamide (TH-302) represents a prototype of such a novel generation HAP. Evofosfamide is currently the most advanced compound in clinical trials of the new generation of bioreductive cytotoxins [10–12].

The development of linear accelerator technology for the precise delivery of radiotherapy has nowadays reached a level of dose conformity to the tumor that allows the application of high dose fractions (even > 10 Gy) to small tumors with very steep dose gradients. Fractionated application of daily doses of IR exploits reoxygenation of hypoxic tumor regions in between fractions and thereby overcomes the hypoxic challenge as part of an iterative process. On the other hand single high doses of IR or a hypofractionated treatment regimen requires other means to improve its efficacy and to control a hypoxic tumor e.g. by the combined treatment modality with a HAP [13, 14].

Here we investigated the potency of evofosfamide in combination with fractionated and single high-dose of IR and tested these regimens in three settings (neoadjuvant, concomitant and adjuvant) routinely applied in clinical practice. Furthermore, the influence of treatment conditions linked to the individual geno- and phenotype of the tumor, including the status of the HAP-activating oxidoreductases, DNA-damage repair machineries and the hypoxic burden, was analyzed.

RESULTS

Evofosfamide in combination with IR *in vivo*

The combined treatment modality of IR with an HAP is based on biological cooperation. However, the most effective scheduling of the two modalities is not predictable. We therefore probed three different treatment schedules (neoadjuvant, concomitant and adjuvant) of a minimally fractionated irradiation regimen (3x2 Gy on 3 consecutive days) and evofosfamide (50 mg/kg, Q3Dx5) in a lung adenocarcinoma (A549) and a head&neck squamous cell carcinoma (UT-SCC-14) tumor xenograft model. The dosage and schedule of evofosfamide was defined based on previous preclinical reports when used as part of a combined treatment modality [15] and closely mimic the settings used in clinical practice. 2 Gy per fraction of IR corresponds to the dose/fraction used as part of a clinical fractionated radiotherapy treatment regimen. Both tumor models were previously characterized to develop tumors with an intermediate hypoxic tumor fraction [16, 17]. Tumor hypoxia was also confirmed by pimonidazole staining (Supplementary Figure 1). Treatment was initiated when tumors reached a volume of 300 mm^3 (+/- 10%). Treatment of A549-derived tumor xenografts with evofosfamide in combination with fractionated irradiation resulted in a strongly enhanced treatment response when compared to treatment with evofosfamide and irradiation alone (Figure 1A). The concomitant schedule induced the strongest tumor growth delay ($P<0.05$ for evofosfamide plus IR versus each monotherapy), however, no statistically significant differences in between the three combined treatment regimens could be determined. Interestingly, evofosfamide alone did not reduce tumor growth of HNSCC UT-SCC-14 xenografts and did not enhance the growth inhibitory effect of fractionated irradiation as part of a combined treatment modality (Figure 1B). These results suggest that the response to evofosfamide and IR is highly dependent on the tumor type.

Due to the differential treatment response in the two tumor models *in vivo*, the effect of evofosfamide was also determined *in vitro* with defined hypoxic conditions (0.2% O_2). Interestingly, A549 cells were also more sensitive than UT-SCC-14 to increasing concentrations of evofosfamide (Supplementary Figure 2). The cytochrome P450 oxidoreductase (POR) has previously been identified as major determinant for the sensitivity of hypoxia-activated prodrugs [18, 19]. Therefore, the expression level of POR was determined on the cellular and tumor level by western blotting and immunohistochemistry, respectively. The POR expression level was strongly reduced in UT-SCC-14 cells and UT-SCC-14-derived tumors in comparison to A549 cells and tumors derived thereof (Figure 2A, 2B). This is most probably the cause for evofosfamide-resistance against the head&neck tumor model used in this study. Furthermore, transient downregulation of POR in A549 cells with POR-directed siRNA resulted in reduced sensitivity to evofosfamide in these cells relative to control siLUC-transfected A549 cells (Supplementary Figure 3), reinforcing the role of POR for evofosfamide sensitivity. Despite several attempts, we could not perform the opposite experimental approach to overexpress POR in UTSCC-14 cells. These cells did always undergo cell death upon genetic manipulation alone.

To further analyze the differential treatment response in between A549 and UT-SCC-14-derived tumors, comprehensive analysis of hypoxia-related secreted factors was performed by Bio-plex analysis. Unfortunately, the levels of serum secreted factors in mice carrying tumor xenografts were below detection limits. Therefore, *in vitro* analysis of conditioned media

derived from A549 and UT-SCC-14 cells was performed. The basal secretory levels of most factors analyzed were different in between the two cell lines (e.g. VEGF, IL-6, Osteopontin, sEGFR, TNFα) and did not change in response to evofosfamide treatment (Supplementary Figure 4). Interestingly, placental growth factor (PlGF) was strongly increased in A549 but not in UT-SCC-14 cells in response to evofosfamide, suggesting that an increase of PlGF might be used as an early response biomarker (Figure 2C).

Next, the potency of evofosfamide was investigated in the evofosfamide-sensitive A549-derived tumor model as part of a combined treatment modality (neoadjuvant, concomitant, adjuvant) with a single high dose of IR (10 Gy). The adjuvant combined treatment modality was most effective and induced a strong tumor growth delay in comparison to evofosfamide and IR alone ($P<0.05$ for evofosfamide plus IR versus each monotherapy). Concomitant treatment with IR and evofosfamide only induced a partial additive tumor growth delay. On the other hand tumors almost doubled in size during the time period of neoadjuvant treatment with evofosfamide. Thereby tumors were irradiated at an increased tumor volume with a single high dose of IR, resulting in a reduced overall treatment response to the neoadjuvant combined treatment regimen (Figure 3A, 3B).

Enhanced radiosensitivity upon evofosfamide treatment *in vitro*

In vitro experiments with A549 cells demonstrated a dose- and hypoxia incubation time-dependent antiproliferative effect of evofosfamide (Figure 4A). To determine cancer cell clonogenicity, A549 cells were incubated with evofosfamide (0.5 μM) for 4 hours under hypoxia (0.2% O_2) and normoxia, respectively, followed by irradiation under reoxygenated conditions. Combined treatment of A549 cells with evofosfamide and increasing doses of IR resulted in a strong, supra-additive reduction of clonogenicity when cells were preincubated with

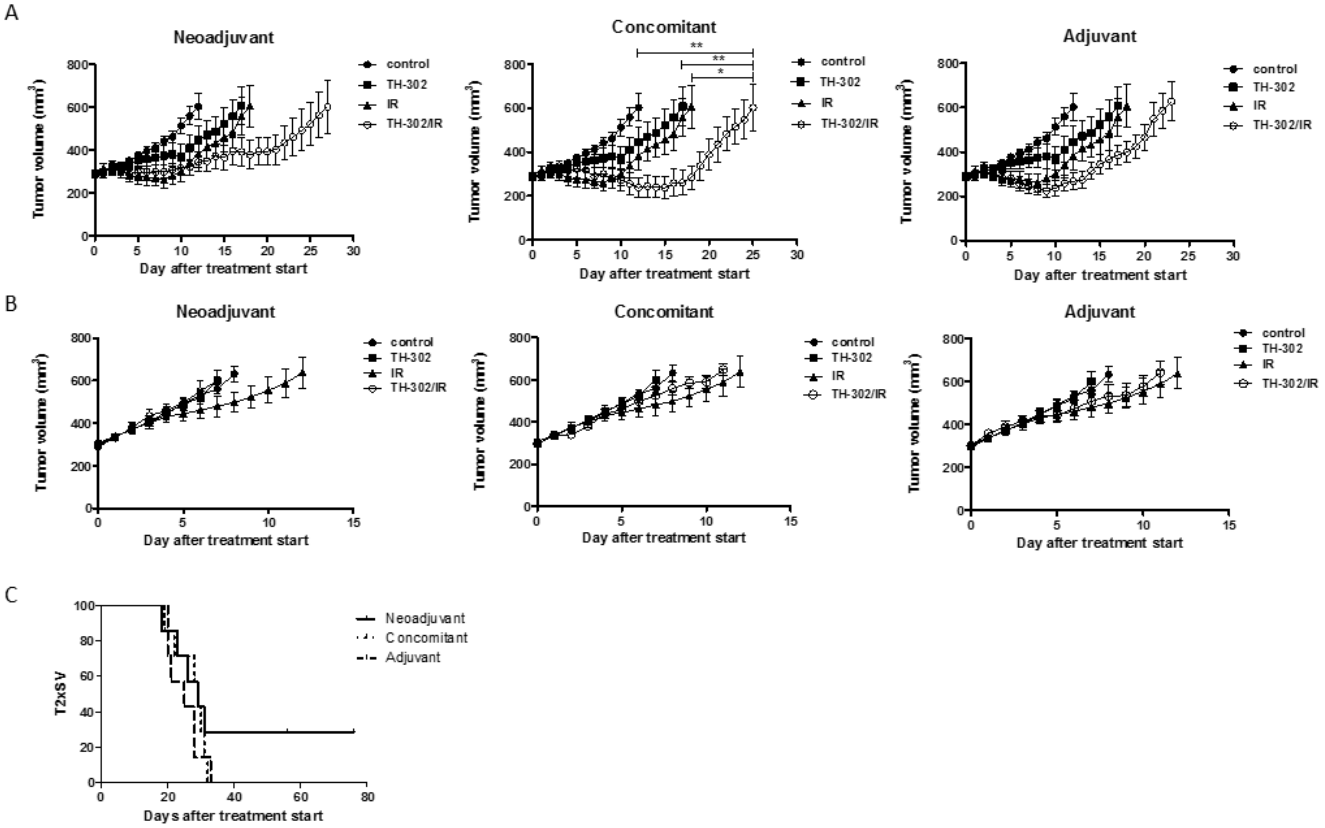

Figure 1: Treatment response to evofosfamide and fractionated irradiation *in vivo*. Tumor growth delay of A549-derived **(A)** and UT-SCC-14-derived **(B)** tumor xenografts in response to different treatment schedules of the combined treatment modality with evofosfamide (50 mg/kg, Q3Dx5) and fractionated irradiation (3x2 Gy). Control mice were treated i.p. with saline. Neoadjuvant (left panel), concomitant (middle panel), and adjuvant (right panel) regimens are shown. Neoadjuvant (left panel), with evofosfamide given on days 1-12 followed by fractionated irradiation; concomitant (middle panel), with evofosfamide given on days 1-12 and IR on days 5-7; adjuvant (right panel), IR given on days 0-2 (fractionated) followed by treatment with evofosfamide. 7-8 mice per treatment groups were used. Error bars represent SEM. **(C)** Kaplan-Meier curves for A549-derived tumors reaching 600mm³ tumor volume.

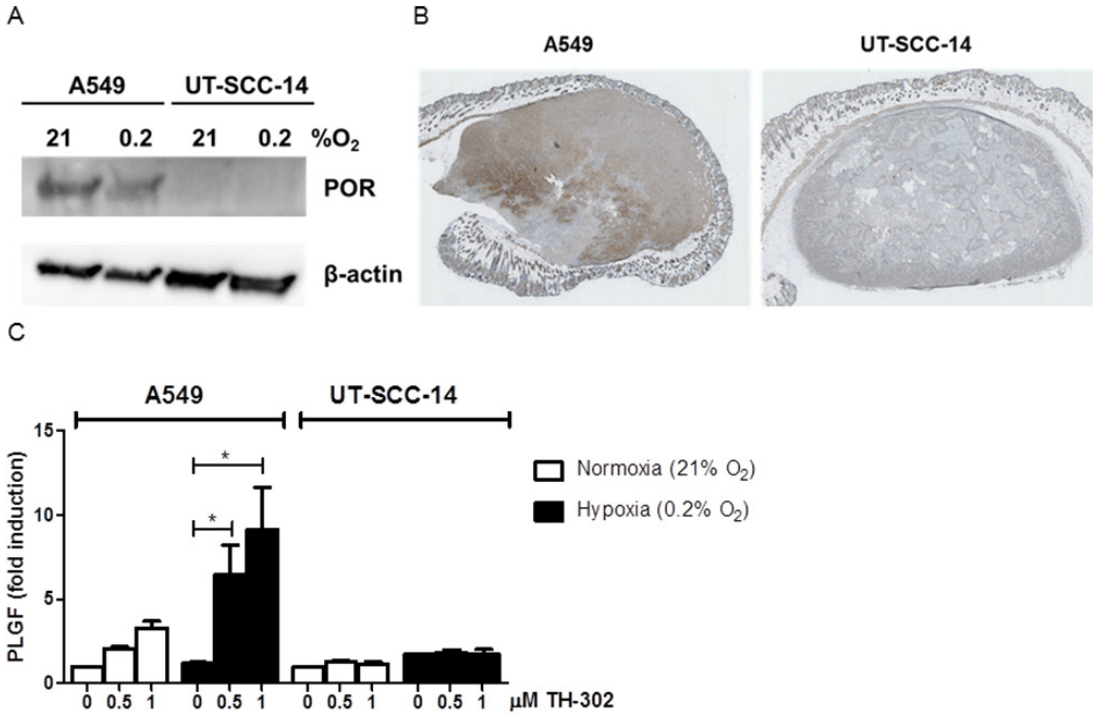

Figure 2: Differential POR- and PLGF-levels in A549 and UT-SCC-14 tumors. (A) Protein levels of cytochrome P450 oxidoreductase (POR) in A549 and UT-SCC-14 cells incubated under normoxia (21% O_2) and hypoxia (0.2% O_2, 24 hours) as determined by western blotting. **(B)** Staining of A549 (left) and UT-SCC-14 (right)-derived tumor xenografts sections with anti–POR antibodies. **(C)** Levels of secreted PLGF in A549 and UT-SCC-14 conditioned medium in normoxia (21% O_2) and hypoxia (0.2% O_2, 24 hours) as determined using Bio-plex assay. Data are shown as fold induction over non-treated normoxic samples in three independent experiments, error bars represent SEM.

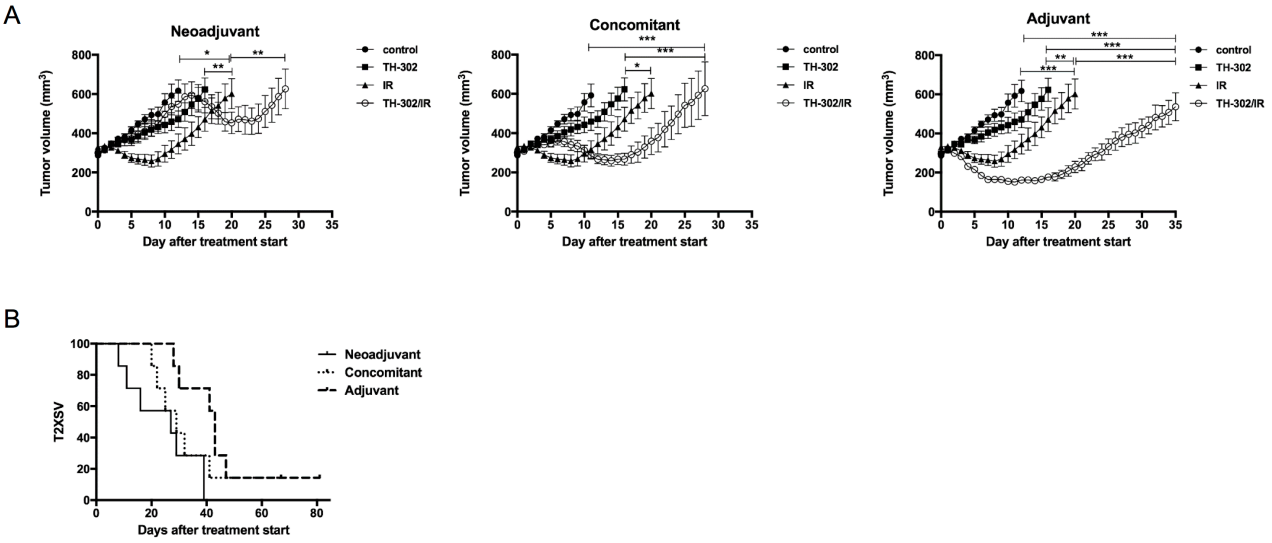

Figure 3: Treatment response to evofosfamide and single high-dose irradiation *in vivo*. Tumor growth delay of A549-derived xenografts in immunocompromised mice in response to combined treatment with evofosfamide (50 mg/kg, Q3Dx5) and single high-dose IR (1x10 Gy). Control mice were treated i.p. with saline. **(A)** Neoadjuvant (left panel), concomitant (middle panel), and adjuvant (right panel) regimens are shown. Neoadjuvant (left panel), with evofosfamide given on days 1-12 followed by irradiation; concomitant (middle panel), with evofosfamide given on days 1-12 and IR on day 6; adjuvant (right panel), IR given on day 0 followed by treatment with evofosfamide. 7-14 mice per treatment groups were used. Error bars represent SEM. **(B)** Kaplan-Meier curves for tumors reaching 600mm^3 tumor volume.

evofosfamide under hypoxic conditions in comparison to preincubation under normoxic conditions ($DEF_{0.1}$=1.44+/-0.07 vs $DEF_{0.1}$ of 1.16 +/- 0.07 respectively, and $DEF_{0.37}$=1.72+/-0.12 vs $DEF_{0.37}$=1.23+/-0.24, respectively) (Figure 4B).

The adjuvant schedule of evofosfamide in combination with IR resulted in a strong tumor growth delay *in vivo*. Therefore a reversed schedule with irradiation of cells (2 Gy) followed by incubation with evofosfamide (0.5 μM for 4 hours, 0.2% O_2) was also probed *in vitro*. Combined treatment also resulted in a statistically significant increase of cell killing in comparison to cellular treatment with evofosfamide and IR alone (Figure 4C).

Induction of DNA damage and senescence in response to evofosfamide

Activation of the prodrug evofosfamide results in the potent DNA-alkylating agent bromo isophosphoramide mustard and induces a strong DNA damage response. Residual DNA damage was determined by γH2AX foci

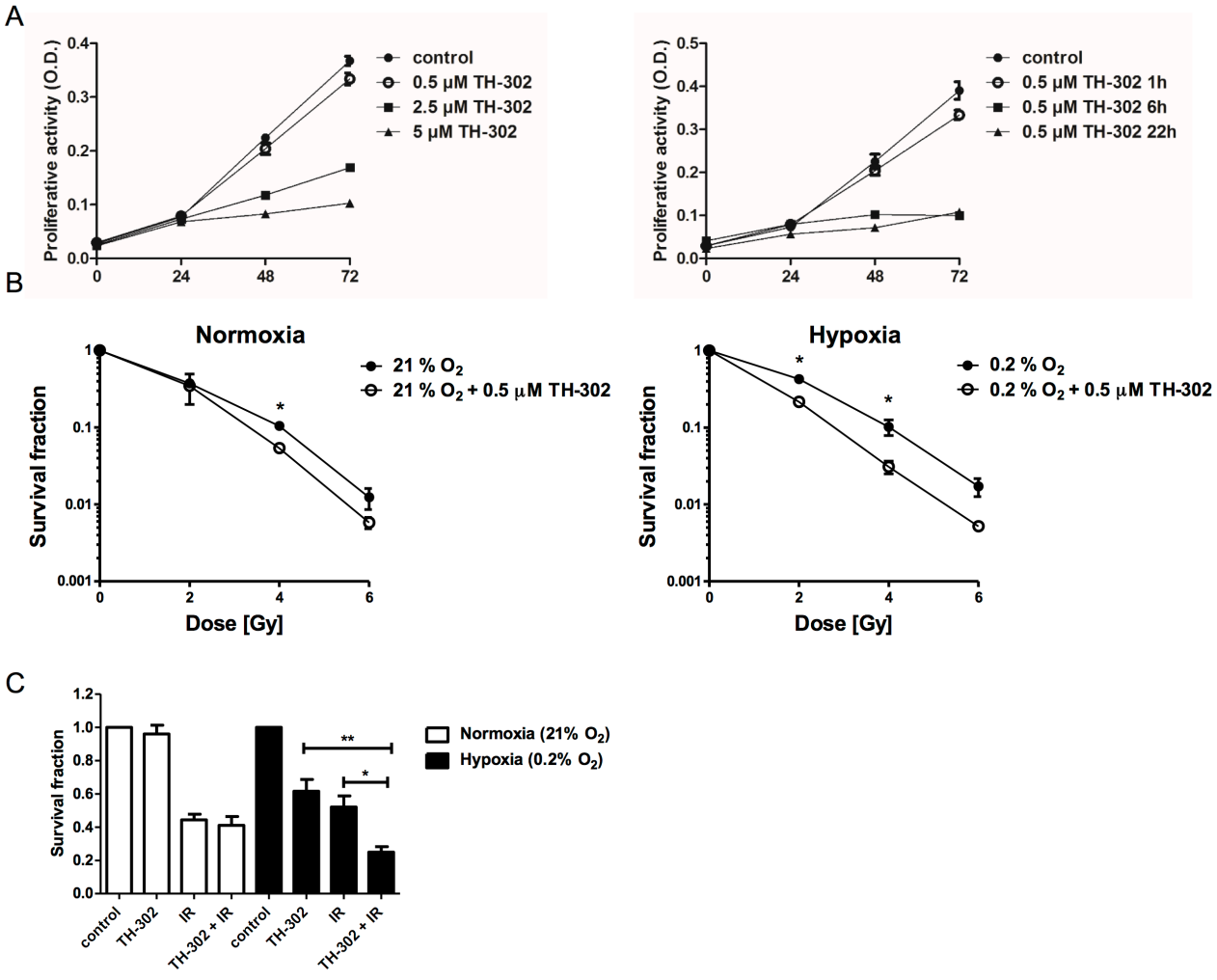

Figure 4: Treatment response to evofosfamide and irradiation *in vitro*. (A) Proliferation of A549 lung adenocarcinoma cells in response to increasing doses of evofosfamide. Cells were pre-incubated in hypoxia (0.2% O_2) for 23 hours, followed by treatment with increasing concentrations of evofosfamide under hypoxic conditions for 1 hour (left panel). Proliferation of A549 cells pre-incubated for 23, 18 and 2h in hypoxia (0.2% O_2), followed by treatment with evofosfamide (0.5 μM) under hypoxia for 1, 6 and 22 hours, respectively (right panel). The proliferative activity of reoxygenated cells was monitored over 72 hours. **(B)** To determine time-dependent effects of evofosfamide, cells were incubated for 23, 18 and 2h in hypoxia (0.2% O_2), followed by treatment with evofosfamide (0.5 μM) for 1, 6 and 22 hours, respectively. The proliferative activity of reoxygenated cells was monitored over 72 hours. **(B)** Clonogenic cell survival assay of A549 cells treated with 0.5 μM evofosfamide under normoxic (21% O_2) and hypoxic (0.2% O_2) conditions for 4 hours. Following reoxygenation, cells were irradiated with increasing doses of IR. **(C)** Clonogenic survival assay of lung carcinoma A549 cells irradiated with 2 Gy and treated thereafter with evofosfamide (0.5 μM) under normoxic (21% O_2) and hypoxic (0.2% O_2) conditions for 4 hours (adjuvant setting); Error bars represent SEM.

detection in A549 cells on treatment with evofosfamide and IR alone and in combination. As expected, a high level of residual DNA-damage was present at the 24 hour time point on initial cellular incubation with evofosfamide for 4 hours under hypoxic but not under normoxic condition. Interestingly, combined treatment with irradiation (2 Gy) only resulted in a minimal but statistically not significant additional increase of residual DNA damage (Figure 5A). Lack of additional residual γH2AX foci in cells treated with both modalities does not correspond with the supra-additive cell killing by the combined treatment modality *in vitro* (see above Figure 4B, 4C). Similar results were obtained when DNA damage was probed on the level of residual 53BP1-foci (Supplementary Figure 5).

Senescence is a well-known mode of cell death induced upon treatment with alkylating agents [20]. A high percentage of β-galactosidase positive A549 cells was induced on treatment with evofosfamide under hypoxic conditions, which was further increased on combined treatment with IR (Figure 5B). These results demonstrate that evofosfamide alone induces a strong DNA damage response and senescence in lung carcinoma cells. The small increase in the number of senescent cells in response to evofosfamide in combination with IR corresponds in part with decreased clonogenicity of A549 cells in response to this combined treatment modality.

Increased cell killing by evofosfamide in BRCA2-deficient ovarian carcinoma cells

Evofosfamide-induced DNA damage requires homologous recombination for efficient DNA repair as previously shown in non-tumorigenic chinese hamster ovary cells [19]. To further investigate evofosfamide in combination with IR in tumorigenic cell lines and with defined HR-deficiency, proliferative activity and clonogenicity was determined in the BRCA2-wildtype PEO4 and the otherwise genetically identical BRCA2-deficient ovarian carcinoma cell line PEO1 [21]. As expected, BRCA2-deficient PEO1 cells were more sensitive to increasing concentrations of evofosfamide in comparison to BRCA2-wildtype PEO4 cells under hypoxic conditions (Figure 6A). Moreover, combined treatment with IR reduced clonogenic cell survival in

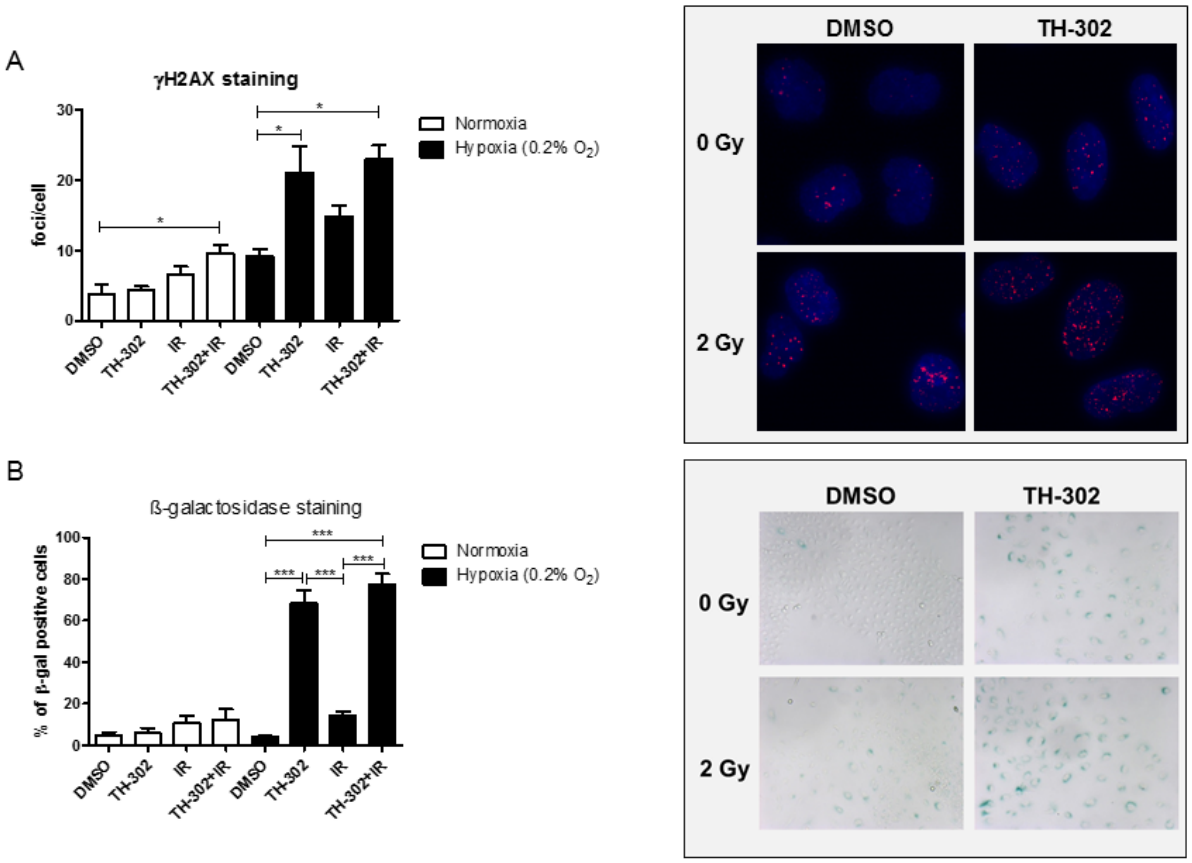

Figure 5: DNA damage in response to evofosfamide and irradiation. (A) Residual γH2AX foci were analyzed in A549 cells treated for 4 hours with evofosfamide and irradiation with 2 Gy. Cells were analyzed 20 hours after irradiation at a magnification of 40x. **(B)** Induction of senescence (β-galactosidase staining) in response to the combined treatment in A549 cells. Cells were analyzed 72 hours after treatment at a magnification of 10x. At least 50 cells/condition were analyzed. Representative pictures are shown. Error bars represent SEM.

PEO1 cells to a higher extent than in the BRCA2-wildtype counterpart cells (Figure 6B). The ratio of survival fractions in response to evofosfamide and evofosfamide in combination with IR was 25.5 and 17.9 for PEO1 and PEO4 cells, respectively. The ratio of survival fractions in response to IR and the combined treatment modality was 7.1 and 2.7 for PEO1 and PEO4, respectively. These results strongly indicate a superior appliance for this combined treatment modality in tumors with homologous recombination-deficiency.

DISCUSSION

Evofosfamide is one of the most promising hypoxia-targeting agents currently tested in several clinical trials. Here we have investigated the combined treatment modality of evofosfamide with IR in a lung and a head&neck carcinoma model with a specific focus on multiple treatment regimens and schedulings. IR is known to target primarily well-oxygenated cells, while hypoxic cells are radiation-resistant. Therefore, the combined treatment modality of IR with evofosfamide is based on the promising rationale named biological cooperativity [5]. Both tumor models stained positive and to similar extent for the hypoxia-marker pimonidazole, however head&neck tumor xenografts were completely resistant to evofosfamide alone and when combined with IR, independent of the treatment scheduling. Subsequent expression studies revealed strongly reduced cytochrome P450 oxidoreductase (POR) levels in this tumor model. On the other hand A549 cells and A549 -derived tumor xenografts stained POR-positive and were highly evofosfamide-sensitive *in vitro* and *in vivo*.

Recently the dual combined treatment modality of IR with evofosfamide was shown to enhance the effect of radiotherapy in a rhabdomyosarcoma R1 and in a H460-derived non-small-cell lung cancer tumor model and as part of a trimodality therapy in sarcoma models with the anti-VEGF receptor-directed antibody DC101 [15, 22]. In both studies only single high doses of IR were applied and scheduling of evofosfamide with IR was not investigated.

We here tested three different treatment regimens (neoadjuvant, concomitant, adjuvant) in combination with fractionated and single high-dose IR in the lung adenocarcinoma tumor model. A more potent neoadjuvant and concomitant versus adjuvant scheduling of the combined treatment modality of evofosfamide with fractionated IR was identified, which might coincide with evofosfamide initially targeting the major tumor hypoxic burden followed by fractionated irradiation including partial reoxygenation of the remaining hypoxic areas.

On the other hand the more potent adjuvant scheduling of evofosfamide in combination with a single high dose of IR could be due to an (transient) increase of tumor hypoxia in response to single high doses of IR [23, 24]. Interestingly own experiments performed independently of this study also demonstrated an increase of tumor hypoxia over time in response to a single high dose of IR in this tumor model (Supplementary Figure 6). Similar to former studies with evofosfamide we only considered tumor growth delay as an endpoint and the hypoxic situation might vary in between different tumors. As such these schedulings will have to be carefully translated to the clinical situation.

Several studies on the activation of HAPs previously demonstrated that cytochrome P450 oxidoreductase is indispensable for several HAPs [18, 19, 25]. However, its

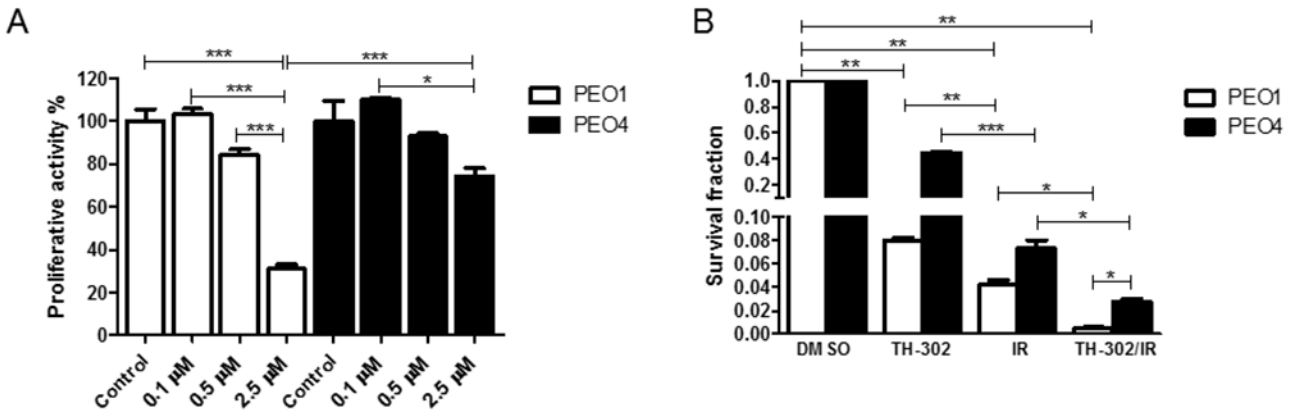

Figure 6: Treatment response of BRCA2-deficient (PEO1) and BRCA2-wild-type (PEO4) ovarian carcinoma cells to evofosfamide and irradiation. (A) Cells were pre-incubated in hypoxia (0.2% O_2) for 20 hours, followed by treatment with increasing concentrations of evofosfamide for 4 hours. The proliferative activity of reoxygenated cells was monitored over 72 hours. **(B)** Clonogenic cell survival assay of BRCA2 deficient (PEO1) and wild-type (PEO4) cells in response to evofosfamide (0.5 µM) and irradiation with 4 Gy. Cells were pre-incubated in hypoxia (0.2% O_2) for 20 hours, followed by evofosfamide treatment under hypoxic conditions (4 hours), reoxygenation and irradiation with 4 Gy. Error bars represent SEM.

relevance for the nitroimidazole mustard evofosfamide is less clear. Su et al. knocked-out POR in multiple tumor cell lines that resulted in resistance to several one-electron reductase substrates but not to evofosfamide, suggesting the existence of structure-dependent oxidoreductase redundancies [26]. On the other hand, Hunter et al. recently demonstrated reduced cytotoxicty of evofosfamide in head&neck carcinoma cells with shRNA-downregulated POR-expression [18]. More important, a heterogeneous POR expression status was retrospectively determined in head&neck squamous cell carcinoma patient samples, and suggests that POR might be a major predictive determinant for HAPs including evofosfamide [18]. Our own studies, which were performed on the cellular level and to our best knowledge for the first time also *in vivo*, strongly suggest that POR co-determines the potency of evofosfamide. As such we demonstrate minimal efficacy of evofosfamide *in vivo* in hypoxic tumor xenografts generated from a patient-derived head&neck carcinoma [27].

Only recently two phase III trials of evofosfamide in advanced soft-tissue sarcoma and in advanced pancreatic cancer in combination with doxorubicin and gemcitabine, respectively, did not meet their primary endpoints of improved overall survival (CancerNetwork Oncology, December 2015). Our *in vivo* data suggest the treatment combination of evofosfamide with radiotherapy is still of strong interest but requires detailed efficacy- and mechanistic-oriented studies towards a successful, personalized treatment approach. Our data demonstrate that both tumor hypoxia and the POR-status are strong co-determinant for the efficacy of evofosfamide. Thus, specific image- and gene expression-guided biomarker analysis to determine tumor hypoxia but also HAP-activation are required for optimized patient stratification. Serial analysis of serum factors specifically released in response to evofosfamide could represent a valid strategy to identify at an early stage evofosfamide-responsive tumors. We probed several angiogenesis- and hypoxia-related serum factors in response to evofosfamide. Interestingly only secretion of the placental growth factor (PlGF) was increased on treatment by evofosfamide under hypoxia and only by the evofosfamide-responsive and not by the evofosfamide-resistant carcinoma cells. Our *in vitro* data also corroborate that evofosfamide in combination with IR is more potent in BRCA2-deficient tumor cells than in their BRCA2-wildtype counterpart cells. Previous studies were only performed in genetically-defined CHO-cells and in combination with cisplatinum against tumor cells [18, 19].

Thus, it will be of highest interest to follow the results of the first clinical study by Larue and colleagues, testing evofosfamide with preoperative chemoradiotherapy in oesophageal adenocarcinoma patients [28]. This study includes repeated hypoxia PET imaging and blood sampling to determine hypoxia blood markers and could also incorporate testing of POR, PlGF and a putative homologous recombination-corrupted genetic background as part of their translational endpoints. Investigated dose levels of evofosfamide will range from 120 mg/m^2 to 340 mg/m^2 in this clinical study. However, it will be difficult to compare these dose levels with the drug concentrations applied in our animal study due to the differential route of drug administration and the differential drug metabolism between humans and mice. For comparative reasons we used similar concentrations of evofosfamide doses in our study as in the previous preclinical study by Peters et al. [15].

Overall our data demonstrate that evofosfamide with IR is a potent combined treatment modality against hypoxic tumors. Our preclinical data suggest that its efficacy on the clinical level could eventually be dependent on scheduling parameters and tumor type. Furthermore, several conditions linked to the individual geno- and phenotype of the tumor including the status of the HAP-activating oxidoreductases, DNA-damage repair machineries and the hypoxic burden have to be fulfilled, rendering this combined treatment modality highly potent towards a personalized treatment approach.

MATERIALS AND METHODS

Cell lines and compounds

The human non-small cell lung cancer (NSCLC) cell line A549 was obtained from ATCC and cultured in RPMI 1640 cell culture media supplemented with 10% FBS, glutamine (2 mM) and penicillin-streptomycin (100 U/ml-100 µg/ml). The head&neck squamous cell carcinoma (HNSCC) UT-SCC-14 cell line was a kind gift from Reidar Grénman (Turku University Hospital, Finland) and was maintained in DMEM, high glucose, NEAA, 10% FCS, 2 mM L-glutamine, 1% Penicillin/Streptomycin (100 U/ml-100 µg/ml) and 1 mM sodium pyruvate [27]. The ovarian cancer cells PEO4 and PEO1 were purchased from the Health Protection Agency Culture Collections (Salisbury, UK) and were kept in RPMI 1640 cell culture media supplemented with 10% FBS, glutamine (2 mM), sodium pyruvate (2 mM) and penicillin-streptomycin (100 U/ml-100 µg/ml). For normoxic conditions, cells were kept in a 5% CO_2 incubator at 37°C, for hypoxic conditions, cells were kept in a 0.2% O_2, 5% CO_2, incubator (*In vivo*$_2$ 300-Ruskinn; Hypoxia Incubator, Siemens) at 37°C. Evofosfamide was obtained from Merck KGaA.

Cell proliferation and clonogenic cell survival assay

The proliferative activities of tumor cells were assessed in 96-well plates with the colorimetric alamarBlue assay (Invitrogen). Cells were preincubated under hypoxia and treated for the indicated time intervals and concentrations of evofosfamide in either normoxic

(21% O_2) or hypoxic (0.2% O_2) conditions. Clonogenic cell survival was determined by the ability of single cells to form colonies *in vitro* as described before [29]. Cells were treated with 0.5 μM of evofosfamide for 4 hours in either normoxic (21% O_2) or hypoxic (0.2% O_2) conditions or as described in the figure legend. Thereafter cells were reoxygenated and irradiated with increased doses of IR and trypsinized. To probe the adjuvant scheduling, cells were first irradiated with 2 Gy, followed by addition of evofosfamide and incubation of cells in either normoxic or hypoxic conditions for 4 hours. Single cell suspensions were seeded into 10 cm-petri dishes. The number of plated cells per dish was adjusted to obtain approx. 50-100 colonies under all experimental conditions. After colony formation (depending on cell lines, approx. 14 days), colonies were fixed (methanol/acetic acid; 3:1) and stained with crystal violet (2%). Colonies (containing > 50 cells) were then counted manually.

Tumor xenografts and application of treatment regimes

A549 lung carcinoma and UT-SCC-14 head&neck squamous cell carcinoma cells were subcutaneously injected on the back of four week old, female CD1 athymic nude mice (Charles River). Tumor volumes were determined from caliper measurements of tumor length (L) and width (l) according to the formula (L x l^2)/2. Treatment was initiated when tumors reached a volume of 300 mm^3 +/- 10%. Tumors were sham-irradiated or irradiated using a customized shielding device with either a fractionated (3x2 Gy) or a single high dose regimen (1x10 Gy) using an Xstrahl 200 kV X-ray unit at 1 Gy/min. Evofosfamide (50 mg/kg in saline) or saline was administered i.p. Q3Dx5. Three treatment regimens were investigated: neoadjuvant, with evofosfamide on days 1-12 followed by either a fractionated or a high dose regimen; concomitant, with evofosfamide on days 1-12 and IR on days 5-7 (fractionated) or day 6 (high dose); adjuvant, IR on days 0-2 (fractionated) or day 0 (high dose) followed by treatment with evofosfamide. All *in vivo* experiments were performed according to the guidelines for the welfare and use of animals of the Veterinäramt Kanton Zürich, Switzerland.

Bio-plex multiplex assay

A549 lung carcinoma and UT-SCC-14 head&neck squamous cell carcinoma cells were seeded in 6-well plates at the density of 150-200'000 cells/well in DMEM medium (high glucose, NEAA, 10% FCS, 2 mM L-glutamine, 1% Penicillin/Streptomycin and 1 mM sodium pyruvate). Cells were irradiated with 5 Gy followed by addition of evofosfamide (0.5; 1 μM) and placed in either normoxic (21% O_2) or hypoxic conditions (0.2% O_2). After 24 hour incubation, conditioned medium was collected, filtered through an 0.45 μM filter and stored at -20° C until analysis. A customized Bio-plex Biomarker Cancer Panel assay was performed with undiluted conditioned medium samples according to the manufacturer protocol (Bio-Rad). Obtained concentrations of measured samples (pg/ml) were normalized to the cell number and are shown as fold induction relative to the determined concentrations derived from normoxic untreated control samples.

Western blotting and immunohistochemistry

For western blot analysis, A549 and UT-SCC-14 cells were incubated in either normoxic (21% O_2) or hypoxic conditions (0.2% O_2) for 24 hours, followed by lysis in RIPA buffer (Sigma) and SDS-PAGE. Membranes were incubated with primary anti-Cytochrome P450 Reductase (POR/CYPOR) antibodies (Santa Cruz Biotechnology (G-5): sc-25263; 1:100) and mouse monoclonal anti–β-actin antibody (Sigma Aldrich, #A5441, 1:1000), followed by secondary anti-mouse ECL IgG HRP-linked (GE Healthcare, NA931V, 1:2000). Immunohistological endpoints were analyzed on paraffin-embedded blocks of A549 and UT-SCC-14-derived tumor xenografts using anti-POR (Invitrogen, PA5-27326; 1:100) and anti-pimonidazole (Hypoxyprobe, HP1-1000, 1:100) antibodies.

γH2AX and 53BP1 foci staining

A549 cells were preincubated in hypoxic conditions (0.2% O_2) for 20 hours, followed by treatment with evofosfamide for 4 hours under hypoxic conditions, reoxygenation and irradiation with 2 Gy. 20 hours after irradiation, cells were washed twice with PBS, fixed with 4% formaldehyde/PBS for 10 min, and washed with PBS (4 x 5 min). Cells were then permeabilized for 5 min with 0.2% ice cold Triton-X-100/PBS, blocked for at least 20 min with 1% BSA, followed by 1 hour incubation with the rabbit monoclonal anti-H2AX-pSer139 (1:100, Abcam, Cambridge, UK) or the rabbit polyclonal anti-53BP1 (1:200, Cell Signaling, Boston MA, USA) primary antibodies, diluted in 1% BSA/PBS. After washing with 1% BSA/PBS (3 x 15 min), cells were incubated with the appropriate secondary antibody diluted 1:1000 (Alexa-488), washed with 1% BSA/PBS (2 x 10 min) followed by PBS (1 x 10 min) and incubated with DAPI/Methanol (1 μg/ml) for 3 min, before fixation with Dako Fluorescent Mounting Medium (Dako, North America). Images were taken using a Leica DM 5500 microscope at a magnification of 40x and quantified using FociCounter software. At least 50 cells/condition were analyzed.

Analysis of cellular senescence

A549 cells were preincubated in hypoxic conditions (0.2% O_2) for 20 hours, followed by treatment with

evofosfamide for 4 hours under hypoxic conditions, reoxygenation and IR with 2 Gy. 72 hours after irradiation, cells were stained for β-galactosidase using the Senescence β-Galactosidase Staining Kit (Cell Signaling, #9860): cells were washed with PBS and fixed (with 2% formaldehyde, 0.2% glutaraldehyde in PBS) for 15 min at room temperature. Cells were washed twice with PBS and stained with 40 mM citric acid/sodium phosphate (pH 6.0), 0.15 M NaCl, 2 mM $MgCl_2$, 5 mM potassium ferrocyanide, 5 mM potassium ferricyanide, 1 mg/ml X-gal (5-bromo-4-chloro-3-indolyl-βD-galactopyranoside) for 24 hours at 37°C. β-galactosidase-positive cells were counted in at least 3 randomly chosen visual fields at a magnification of 10x in each treatment setup.

Short interfering RNA treatment

A549 cells were transfected with POR-directed siRNA (Santa Cruz Biotechnology) for 24h using Lipofectamine RNAiMAX (Invitrogen). Cells were preincubated under hypoxia (0.2% O_2) for 20 hours, followed by incubation with evofosfamide for 4 hours under hypoxia and reoxygenation.

Statistical analysis

For *in vivo* treatment response to evofosfamide with fractionated and single high dose irradiation, the mean slopes of tumor growth curves for individual animals (day 0-15) were calculated and analyzed by one way ANOVA with Tukey post test using the GraphPad software. To calculate statistical significance between two or more groups of variables in *in vitro* experiments, either unpaired t-test or ANOVA with Tukey post test was used, respectively. P values <0.05 were considered significant. For all experiments, *P<0.05, **P<0.01, ***P<0.001.

ACKNOWLEDGMENTS

We thank Reidar Grénman (Turku University Hospital, Finland) for the kind gift of the head&neck squamous cell carcinoma (HNSCC) UT-SCC-14 cell line. We thank the Department of Pathology, University Hospital Zurich, for excellent technical support, the Biologisches Zentrallabor of the University Hospital of Zurich for animal housing.

CONFLICTS OF INTEREST

No potential conflicts of interest exist.

GRANT SUPPORT

This work was supported in part by grants from the CCRP Tumor Oxygenation of the University of Zurich, Merck KGaA, and Threshold Pharmaceuticals, the Kanton Zurich and the Swiss Cancer League (KLS-02788-02-2011), the Swiss National Science Foundation (144060).

REFERENCES

1. Brizel DM, Sibley GS, Prosnitz LR, Scher RL, Dewhirst MW. Tumor hypoxia adversely affects the prognosis of carcinoma of the head and neck. International Journal of Radiation Oncology Biology Physics. 1997; 38:285-289.
2. Nordsmark M, Alsner J, Keller J, Nielsen OS, Jensen OM, Horsman MR, Overgaard J. Hypoxia in human soft tissue sarcomas: Adverse impact on survival and no association with p53 mutations. British Journal of Cancer. 2001; 84:1070-1075.
3. Wilson WR, Hay MP. Targeting hypoxia in cancer therapy. Nat Rev Cancer. 2011; 11:393-410.
4. Horsman MR, Overgaard J. The impact of hypoxia and its modification of the outcome of radiotherapy. J Radiat Res. 2016.
5. Bentzen SM, Harari PM, Bernier J. Exploitable mechanisms for combining drugs with radiation: concepts, achievements and future directions. Nature Clinical Practice Oncology. 2007; 4:172-180.
6. Overgaard J. Hypoxic modification of radiotherapy in squamous cell carcinoma of the head and neck - A systematic review and meta-analysis. Radiotherapy and Oncology. 2011; 100:22-32.
7. Ahn GO, Brown M. Targeting tumors with hypoxia-activated cytotoxins. Front Biosci. 2007; 12:3483-3501.
8. Adams GE, Cooke MS. Electron-affinic sensitization I. A structural basis for chemical radiosensitizers in bacteria. International Journal of Radiation Biology and Related Studies in Physics Chemistry and Medicine. 1969; 15:457-471.
9. Mohindra JK, Rauth AM. Increased cell killing by metronidazole and nitrofurazone of hypoxic compared to aerobic mammalian cells. Cancer Res. 1976; 36:930-936.
10. Liu Q, Sun JD, Wang J, Ahluwalia D, Baker AF, Cranmer LD, Ferraro D, Wang Y, Duan JX, Ammons WS, Curd JG, Matteucci MD, Hart CP. TH-302, a hypoxia-activated prodrug with broad *in vivo* preclinical combination therapy efficacy: optimization of dosing regimens and schedules. Cancer Chemotherapy and Pharmacology. 2012; 69:1487-1498.
11. McKeage MJ, Jameson MB, Ramanathan RK, Rajendran J, Gu YC, Wilson WR, Melink TJ, Tchekmedyian NS. PR-104 a bioreductive pre-prodrug combined with gemcitabine or docetaxel in a phase Ib study of patients with advanced solid tumours. Bmc Cancer. 2012; 12.
12. Sun JD, Liu Q, Wang JL, Ahluwalia D, Ferraro D, Wang Y, Duan JX, Ammons WS, Curd JG, Matteucci MD, Hart CP. Selective Tumor Hypoxia Targeting by Hypoxia-Activated Prodrug TH-302 Inhibits Tumor Growth in

Preclinical Models of Cancer. Clinical Cancer Research. 2012; 18:758-770.

13. Brown JM, Carlson DJ, Brenner DJ. The Tumor Radiobiology of SRS and SBRT: Are More Than the 5 Rs Involved? International Journal of Radiation Oncology Biology Physics. 2014; 88:254-262.
14. Brown JM. The hypoxic cell: A target for selective cancer therapy - Eighteenth Bruce F. Cain Memorial Award lecture. Cancer Res. 1999; 59:5863-5870.
15. Peeters SG, Zegers CM, Biemans R, Lieuwes NG, van Stiphout RG, Yaromina A, Sun JD, Hart CP, Windhorst AD, van Elmpt W, Dubois LJ, Lambin P. TH-302 in Combination with Radiotherapy Enhances the Therapeutic Outcome and Is Associated with Pretreatment F-18 HX4 Hypoxia PET Imaging. Clinical Cancer Research. 2015; 21:2984-2992.
16. Orlowski K, Bley CR, Zimmermann M, Van V, Hug D, Soltermann A, Broggini-Tenzer A and Pruschy M. Dynamics of Tumor Hypoxia in Response to Patupilone and Ionizing Radiation. Plos One. 2012; 7.
17. Maftei CA, Bayer C, Astner ST, Shi K, Vaupel P. Quantitative assessment of hypoxia subtypes in xenografted human tumors. Strahlentherapie Und Onkologie. 2010; 186:69-69.
18. Hunter FW, Young RJ, Shalev Z, Vellanki RN, Wang JL, Gu YC, Joshi N, Sreebhavan S, Weinreb I, Goldstein DP, Moffat J, Ketela T, Brown KR, et al. Identification of P450 Oxidoreductase as a Major Determinant of Sensitivity to Hypoxia-Activated Prodrugs. Cancer Res. 2015; 75:4211-4223.
19. Meng F, Evans JW, Bhupathi D, Banica M, Lan L, Lorente G, Duan JX, Cai X, Mowday AM, Guise CP, Maroz A, Anderson RF, Patterson AV, et al. Molecular and Cellular Pharmacology of the Hypoxia-Activated Prodrug TH-302. Molecular Cancer Therapeutics. 2012; 11:740-751.
20. Jaiswal AS, Multani AS, Pathak S, Narayan S. N-methyl-N'-nitro-N-nitrosoguanidine-induced senescence-like growth arrest in colon cancer cells is associated with the loss of adenomatous polyposis coli protein, microtubule organization and telomeric DNA. Proceedings of the American Association for Cancer Research Annual Meeting. 2004; 45:1169-1169.
21. Sakai W, Swisher EM, Jacquemont C, Chandramohan KV, Couch FJ, Langdon SP, Wurz K, Higgins J, Villegas E, Taniguchi T. Functional Restoration of BRCA2 Protein by Secondary BRCA2 Mutations in BRCA2-Mutated Ovarian Carcinoma. Cancer Res. 2009; 69:6381-6386.
22. Yoon C, Lee HJ, Park DJ, Lee YJ, Tap WD, Eisinger-Mathason TSK, Hart CP, Choy E, Simon MC, Yoon SS. Hypoxia-activated chemotherapeutic TH-302 enhances the effects of VEGF-A inhibition and radiation on sarcomas. British Journal of Cancer. 2015; 113:46-56.
23. Goda F, O'Hara JA, Rhodes ES, Liu KJ, Dunn JF, Bacic G, Swartz HM. Changes of oxygen tension in experimental tumors after a single dose of X-ray irradiation. Cancer Res. 1995; 55:2249-2252.
24. Park HJ, Griffin RJ, Hui S, Levitt SH, Song CW. Radiation-induced vascular damage in tumors: implications of vascular damage in ablative hypofractionated radiotherapy (SBRT and SRS). Radiat Res. 2012; 177:311-327.
25. Guise CP, Wang AT, Theil A, Bridewell DJ, Wilson WR, Patterson AV. Identification of human reductases that activate the dinitrobenzamide mustard prodrug PR-104A: A role for NADPH : cytochrome P450 oxidoreductase under hypoxia. Biochem Pharmacol. 2007; 74:810-820.
26. Su JC, Gu YC, Pruijn FB, Smaill JB, Patterson AV, Guise CP, Wilson WR. Zinc Finger Nuclease Knock-out of NADPH: Cytochrome P450 Oxidoreductase (POR) in Human Tumor Cell Lines Demonstrates That Hypoxia-activated Prodrugs Differ in POR Dependence. J Biol Chem. 2013; 288:37138-37153.
27. Eicheler W, Zips D, Dorfler A, Grenman R, Baumann M. Splicing mutations in TP53 in human squamous cell carcinoma lines influence immunohistochemical detection. Journal of Histochemistry & Cytochemistry. 2002; 50:197-204.
28. Larue RT, Van De Voorde L, Berbee M, van Elmpt WJ, Dubois LJ, Panth KM, Peeters SG, Claessens A, Schreurs WM, Nap M, Warmerdam FA, Erdkamp FL, Sosef MN, et al. A phase 1 'window-of-opportunity' trial testing evofosfamide (TH-302), a tumour-selective hypoxia-activated cytotoxic prodrug, with preoperative chemoradiotherapy in oesophageal adenocarcinoma patients. BMC Cancer. 2016; 16:644.
29. Fontana AO, Augsburger MA, Grosse N, Guckenberger M, Lomax AJ, Sartori AA, Pruschy MN. Differential DNA repair pathway choice in cancer cells after proton- and photon-irradiation. Radiotherapy and Oncology. 2015; 116:374-380.

The hypoxia-activated prodrug evofosfamide in combination with multiple regimens of radiotherapy

SUPPLEMENTARY DATA

REFERENCE

1. Orlowski K, Bley CR, Zimmermann M, Van V, Hug D, Soltermann A, et al. Dynamics of Tumor Hypoxia in Response to Patupilone and Ionizing Radiation. Plos One. 2012; 7.

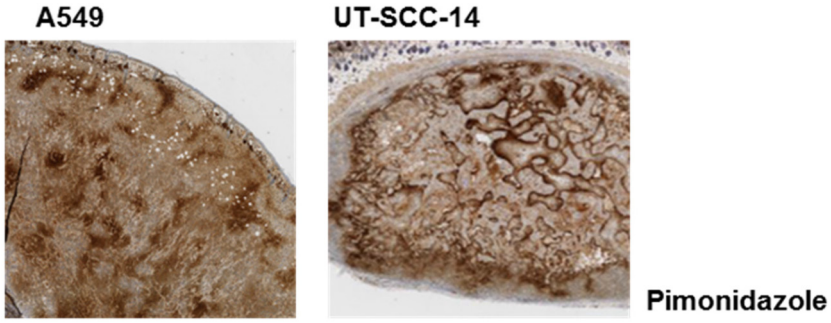

Supplementary Figure 1: Tumor hypoxia in A549 and UT-SCC-14-derived tumor xenografts. Staining of A549 (left) and UT-SCC-14 (right)-derived tumor xenografts for pimonidazole uptake. Pimonidazole was injected 1 hour (i.p.) prior euthanasia and tumor extraction.

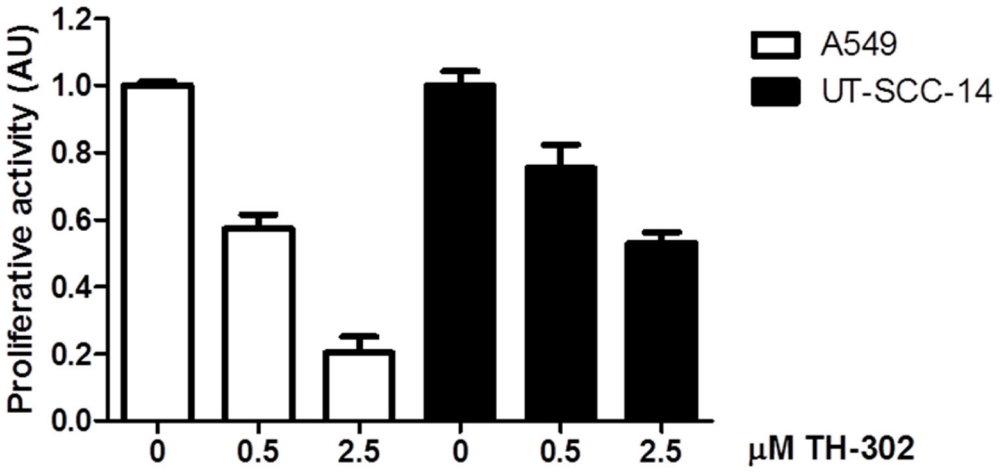

Supplementary Figure 2: Differential sensitivity of A549 and UT-SCC-14 cells to evofosfamide *in vitro*. Proliferative activity of A549 and UT-SCC-14 cells 72 hours after evofosfamide treatment. Cells were preincubated under hypoxia (0.2% O_2) for 20 hours, followed by treatment with increasing concentrations of evofosfamide for 4 hours, followed by reoxygenation. Error bars represent SEM.

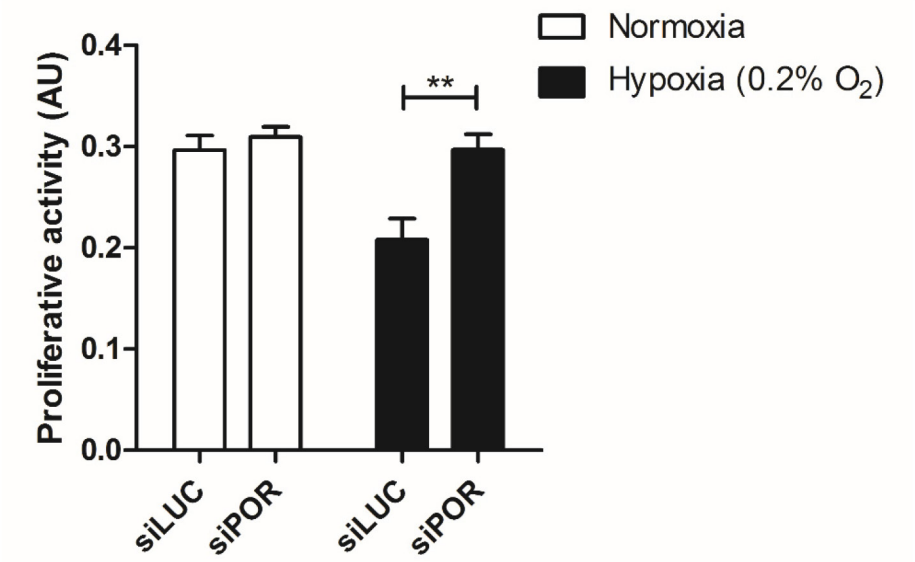

Supplementary Figure 3: Effect of POR downregulation on A549 cell sensitivity towards evofosfamide *in vitro*. Proliferative activity of siLUC and siPOR-pretreated A549 cells 48 hours after evofosfamide treatment. Cells were preincubated under hypoxia (0.2% O_2) for 20 hours, followed by treatment with evofosfamide (0.5μM) for 4 hours and reoxygenation. Error bars represent SEM.

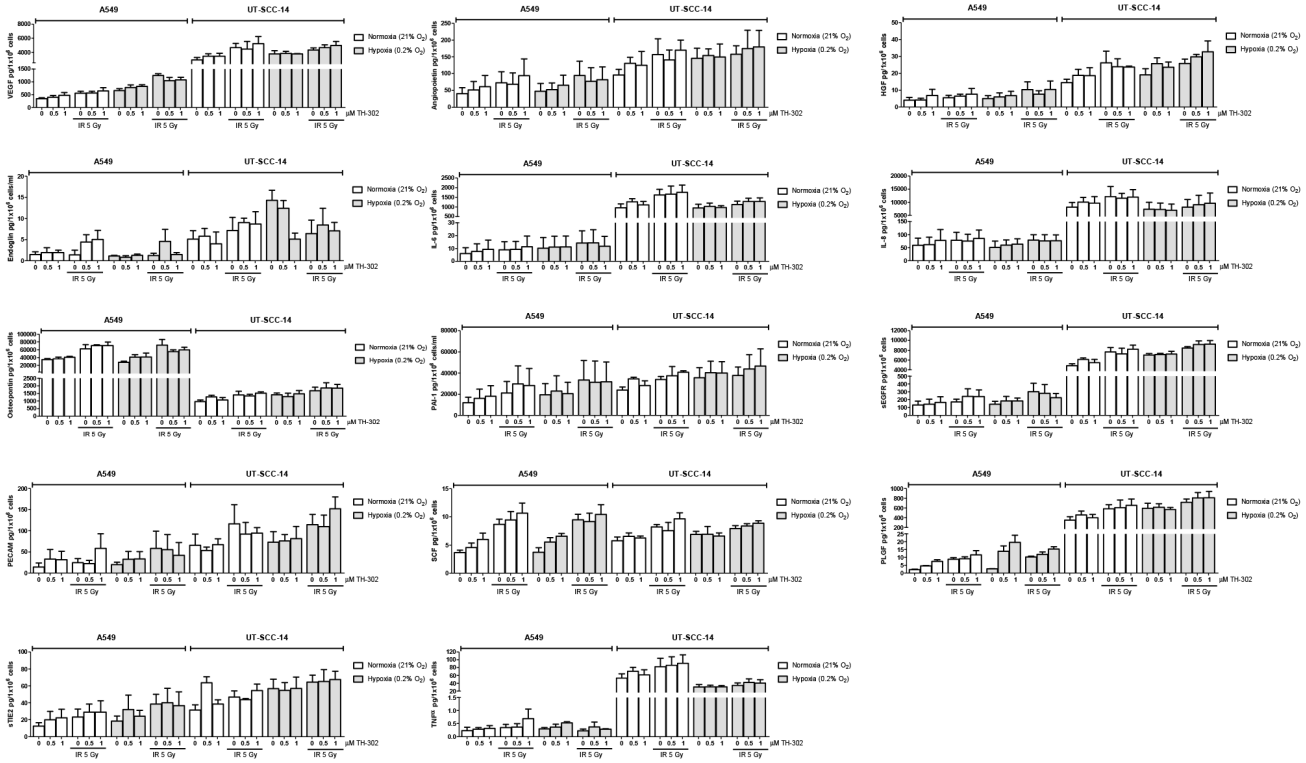

Supplementary Figure 4: Analysis of secreted factors in response to evofosfamide and irradiation. Raw data of Bioplex analysis of secreted factors in A549 and UT-SCC-14 cells in reponse to evofosfamide (0.5, 1 µM) and irradiation (5 Gy) under normoxic (21% O_2) and hypoxic conditions (0.2% O_2). Error bars represent SEM.

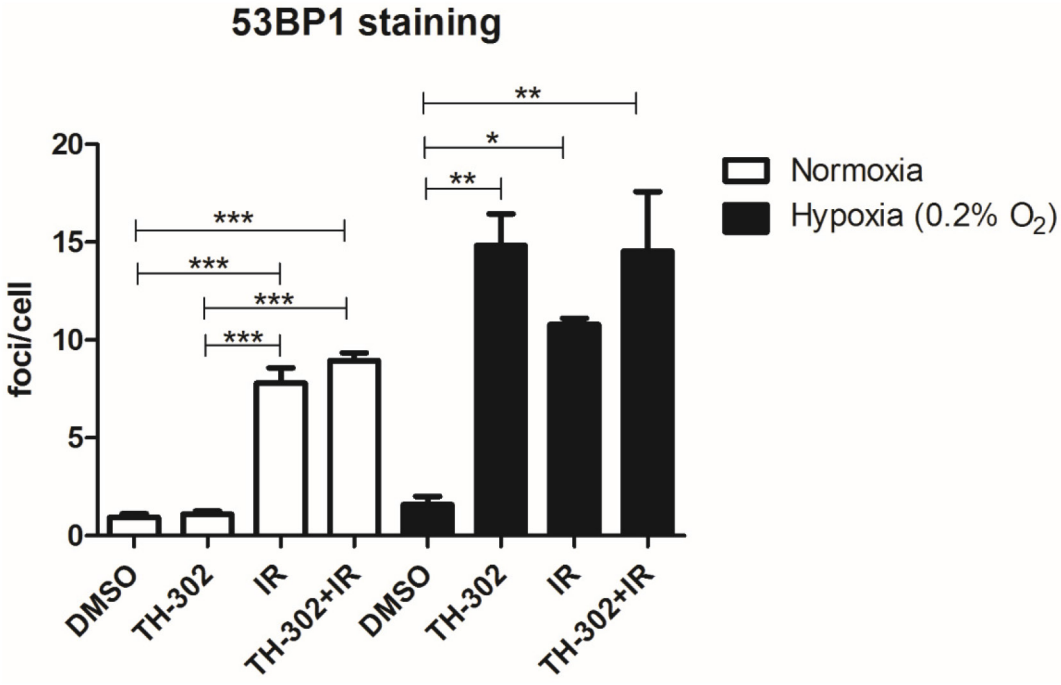

Supplementary Figure 5: DNA damage in response to evofosfamide and irradiation. 53BP1 foci were analyzed in A549 cells treated for 4 hours with evofosfamide and irradiation with 2 Gy. Cells were analyzed 20 hours after irradiation. Error bars represent SEM.

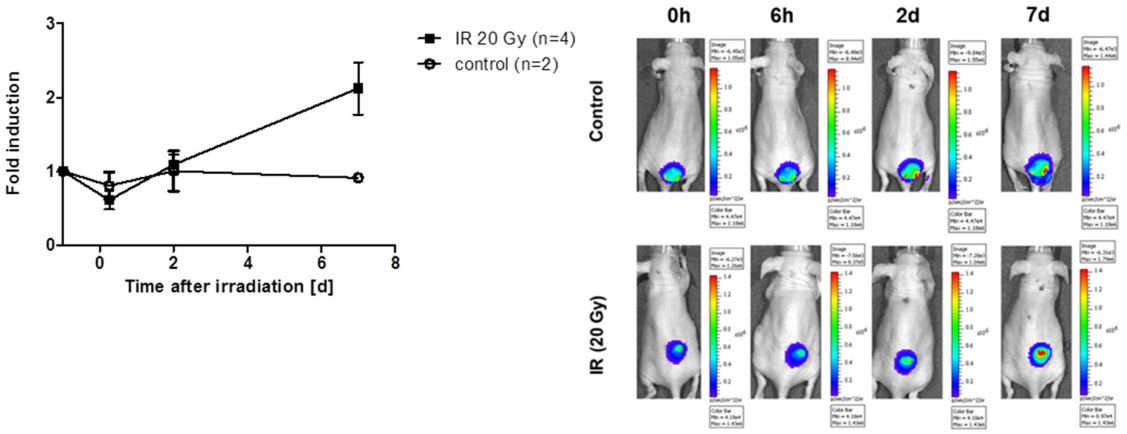

Supplementary Figure 6: Luciferase-activity of A549 ODD-Luc-derived tumor xenografts untreated and treated with single high-dose IR (20 Gy). Representative *in vivo* bioimages of control and irradiated mice. Measurements were performed as described in [1]. Data are shown as fold induction of the total flux normalized to the tumor volume at the indicated time point. Error bars represent SEM.

3.2 Neoadjuvant tumor reoxygenation with myo-inositol trispyrophosphate increases the radiosensitivity of hypoxic tumors

Ivo Grgic[1], Fabienne Tschanz[1], Nathalie Borgeaud[2], Rolf Graf[2], Matthias Guckenberger[1], Martin Pruschy[1]

[1]Laboratory for Applied Radiobiology, Dept. Radiation Oncology University Hospital Zurich, University Zurich

[2]Laboratory of the Swiss-Hepato-Pancreatico-biliary (HPB) Centre, Dept. of Visceral Surgery, University Hospital Zurich, University Zurich

Status of the manuscript: Submitted

Author contribution I. Grgic:

- Planning, data acquisition, analysis and interpretation of the experiments
- Fig.1 – a, b
- Fig.2 – c, d
- Fig.4 – all
- Fig.5 – all
- Fig.6 – all
- Writing of the manuscript

Neoadjuvant tumor reoxygenation with myo-inositol trispyrophosphate increases the radiosensitivity of hypoxic tumors

Ivo Grgic[1], Fabienne Tschanz[1], Nathalie Borgeaud[2], Rolf Graf[2], Matthias Guckenberger[1], Martin Pruschy[1]*

[1]Laboratory for Applied Radiobiology, Dept. Radiation Oncology University Hospital Zurich, University Zurich

[2]Laboratory of the Swiss-Hepato-Pancreatico-biliary (HPB) Centre, Dept. of Visceral Surgery, University Hospital Zurich, University Zurich

Running Title: ITPP in combination with Radiotherapy

Keywords: Ionizing Radiation, Tumor Oxygenation, myo-inositol trispyrophosphate, ITPP, DNA damage,

Grant Support: This work was supported in part by grants from the KFSP Tumor Oxygenation, the KFSP Molecular Imaging Network Zurich of the University of Zurich and from NormOxys, Inc.

*Corresponding Author: Martin Pruschy, Dept. Radiation Oncology, University Hospital Zurich, Raemistr. 100, CH-8091 Zurich, Switzerland.

Phone: +4144 255 8549, Fax: +41442554435, E-mail: martin.pruschy@usz.ch

Disclosure of Potential Conflicts of Interest: No potential conflicts of interest exist.

Word count (excluding references and figure legends): 4189

Total number of Fig. and tables: 6

Abstract

Purpose: Tumor hypoxia is a major limiting factor for successful radiotherapy outcome. Here we investigate the combined treatment modality of the reoxygenating compound *myo*-inositol trispyrophosphate (ITPP) in combination with ionizing radiation (IR) in preclinical animal tumor models.

Experimental Design: ITPP-mediated tumor reoxygenation was serially probed by a non-invasive, hypoxia-directed luciferase-based bioimaging approach in tumor xenografts derived from FaDu head and neck squamous carcinoma (HNSCC) and A549 non-small cell lung carcinoma (NSCLC) cells. The efficacy of ITPP in combination with irradiation was determined in vitro and in vivo. Initial and residual DNA-damage- and tumor microenvironment-oriented endpoints in response to treatment were determined by immunohistochemistry.

Results: ITPP-dependent tumor reoxygenation could be detected in the HNSCC- and the NSCLC tumor models already 2 hours following ITPP bolus application. ITPP alone did not affect cellular radiosensitivity in vitro and tumor growth in vivo, but significantly reduced tumor growth when combined with single high dose fractions of IR. Immunohistochemical analysis of γH2AX foci demonstrated increased initial and residual DNA damage within initially hypoxic tumor regions after combined treatment with ITPP and IR in comparison to IR alone. Interestingly, increased tumor hypoxia and vascular damage was detected 4 days after irradiation alone, which were both prevented by the combined treatment with ITPP and thereby exploitable for second high dose fraction of IR.

Conclusions: Our investigations on the combined treatment modality of ITPP with irradiation demonstrate an immediate tumor oxygenating and secondary tumor vasculature protective effect of ITPP, with subsequently increased IR-induced DNA damage and tumor-oriented cytotoxicity.

Introduction

Approximately 50% of all cancer patients receive radiotherapy, either alone or in combination with surgery or chemotherapy (1). One of the major obstacles for successful treatment outcome is tumor hypoxia due to enhanced radiation resistance in low oxygenated tumor areas (2), with hypoxic cells being up to three fold more radiation resistant than normoxic cells. Classic radiotherapy protocols use low dose fractionated treatment regimens, which exploit partial reoxygenation of hypoxic tumor areas in between daily fractions of radiotherapy to reduce the hypoxic, radiation resistant tumor burden.(3).

Hypoxic tumors arise as a result of inadequate perfusion due to structural and functional abnormalities of the tumor microvasculature, which is mainly caused by overexpression of the vascular endothelial growth factor (VEGF) in tumor tissues (4,5). Attempts to prevent and reverse a chaotic microvasculature and to subsequently reduce tumor hypoxia include the clinically relevant anti-VEGF-directed monoclonal antibody bevacicumab (Avastin). However, clinical trials combining radiotherapy with bevacizumab failed to be of significant clinical benefit (6,7). More recently, normalization of the tumor vasculature was successfully shown to be induced by inhibitors of classic signal transduction cascades. With this rational, agents targeting the EGFR/PI3K/Akt-pathway, are also tested in tumor xenografts in combination with ionizing radiation (8,9).

Constant improvements of imaging and linear accelerator technology have resulted in high conformity irradiation of the tumor, which nowadays allows hypofractionation and stereotactic body radiation therapy (SBRT) (10). However, SBRT and hypofractionation with only a few high dose fractions of radiotherapy does not anymore exploit iterative reoxygenation in between fractions. To achieve tumor control and to further minimize normal tissue toxicity, a combined treatment modality with pharmaceutical compounds that preferentially kill the hypoxic tumor burden, such as hypoxia-activated prodrugs, or that increase the partial oxygen pressure and

normalize the tumor vasculature in the tumor is of even higher interest when combined with SBRT and hypofractionation (11).

Myo-inositol trispyrophosphate (ITPP) was developed as an allosteric effector of hemoglobin (12) and potentially combines several of the above described mechanisms to overcome tumor hypoxia. ITPP is actively taken up by red blood cells and triggers a decrease of the affinity of oxygen to hemoglobin, which leads to an increased release of oxygen upon tissue demand i.e. in hypoxic tumors (12,13). Subsequent to this rapidly induced and persistent physicochemical effect, ITPP normalizes the tumor vasculature on downregulation of pro-angiogenic factors like HIF-1α and VEGF. (14). In addition, ITPP selectively activates the tumor suppressor PTEN in endothelial cells thereby inhibiting signaling downstream of PI3K and subsequently normalizing the tumor vasculature (15).

Here we investigated the impact of ITPP on the DNA damage response and on tumor hypoxia, and probed the combined treatment modality of ITPP in combination with hypofractionated radiotherapy in a lung adenocarcinoma and head&neck carcinoma tumor model.

Material and Methods

Cell culture and compounds

The human head&neck squamous cell carcinoma (HNSCC) cell line FaDu was obtained from ATCC and cultured in EMEM cell culture medium supplemented with 10% FBS and 1% penicillin-streptomycin at 37°C in 5% CO_2. The human non-small cell lung cancer (NSCLC) cell line A549 was obtained from ATCC and maintained in RPMI 1640 cell culture medium supplemented with 10% FBS, 1% L-glutamine and 1% penicillin-streptomycin at 37°C in 5% CO_2. Myo-inositol trispyrophosphate (ITPP) was provided by NormOxys and dissolved in PBS.

Tumor xenografts and application of treatment regimens

FaDu HNSCC and A549 NSCLC cells (4 x 10^6 cells/150 µL saline) were subcutaneously injected in the back of 4-week old, female athymic CD1 nude mice (Charles River). Tumor volumes were determined by caliper measurements of tumor length (L) and width (l) according to the formula (L x l^2)/2. Treatment was started when tumors reached a volume of 300 mm^3 ± 10%. ITPP (dissolved in PBS) was administered intraperitoneally at 3 g/kg on two consecutive days. Tumors were sham-irradiated or irradiated using a customized shielding device with either 1 x 10 Gy (2 hours after second ITPP injection) or 2 x 10 Gy (2 hours after second ITPP injection, 5 days after second ITPP injection). All *in vivo* experiments were performed according to the guidelines for the welfare and use of animals of the Veterinäramt Kanton Zürich, Switzerland.

Irradiation

If not stated differently, irradiation was performed using an Xstrahl 200 kV X-ray unit at 1 Gy/min. For ionizing radiation (IR)-induced DNA damage analysis in FaDu xenografts and for the tumor growth delay experiment in A549 xenografts, an image-guided small animal radiotherapy platform (Precision X-Ray, X-Rad SmART) 225 kV unit with a dose rate of 3 Gy/min was used.

Cell proliferation and clonogenic survival assay

The proliferative activities of tumor cells were assessed in 96-well plates with the colorimetric alamarBlue assay (Invitrogen). Clonogenic cell survival was determined by the ability of single cells to form colonies *in vitro* as described previously (16). Briefly, cells were treated with ITPP or vehicle for 6 hours. Thereupon, cells were irradiated with increasing doses of IR, trypsinized and reseeded in petri dishes. After 14 days, colonies were fixed (methanol/acetic acid 3:1) and stained with crystal violet (2%). Colonies were then counted manually.

Western blotting

For sample preparation, cells were detached in Lämmli Buffer, heated for 5 minutes at 95°C and their protein concentration was determined by Nanodrop 1000 (Spectrophotometer, Thermo Scientific). The samples were size separated by SDS-PAGE and transferred to a polyvinylidene difluoride (PVDF) membrane using a semi-dry transfer unit (TE70X, Hoefer). After the transfer, membranes were blocked in 5% non-fat milk solution (NFMS) for 1 hour at room temperature before overnight incubation at 4°C with different primary antibodies (pAKT (Ser473) Cell Signaling, PTEN (138G6) Cell Signaling, PI3K (p110 α) Upstate Biotechnology, β-actin Sigma Aldrich, 1:1000 in 5% NFMS). Membranes were probed for primary antibody with anti-rabbit (1:2000) and anti-mouse (1:2000) ECL peroxidase conjugates. Chemiluminescence was identified with ECLTM Western Blotting detection agents by a Vilber Lourmat Fusion FX Detector.

***In vivo* bioluminescence imaging and analysis**

FaDu and A549 cell lines were transfected with SV40-luciferase and SV40-ODD-luciferase vectors as described previously (17). Tumor-bearing mice were intraperitoneally (i.p.) injected with 150 mg/kg D-Luciferin (Perkin Elmer) 5 minutes before anesthesia. Sequential measurements of photon emission (flux/s) were acquired approximately 10 minutes after D-Luciferin injection with the IVIS200 (Xenogen). The measurement with the highest photon flux within the tumor of each mouse was used for the pharmacodynamic survey. The values were normalized to the baseline value (t=0) and divided by the tumor volume.

Immunohistochemistry

Immunohistological endpoints were analyzed on formalin-fixed paraffin-embedded (FFPE) blocks for hematoxyline & eosine, pimonidazole (1:12000, Hypoxyprobe), CAIX (1:6000, abcam, ab184006), CD31 (1:10, Dako, M0823), SMA (1:50, Dako, M0851) and γH2AX (1:500, Novus Biologicals, NB100-2280). Viable areas (as determined by H&E staining) of

whole tumor sections were manually quantified for specific pimonidazole or CAIX staining percentage. Number of blood vessels (CD31) and their respective SMA coverage were counted in at least 3 randomly chosen visual fields (magnification 100x) in each xenograft.

IR-induced DNA damage analysis

FaDu xenograft-bearing mice received 60 mg/kg pimonidazole 4 hours prior to the previously established treatment schedule, i.e. 3g/kg ITPP or PBS on 2 consecutive days, followed by a single fraction of 4 Gy. Tumors were harvested 30 minutes or 24 hours after IR, immediately fixed in formalin and embedded into paraffin 24 hours thereafter. Three consecutive 3 µm tissue sections were stained for H&E, pimonidazole and γH2AX. For the evaluation, 3 hypoxic (pimonidazole-positive) and 3 normoxic (pimonidazole-negative) areas per tissue section were selected and the individual number of γH2AX foci per nucleus was counted in at least 100 cells of the chosen area. The individual number of foci per cell was normalized to the according nuclear volume using ImageJ. Foci analysis was performed in viable, non-dividing cells only.

Statistical analysis

In vivo luciferase activity data were analyzed by Student's t-test. For the treatment response to ITPP in combination with IR, the time to reach a tripling of the initial tumor volume (T3xSV) was analyzed by one-way ANOVA with Tukey post test. Immunohistochemical data were analyzed by one-way ANOVA on replicate tumor samples (n =3) and pair-wise analysis was performed using the Tukey test.

Results

To monitor tumor reoxygenation on ITPP administration we used a functional hypoxia-oriented luciferase-based reporter gene assay, which was previously developed in our laboratory (17). Briefly, the oxygen-dependent degradation (ODD) domain of HIF-1α is fused 5` to the luciferase reporter gene. The construct in constantly expressed in cells under control of a hypoxia-independent SV40 promoter. In the presence of oxygen, the SV40-ODD-Luc construct is degraded, resulting in low bioluminescent photon flux upon luciferin administration. The tumor oxygenation status was determined at different timepoints after intraperitoneal ITPP (3 g/kg) injection in stably transfected lung adenocarcinoma (A549) and head&neck squamous cell carcinoma (FaDu) tumor xenograft models. These cell lines were previously shown to develop xenografts with high (A549) and intermediate (FaDu) hypoxic tumor fractions (18,19). The first measurements were performed when tumors reached a volume of 300 mm^3 (± 10%).

In the more hypoxic A549 xenograft model, tumor oxygenation was significantly increased already 2 hours after intraperitoneal ITPP administration (Fig. 1A). The hypoxic tumor fraction was decreased 2.2-fold as compared to the initial baseline level. Serial measurements of tumor oxygenation revealed a time-dependent, partial reversion of tumor hypoxia. ITPP-mediated tumor reoxygenation was stable for up to 10 hours after ITPP injection (Supplementary Fig. S1). Only minimal changes in luminescence were detected in A549-derived tumor xenografts expressing the ODD-luciferase reporter gene on administration of PBS.

To validate that ITPP-induced changes in luciferase activity are mediated by alterations in tumor oxygenation, we determined luminescence in tumor xenografts derived from A549 cells stably transfected with a SV40-Luc construct lacking the oxygen-dependent degradation domain (ODD). Neither PBS- nor ITPP-administration affected luciferase activity in these control tumors (Fig. 1B).

To determine the capacity of ITPP to reoxygenate tumors with a lower hypoxic fraction, we probed the previously developed treatment schedule in FaDu-derived xenografts also expressing the ODD-luciferase construct. ITPP-mediated reoxygenation of FaDu xenografts was less effective in comparison to the response observed in the lung adenocarcinoma derived tumor xenograft, which most probably due to their lower hypoxic fraction. Nevertheless, a significant decrease in tumor hypoxia was detected 2 hours after the second ITPP administration ($p = 0.03$), whereas PBS treatment had no impact on tumor oxygenation (Fig. 1C). Overall, these results demonstrate that ITPP efficiently reoxygenates hypoxic tumors in a dose-and time dependent manner.

Increased tumor response to radiotherapy in combination with ITPP

The tumor response to a combined treatment modality of ITPP and IR was determined in the A549-derived tumor xenograft model that was treated on two consecutive days with ITPP (3 g/kg) and PBS, respectively, followed by a single dose of IR (5 Gy) 2 hours after the second ITPP administration. While tumor growth was not affected by treatment with ITPP alone, irradiation induced a tumor growth delay that was further extended in ITPP-pretreated tumors. The time to reach 2.5fold of the initial tumor volume (300 mm^3) was significantly delayed by administration of ITPP prior to a single high dose of irradiation in comparison to IR alone (31 versus 22 days, $p = 0.01$), with many tumors becoming necrotic thereafter (Fig. 2A). To investigate the tumor response in the less hypoxic FaDu-tumor cell derived tumor model, mice were treated with the same treatment schedule as for the A549-derived tumor xenograft model, but received a higher dose of IR (1 x 10 Gy) due to the lower radiosensitivity of FaDu cells in comparison to A549 cells. ITPP alone did not affect tumor growth rate, whereas neoadjuvant administration significantly enhanced the time to triple the initial tumor volume at treatment start in comparison to IR alone ($p = 0.03$) (Fig. 2B). Overall, these results demonstrate that

ITPP reoxygenate hypoxic tumors and enhance the treatment response to a single dose of ionizing radiation.

ITPP does not enhance cellular response to ionizing radiation in vitro.

Given its structural relationship to the substrates of the phosphatidylinositol-4,5-bisphosphate 3-kinase (PI3K) family, ITPP could interfere with cellular PI3K/AKT signalling, which is important for tumor cell proliferation and cellular radiation sensitivity (20) and unpublished Data by NormOxys). Interestingly, we observed a time-dependent decrease in phosphoAKT levels in cell lysates derived from ITPP treated A549 and FaDu cells (Fig. 3A). Furthermore, decreasing phosphoAKT levels correlated in FaDu but not in A549 cells with increasing Phosphatase and tensin homolog (PTEN) protein levels, which is known to counteract PI3K-signaling. Since high phosphoAKT levels are associated with increased radioresistance (21) cell proliferation and clonogenic cell survival assays were performed on combined treatment with ITPP and ionizing radiation. Increasing concentration of ITPP did not affect cellular proliferative activity and did not enhance cellular sensitivity of A549 and FaDu cells to IR (Fig. 3B and 3C). These results strongly suggest that increased ITPP-mediated tumor growth delay in response to irradiation is primarily caused by neoadjuvant tumor reoxygenation prior to irradiation.

ITPP increases IR-induced DNA damage in hypoxic tumor areas

Increased ITPP-mediated oxygen availability within the tumor at the timepoint of irradiation could result in the generation of a differential amount of DNA double strand breaks (DSB) in response to IR. Therefore the initial and residual amount of γH2AX-foci were assessed in FaDu-derived xenografts that were treated with PBS and ITPP, irradiated with a single IR-dose of 4 Gy and harvested 30 minutes and 24 hours, respectively, after irradiation. A reduced dose of 4 Gy was applied since the amount of γH2AX-foci induced after 10 Gy was technically not

feasible to count (22,23). Pimonidazole was injected 4 hours prior to our established treatment regimen to covalently label initially hypoxic tumor areas and to identify them retroactively after treatment and tumor harvesting. (Fig. 4A).

Within initially hypoxic tumor regions, the average number of γH2AX foci per nucleus detectable 30 minutes after irradiation was 22.8 ± 3.7. A significantly increased number of γH2AX foci per nucleus (34.3 ± 4.9, p = 0.0006) was determined in neoadjuvant ITPP-treated and irradiated tumors that were harvested at this early time point. Moreover, frequency distribution analysis revealed that in almost 10% of irradiated hypoxic tumor cells no γH2AX-foci were detectable, whereas less than 1% of cells remained undamaged after ITPP-treatment and irradiation (Fig. 4B). To validate that ITPP specifically increases DNA damage in hypoxic tumor cells, initially normoxic, pimonidazole-negative areas were analysed for γH2AX foci. As expected, the average number of γH2AX foci per nucleus after PBS and IR treatment was higher in these normoxic cells (31.6 ± 6.7) in comparison to hypoxic cells (see above) but was not significantly further increased in ITPP-pretreated tumors (37.1 ± 4.5, p = 0.09). The frequency distribution of γH2AX-foci in the ITPP- and PBS-pretreated, pimonidazole-negative areas was similar, indicating a DNA-damage enhancing effect of ITPP specifically in the pimonidazole-positive, pretreatment hypoxic tumor areas (Fig. 4C).

Eventually it is the amount of residual DNA damage, which is relevant for irradiation-induced cell death. The average number of residual γH2AX foci per cell in initially hypoxic, pimonidazole-positive tumor areas was significantly higher in ITPP versus PBS-pretreated tumors (31.3 ± 4.2 vs 17.5 ± 4.0, respectively; p = 0.0001). The amount of residual γH2AX foci per cell in normoxic, pimonidazole-negative tumor areas was also higher in ITPP versus PBS-pretreated tumors, but not to an extent as determined in the initially hypoxic and ITPP-reoxygenated tumor areas (28.9 ± 5.3 vs 21.7 ± 5.2, respectively; p = 0.003; compare Fig. 4D and 4E). This partial ITPP-related effect in normoxic areas might be due to a slight increase of the pO_2 at a pO_2-level not sufficiently low for pimonidazole staining. Overall, these results

illustrate the higher incidence of DNA damage induced in ITPP-pretreated tumors in particular in initially hypoxic tumor areas, which is most probably the key source for enhanced IR-efficacy in ITPP-pretreated tumors. ITPP treatment without subsequent irradiation has no effect on the number or distribution of induced DNA DSBs (Supplementary Fig. 2).

ITPP protects from IR-induced vascular damage and IR-enhanced tumor hypoxia

Single high dose irradiation damages the tumor vasculature with subsequently increased tumor hypoxia (24,25). On the other hand ITPP treatment was previously shown to normalize the tumor vasculature (15). Therefore a differential treatment-induced effect on the tumor microenvironment was determined after ITPP-treatment (on two consecutive days, 3 g/kg) and irradiation (10 Gy) alone and in combination in FaDu-derived tumor xenografts at the time point 5 days after treatment start.

Tumor irradiation resulted in decreased microvessel density (MVD; CD31-positive vessels per visual field) in comparison to the MVD in unirradiated tumors of PBS-treated mice (113 ± 34 vs 74 ± 37; $p = 0.01$). Interestingly, irradiation-induced vascular damage (vessels/field) was completely prevented in tumors of mice pretreated with ITPP [103 ± 32 (ITPP) vs. 112 ± 41 (ITPP + IR), $p = 0.93$] (Fig. 5A). Likewise, pericyte coverage of CD31-positive vessels in control tumors decreased on irradiation, but remained stable in ITPP-pretreated tumors (Fig. 5B). Staining for carbonic anhydrase IX (CAIX) was used to determine tumor hypoxia in response to treatment. The hypoxic tumor fraction increased from 7.2 ± 4.7% to 11.1 ± 5.2% during 4 days after irradiation, but remained low in ITPP-pretreated tumors (5.1 ± 1.5% before vs 5.0 ± 2.5% after irradiation) (Fig. 5C). The protective ITPP-related effect could also be observed on staining for the exogenous hypoxia marker CCI-103F (Fig. 5D). These results indicate that ITPP protects the tumor vasculature from high dose ionizing radiation-induced damage.

To exploit the tumor vasculature-protective effect of ITPP and subsequently altered tumor microenvironment, FaDu-derived xenografts were irradiated with a second high dose fraction of 10 Gy 4 days after the initial treatment sequence. The second fraction of IR further delayed tumor growth of ITPP and IR-pretreated tumors in comparison to IR-pretreated tumors alone (Fig. 6A and see also Fig. 3C above, $p = 0.02$). Moreover, the tumor vasculature-oriented protective effect of ITPP remained effective even after the second high-dose fraction of IR. The MVD of mice receiving irradiation alone (2 x 10 Gy) was reduced from 77 ± 21 to 40 ± 14 ($p = 0.004$) $CD31^+$-vessels/field 9 days after treatment start. In contrast, initial ITPP treatment prevented an MVD-decrease even after two high dose fractions of irradiation [60 ± 26 (ITPP alone) vs. 67 ± 22 (ITPP plus IR), $p = 0.94$] (Fig. 6C).

Overall, our investigations on the combined treatment modality of ITPP with irradiation demonstrate an immediate oxygenating and delayed tumor vasculature protective effect of ITPP, with subsequently increased IR-induced tumor-oriented cytotoxicity.

Discussion

Only limited approaches exist to reduce the hypoxic tumor burden for successful radiotherapy. Classic fractionated radiotherapy regimens exploit reoxygenation in between individual fractions, which can be further enhanced e.g. as part of a combined treatment modality with nicotinamide and carbogen breathing. But novel approaches are of great need to either reverse or to exploit tumor hypoxia as part of high dose hypofractionated and stereotactic body radiotherapy, in particular since high dose fractions of ionizing radiation might even further enhance tumor hypoxia (new references). (6,7,26-29). Here, we probed to enhance the radiation response with myo-inositol trispyrophosphate (ITPP) and identified by invasive and non-invasive approaches that hypoxic tumor xenografts were rapidly reoxygenated on ITPP administration. Subsequent irradiation of the reoxygenated tumor xenografts significantly delayed tumor growth as compared to tumor irradiation alone, while ITPP alone did not

interfere with tumor growth. Immediate ITPP-induced reoxygenation resulted in an enhanced level of both IR-induced and residual DNA damage in these pretreatment hypoxic areas, which are most probably the major contributing factor for the enhanced tumor response to the combined treatment modality. Besides this immediate effect, we demonstrated a delayed protective effect of ITPP on the tumor vasculature. ITPP treatment increased pericyte coverage of the tumor vasculature and thereby prevented RT-induced vascular damage and subsequential increase of tumor hypoxia, which could be further exploited by a second high dose of irradiation. Overall, these results strongly support the hypothesis of Raykov et al, who originally postulated early and delayed antitumor-directed mechanisms of ITPP (14).

These in vivo experiments were performed in athymic immuno-compromised mice. Thereby, a probable involvement of the adaptive immune system in response to high dose radiotherapy could be excluded, However, the protected and still intact vasculature in response to the combined treatment modality could promote an increased immune cell infiltration, which might further affect the outcome in response to ITPP in combination with high dose radiotherapy (30) We are currently testing this hypothesis in follow-up experiments in C57BL/6 mice.

In vitro experiments revealed that ITPP also interferes with the PI3K/Akt-pathway and downregulates phosphoAkt levels in the pretreated tumor cells. However, ITPP did not increase the antiproliferative effect of ionizing radiation and did not enhance the radiosensitivity of tumor cells under normoxic conditions, thereby excluding a direct ITPP-mediated effect on cellular radiosensitivity. Hence, the enhanced tumor growth delay in response to the combined treatment modality might primarily be linked to ITPP-induced tumor reoxygenation with subsequently enhanced tumor cell killing due to the increased number of induced and residual DNA DSBs on irradiation. Eventually, it will be of interest to apply curative treatment regimens of ITPP in combination with radiotherapy and to probe this combined treatment modality even in combination with chemotherapy and immunotherapy.

A combined treatment modality of ITPP in combination with chemotherapy and radiotherapy, respectively, has previously investigated on the preclincial level but applying different treatment regimens. A low dose regimen of ITPP over 10 days potentiated the capacity of FOLFOX chemotherapy in a hypoxic colorectal liver metastasis tumor model, which is most probably based on the long-term tumor vascular normalization effect of ITPP (31). An extended neoadjuvant low dose regimen of ITPP was probed in an orthotopic glioblastoma tumor model in combination with hypofractionated radiotherapy but failed to enhance the potency of radiotherapy, which might be due to lack of vascular normalization in glioblastoma in response to low dose of ITPP or failure of ITPP to cross the blood brain barrier as suggested by Förnvik et al. (32). Our data demonstrate lack of antitumor activity of ITPP alone but an enhanced treatment response in combination with radiotherapy, best applied as a boost immediately prior to radiotherapy. Own dose response investigations revealed no treatment enhancement with reduced dose of ITPP and delayed irradiation (Supplementary Fig. 3).

ITPP is currently tested as part of a phase Ia/IIb clinical trial in combination with chemotherapy for non-resectable abdominal tumors Based on its capacity to reoxygenate hypoxic tumor and using tumor hypoxia-oriented image-guidance, our results support the strong rationale to combine ITPP also with hypofractionated radiotherapy.

Acknowledgements

This work was supported in part by grants from the KFSP Tumor Oxygenation, the KFSP Molecular Imaging Network Zurich of the University of Zurich and from NormOxys, Inc. We thank Sofie Deschoemaeker and Arne Heyerick for constructive inputs on the experimental designs. We thank the Department of Pathology, University Hospital Zurich, for excellent technical support, the Biologisches Zentrallabor of the University Hospital of Zurich for animal housing and Janosch Ott for technical support during animal experiments.

Figure legends

Fig. 1. ITPP induces rapid tumor reoxygenation. (**A**) Bioluminescent photon flux is significantly decreased in tumors derived from A549 cells transfected with the hypoxia reporter construct (SV40-ODD-Luc, n = 4-5 mice per group) 2 hours after ITPP injection, whereas PBS administration does not result in significant alterations. (**B**) Neither PBS nor ITPP treatment induce significant changes in bioluminescent photon flux in tumors derived from A549 cells transfected with the control construct (SV40-Luc, n = 3-4 mice per group). (**C**) Bioluminescent photon flux is significantly decreased in tumors derived from FaDu cells transfected with the hypoxia reporter construct (SV40-ODD-Luc, n = 3-4 mice per group) 2 hours after ITPP injection, whereas PBS administration does not result in significant alterations. Bar graphs represent the fold change in photon flux as compared to baseline as mean ± SEM. The students t-test was used to compare changes in reoxygenation.

Fig. 2. Tumor growth is delayed on combined treatment with ITPP and IR. Effect of ITPP in combination with IR in mice bearing A549- (**A)** (n = 6-9 per group) and FaDu- (**B**) (n = 10 per group) derived tumors. Mice were treated with two doses of ITPP (3 g/kg, i.p.), and IR (single dose of 5 Gy and 10 Gy, respectively) alone and in combination. Each curve represents the mean tumor volume per group ± SEM. Kaplan–Meier curves for A549- (**C**) and FaDu- (**D**) derived tumor xenografts for reaching tripling tumor volumes (900 mm^3). One-way ANOVA test was used to statistically compare tumor growth rates.

Fig. 3. ITPP interferes with PI3K/AKT pathway but does not affect cellular sensitivity to ionizing radiation. (**A**) A549 and FaDu cells were treated with ITPP (10 mM) for up to 48 hours and whole cell lysates were analyzed against the indicated proteins by western blotting. (**B**) Relative proliferative activity of irradiated A549 and FaDu cells (5 Gy) pretreated for 24 hours with increasing concentrations of ITPP. (**C**) Clonogenic cell survival of A549 and FaDu

cells pretreated for 24 hours with PBS or ITPP (10 mM) and irradiated with increasing doses of IR. Data are represented as mean ± SD.

Fig. 4. Reoxygenation by ITPP increases the number of IR-induced DNA DSBs in initially hypoxic tumor areas. (**A**) Treatment schedule and representative pimonidazole-stained tumor slice of a FaDu-derived tumor xenograft. γH2AX foci in control and ITPP-pretreated tumors, 30 minutes after IR (4 Gy) in initially hypoxic (**B**) and normoxic (**C**) tumor regions. 1 dot represents mean of γH2AX foci/cell of at least 100 cells counted in either initially hypoxic or normoxic tumor regions. Representative cell nuclei and frequency distribution plots (γH2AX foci/cell) are also shown. γH2AX foci in control and ITPP-pretreated tumors, 24 hours after IR (5 Gy) in initially hypoxic (**D**) and normoxic (**E**) tumor regions. 1 dot represents mean of γH2AX foci/cell of at least 100 cells counted in either initially hypoxic or normoxic tumor regions. Representative cell nuclei and frequency distribution plots (γH2AX foci/cell) are also shown. Data are represented as mean ± SD. The students t-test was used to compare numbers of γ-H2AX foci.

Fig. 5. ITPP protects from IR-induced vascular damage and increase of tumor hypoxia. (**A**) Quantification of CD31+ blood vessels per visual field 4 days after IR. Representative stainings are shown. (**B**) Percentage of SMA+ CD31+ blood vessels (pericyte coverage) of total amount of CD31+ blood vessel. (**C**) Percentage of CAIX-positive tumor area of total viable tumor area. Representative stainings are shown. (**D**) Percentage of CCI-103-F-positive tumor are of total viable tumor area. CCL-103-F was injected 2 hours prior to tumor collection. The students t-test was used to analyse data.

Fig. 6. Extended tumor growth delay and tumor vasculature protection on reirradiation. Tumor growth delay (**A**) and Kaplan-Meier (**B**)curves of FaDu-derived tumor xenografts (n = 10 per group) pretreated with PBS or ITPP, and irradiated with the first fractions of 10 Gy, 2 hours after the 2nd IPTT-dose and the second fraction of 4 Gy 4 days thereafter. (**C)** Quantification of CD31+ blood vessels per visual field in FaDu-derived tumor sections 4 days

after the second IR fraction. One-way ANOVA test was used to compare tumor growth rates. The students t-test was used to analyse blood vessel data.

Supplementary Figure Legends

Supl. Fig. 1 ITPP-mediated tumor reoxygenation in tumors is effective for up to 10 hours after injection. (**A**) Bioluminescent photon flux is decreased 2 hours after ITPP injection and remains low for up to 10 hours in tumors derived from A549 cells, transfected with the hypoxia reporter construct (SV40-ODD-Luc, n = 4-5 mice per group). (**B**) Neither PBS nor ITPP treatment induce significant changes in bioluminescent photon flux in tumors derived from A549 cells transfected with the control construct (SV40-Luc) (n = 3-4 mice per group). Bar graphs represent the fold change in photon flux as compared to baseline as mean ± SEM.

Suppl. Fig. 2 ITPP-mediated tumor reoxygenation does not increase the number of DNA DSBs in unirradiated tumors. (**A**) Treatment schedule. γ-H2AX foci in control and ITPP-treated tumors in initially hypoxic (**B**) and normoxic (**C**) tumor regions. Tumors were collected 30 minutes after treatment. 1 dot represents mean of γH2AX foci/cell of at least 100 cells counted in either initially hypoxic or normoxic tumor regions. Representative cell nuclei and frequency distribution plots (γH2AX foci/cell) are also shown. γ-H2AX foci in control and ITPP-treated tumorsin initially hypoxic (**D**) and normoxic (**E**) tumor regions. Tumors were collected 24.5 hours min after treatment. 1 dot represents mean of γH2AX foci/cell of at least 100 cells counted in either initially hypoxic or normoxic tumor regions. Representative cell nuclei and frequency distribution plots (γH2AX foci/cell) are also shown. Data are represented as mean ± SD. The students t-test was used to compare numbers of γ-H2AX foci.

Suppl. Fig. 3 No additional tumor growth delay in tumors treated with reduced ITPP-dose and delayed irradiation Effect of ITPP in combination with IR in mice bearing A549-derived

tumors. Mice were treated with two doses of ITPP (1.5 g/kg, i.p.), and one IR-fraction of 10 Gy, 24 hours after the second ITPP injection.

References

1. Begg AC, Stewart FA, Vens C. Strategies to improve radiotherapy with targeted drugs. Nat Rev Cancer **2011**;11(4):239-53 doi 10.1038/nrc3007.
2. Brown JM, Wilson WR. Exploiting tumour hypoxia in cancer treatment. Nat Rev Cancer **2004**;4(6):437-47 doi 10.1038/nrc1367.
3. Steel GG, McMillan TJ, Peacock JH. The 5Rs of radiobiology. Int J Radiat Biol **1989**;56(6):1045-8.
4. Vaupel P, Mayer A. Hypoxia in cancer: significance and impact on clinical outcome. Cancer Metastasis Rev **2007**;26(2):225-39 doi 10.1007/s10555-007-9055-1.
5. Nagy JA, Chang SH, Dvorak AM, Dvorak HF. Why are tumour blood vessels abnormal and why is it important to know? Br J Cancer **2009**;100(6):865-9 doi 10.1038/sj.bjc.6604929.
6. Carlson JA, Reddy K, Gaspar LE, Ney D, Kavanagh BD, Damek D, *et al.* Hypofractionated-intensity modulated radiotherapy (hypo-IMRT) and temozolomide (TMZ) with or without bevacizumab (BEV) for newly diagnosed glioblastoma multiforme (GBM): a comparison of two prospective phase II trials. J Neurooncol **2015**;123(2):251-7 doi 10.1007/s11060-015-1791-4.
7. Taphoorn MJ, Henriksson R, Bottomley A, Cloughesy T, Wick W, Mason WP, *et al.* Health-Related Quality of Life in a Randomized Phase III Study of Bevacizumab, Temozolomide, and Radiotherapy in Newly Diagnosed Glioblastoma. J Clin Oncol **2015**;33(19):2166-75 doi 10.1200/JCO.2014.60.3217.
8. Qayum N, Muschel RJ, Im JH, Balathasan L, Koch CJ, Patel S, *et al.* Tumor vascular changes mediated by inhibition of oncogenic signaling. Cancer Res **2009**;69(15):6347-54 doi 10.1158/0008-5472.CAN-09-0657.

9. Fokas E, Im JH, Hill S, Yameen S, Stratford M, Beech J, *et al.* Dual inhibition of the PI3K/mTOR pathway increases tumor radiosensitivity by normalizing tumor vasculature. Cancer Res **2012**;72(1):239-48 doi 10.1158/0008-5472.CAN-11-2263.

10. Tipton K, Launders JH, Inamdar R, Miyamoto C, Schoelles K. Stereotactic body radiation therapy: scope of the literature. Ann Intern Med **2011**;154(11):737-45 doi 10.7326/0003-4819-154-11-201106070-00343.

11. Higgins GS, O'Cathail SM, Muschel RJ, McKenna WG. Drug radiotherapy combinations: review of previous failures and reasons for future optimism. Cancer Treat Rev **2015**;41(2):105-13 doi 10.1016/j.ctrv.2014.12.012.

12. Duarte CD, Greferath R, Nicolau C, Lehn JM. myo-Inositol trispyrophosphate: a novel allosteric effector of hemoglobin with high permeation selectivity across the red blood cell plasma membrane. Chembiochem **2010**;11(18):2543-8 doi 10.1002/cbic.201000499.

13. Fylaktakidou KC, Lehn JM, Greferath R, Nicolau C. Inositol tripyrophosphate: a new membrane permeant allosteric effector of haemoglobin. Bioorg Med Chem Lett **2005**;15(6):1605-8 doi 10.1016/j.bmcl.2005.01.064.

14. Raykov Z, Grekova SP, Bour G, Lehn JM, Giese NA, Nicolau C, *et al.* Myo-inositol trispyrophosphate-mediated hypoxia reversion controls pancreatic cancer in rodents and enhances gemcitabine efficacy. Int J Cancer **2014**;134(11):2572-82 doi 10.1002/ijc.28597.

15. Kieda C, El Hafny-Rahbi B, Collet G, Lamerant-Fayel N, Grillon C, Guichard A, *et al.* Stable tumor vessel normalization with pO(2) increase and endothelial PTEN activation by inositol trispyrophosphate brings novel tumor treatment. J Mol Med (Berl) **2013**;91(7):883-99 doi 10.1007/s00109-013-0992-6.

16. Franken NA, Rodermond HM, Stap J, Haveman J, van Bree C. Clonogenic assay of cells in vitro. Nat Protoc **2006**;1(5):2315-9 doi 10.1038/nprot.2006.339.

17. Orlowski K, Bley CR, Zimmermann M, Van V, Hug D, Soltermann A, *et al.* Dynamics of Tumor Hypoxia in Response to Patupilone and Ionizing Radiation. Plos One **2012**;7(12) doi 10.1371/journal.pone.0051476.

18. Fokas E, Hanze J, Kamlah F, Eul BG, Lang N, Keil B, *et al.* Irradiation-dependent effects on tumor perfusion and endogenous and exogenous hypoxia markers in an A549 xenograft model. Int J Radiat Oncol Biol Phys **2010**;77(5):1500-8 doi 10.1016/j.ijrobp.2010.01.060.

19. Maftei CA, Bayer C, Shi K, Vaupel P. Intra- and intertumor heterogeneities in total, chronic, and acute hypoxia in xenografted squamous cell carcinomas. Detection and quantification using (immuno-)fluorescence techniques. Strahlenther Onkol **2012**;188(7):606-15 doi 10.1007/s00066-012-0105-4.

20. Toulany M, Rodemann HP. Phosphatidylinositol 3-kinase/Akt signaling as a key mediator of tumor cell responsiveness to radiation. Semin Cancer Biol **2015**;35:180-90 doi 10.1016/j.semcancer.2015.07.003.

21. Tanno S, Yanagawa N, Habiro A, Koizumi K, Nakano Y, Osanai M, *et al.* Serine/threonine kinase AKT is frequently activated in human bile duct cancer and is associated with increased radioresistance. Cancer Res **2004**;64(10):3486-90 doi 10.1158/0008-5472.CAN-03-1788.

22. Menegakis A, Eicheler W, Yaromina A, Thames HD, Krause M, Baumann M. Residual DNA double strand breaks in perfused but not in unperfused areas determine different radiosensitivity of tumours. Radiother Oncol **2011**;100(1):137-44 doi 10.1016/j.radonc.2011.07.001.

23. Menegakis A, von Neubeck C, Yaromina A, Thames H, Hering S, Hennenlotter J, *et al.* gammaH2AX assay in ex vivo irradiated tumour specimens: A novel method to determine tumour radiation sensitivity in patient-derived material. Radiother Oncol **2015**;116(3):473-9 doi 10.1016/j.radonc.2015.03.026.

24. El Kaffas A, Giles A, Czarnota GJ. Dose-dependent response of tumor vasculature to radiation therapy in combination with Sunitinib depicted by three-dimensional high-frequency power Doppler ultrasound. Angiogenesis **2013**;16(2):443-54 doi 10.1007/s10456-012-9329-2.

25. Song CW, Lee YJ, Griffin RJ, Park I, Koonce NA, Hui S, *et al.* Indirect Tumor Cell Death After High-Dose Hypofractionated Irradiation: Implications for Stereotactic Body Radiation Therapy and Stereotactic Radiation Surgery. Int J Radiat Oncol Biol Phys **2015**;93(1):166-72 doi 10.1016/j.ijrobp.2015.05.016.

26. Overgaard J, Hansen HS, Andersen AP, Hjelm-Hansen M, Jorgensen K, Sandberg E, *et al.* Misonidazole combined with split-course radiotherapy in the treatment of invasive carcinoma of larynx and pharynx: report from the DAHANCA 2 study. Int J Radiat Oncol Biol Phys **1989**;16(4):1065-8.

27. Overgaard J, Hansen HS, Overgaard M, Bastholt L, Berthelsen A, Specht L, *et al.* A randomized double-blind phase III study of nimorazole as a hypoxic radiosensitizer of primary radiotherapy in supraglottic larynx and pharynx carcinoma. Results of the Danish Head and Neck Cancer Study (DAHANCA) Protocol 5-85. Radiother Oncol **1998**;46(2):135-46.

28. Hoskin PJ, Rojas AM, Bentzen SM, Saunders MI. Radiotherapy with concurrent carbogen and nicotinamide in bladder carcinoma. J Clin Oncol **2010**;28(33):4912-8 doi 10.1200/JCO.2010.28.4950.

29. Tap WD, Papai Z, Van Tine BA, Attia S, Ganjoo KN, Jones RL, *et al.* Doxorubicin plus evofosfamide versus doxorubicin alone in locally advanced, unresectable or metastatic soft-tissue sarcoma (TH CR-406/SARC021): an international, multicentre, open-label, randomised phase 3 trial. Lancet Oncol **2017**;18(8):1089-103 doi 10.1016/S1470-2045(17)30381-9.

30. Filatenkov A, Baker J, Mueller AM, Kenkel J, Ahn GO, Dutt S, *et al.* Ablative Tumor Radiation Can Change the Tumor Immune Cell Microenvironment to Induce Durable Complete Remissions. Clin Cancer Res **2015**;21(16):3727-39 doi 10.1158/1078-0432.CCR-14-2824.

31. Iyengar S, Schwartz D. Failure of Inositol Trispyrophosphate to Enhance Highly Effective Radiotherapy of GL261 Glioblastoma in Mice. Anticancer Res **2017**;37(3):1121-5 doi 10.21873/anticanres.11425.

32. Fornvik K, Zolfaghari S, Salford LG, Redebrandt HN. ITPP Treatment of RG2 Glioblastoma in a Rat Model. Anticancer Res **2016**;36(11):5751-5 doi 10.21873/anticanres.11158.

Fig.1

PBS

ITPP

A

A549

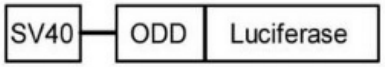

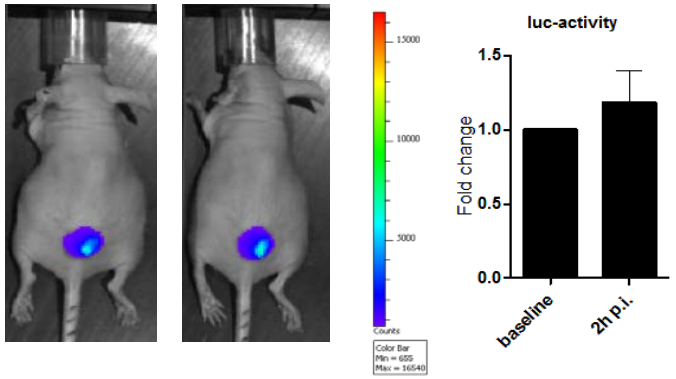

baseline 2h p.i.

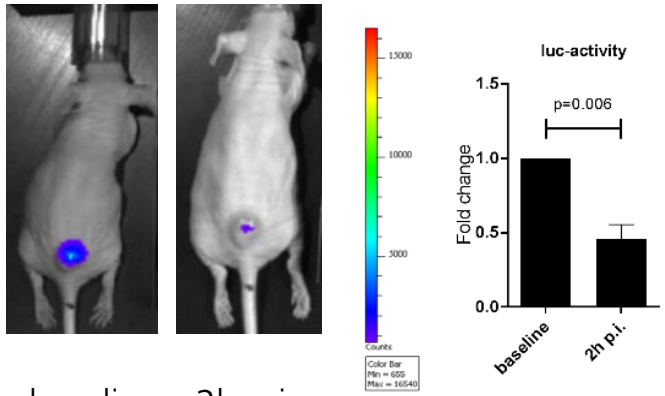

baseline 2h p.i.

B

A549

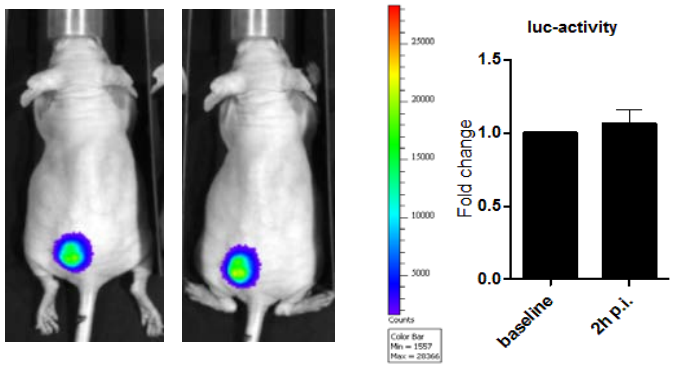

baseline 2h p.i.

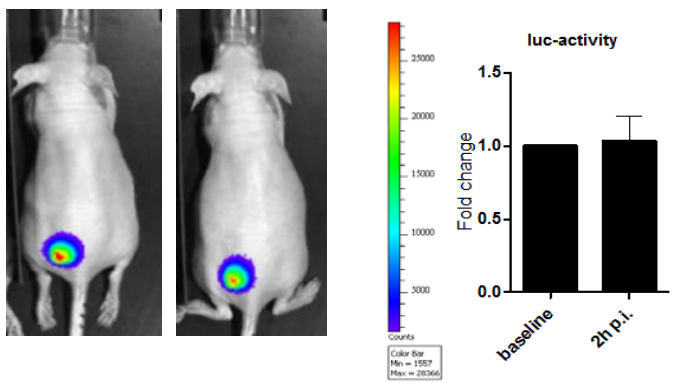

baseline 2h p.i.

C

FaDu

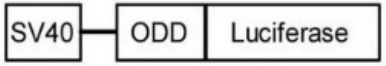

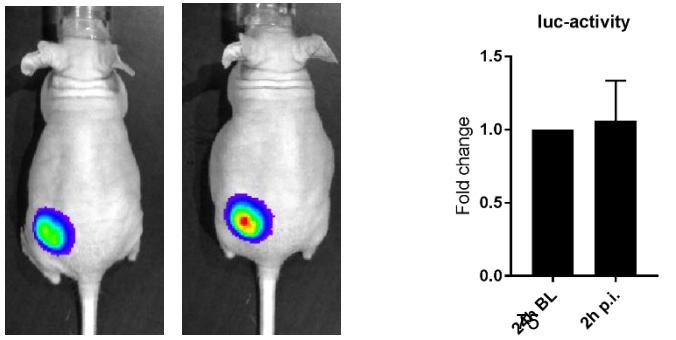

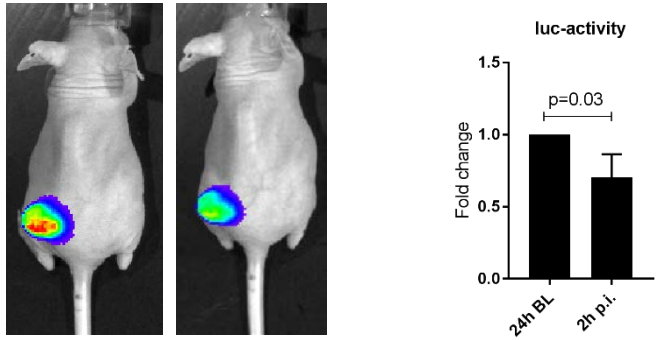

Fig.2

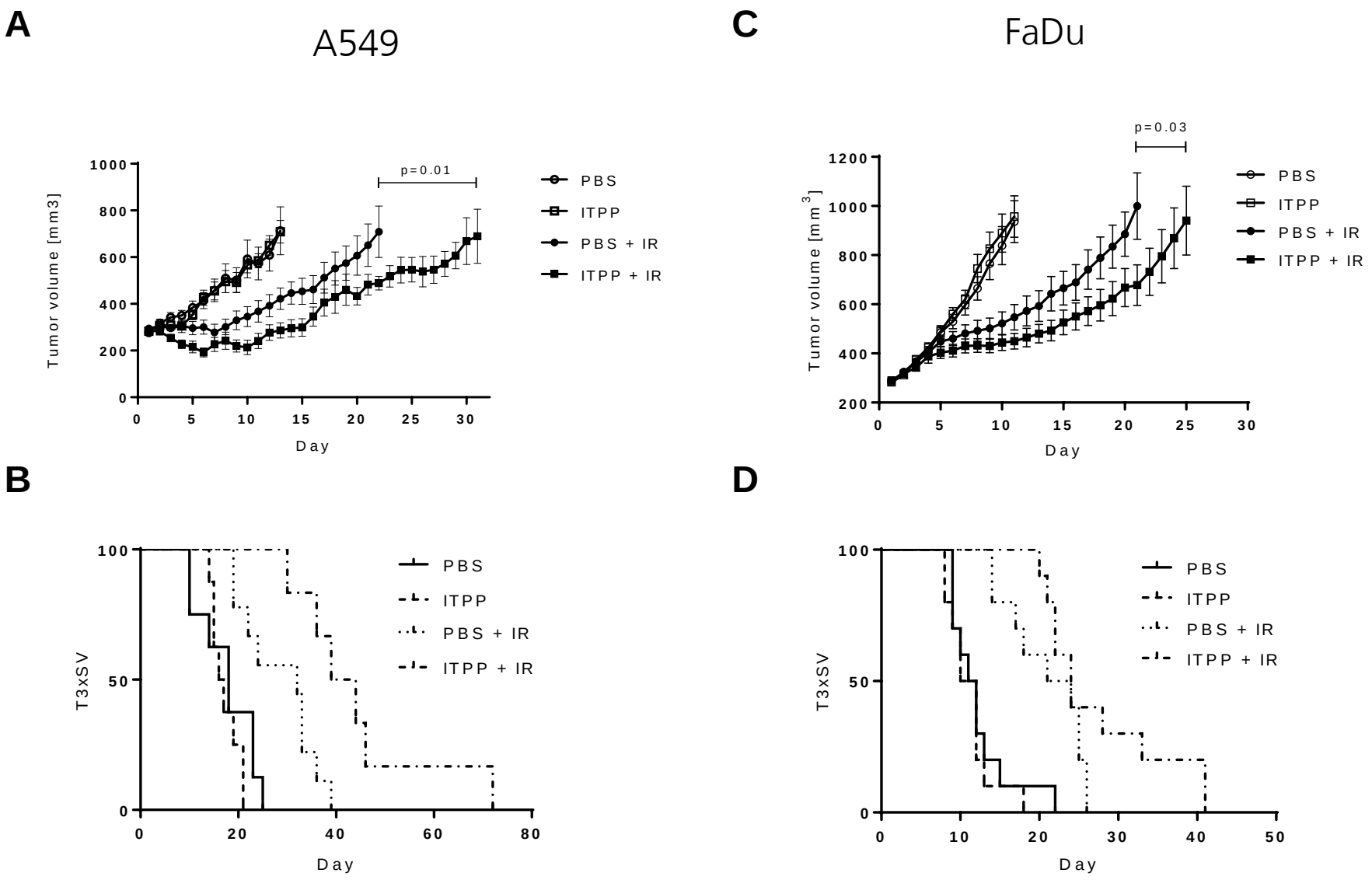
A
A549
Tumor volume [mm3]
Day
p=0.01
PBS
ITPP
PBS + IR
ITPP + IR
B
T3xSV
Day
PBS
ITPP
PBS + IR
ITPP + IR
C
FaDu
Tumor volume [mm3]
Day
p=0.03
PBS
ITPP
PBS + IR
ITPP + IR
D
T3xSV
Day
PBS
ITPP
PBS + IR
ITPP + IR

Fig.3

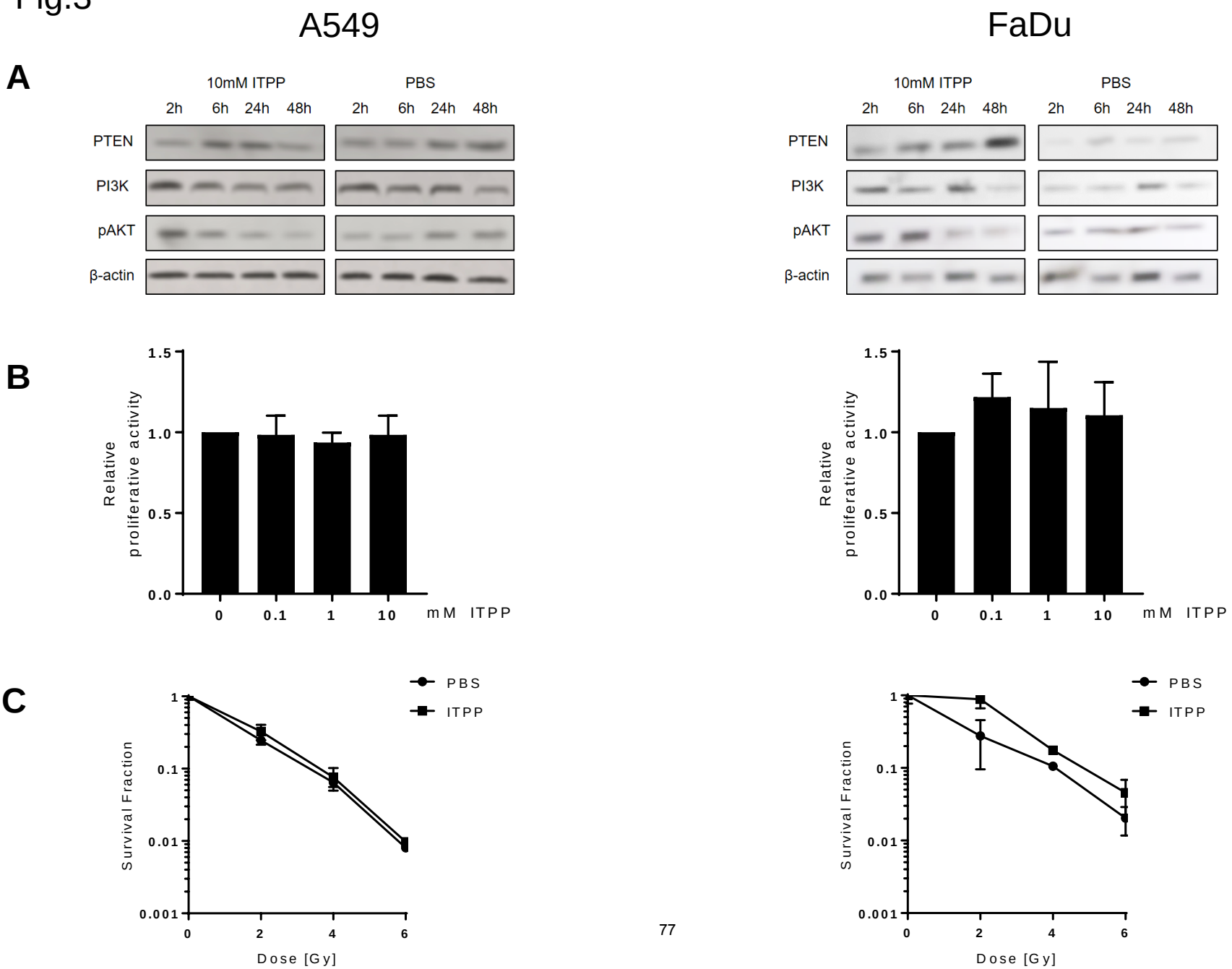
A549
FaDu
A
10mM ITPP
PBS
2h 6h 24h 48h 2h 6h 24h 48h
PTEN
PI3K
pAKT
β-actin
B
Relative proliferative activity
1.5
1.0
0.5
0.0
0 0.1 1 10 mM ITPP
C
PBS
ITPP
Survival Fraction
1
0.1
0.01
0.001
0 2 4 6
Dose [Gy]

Fig.4

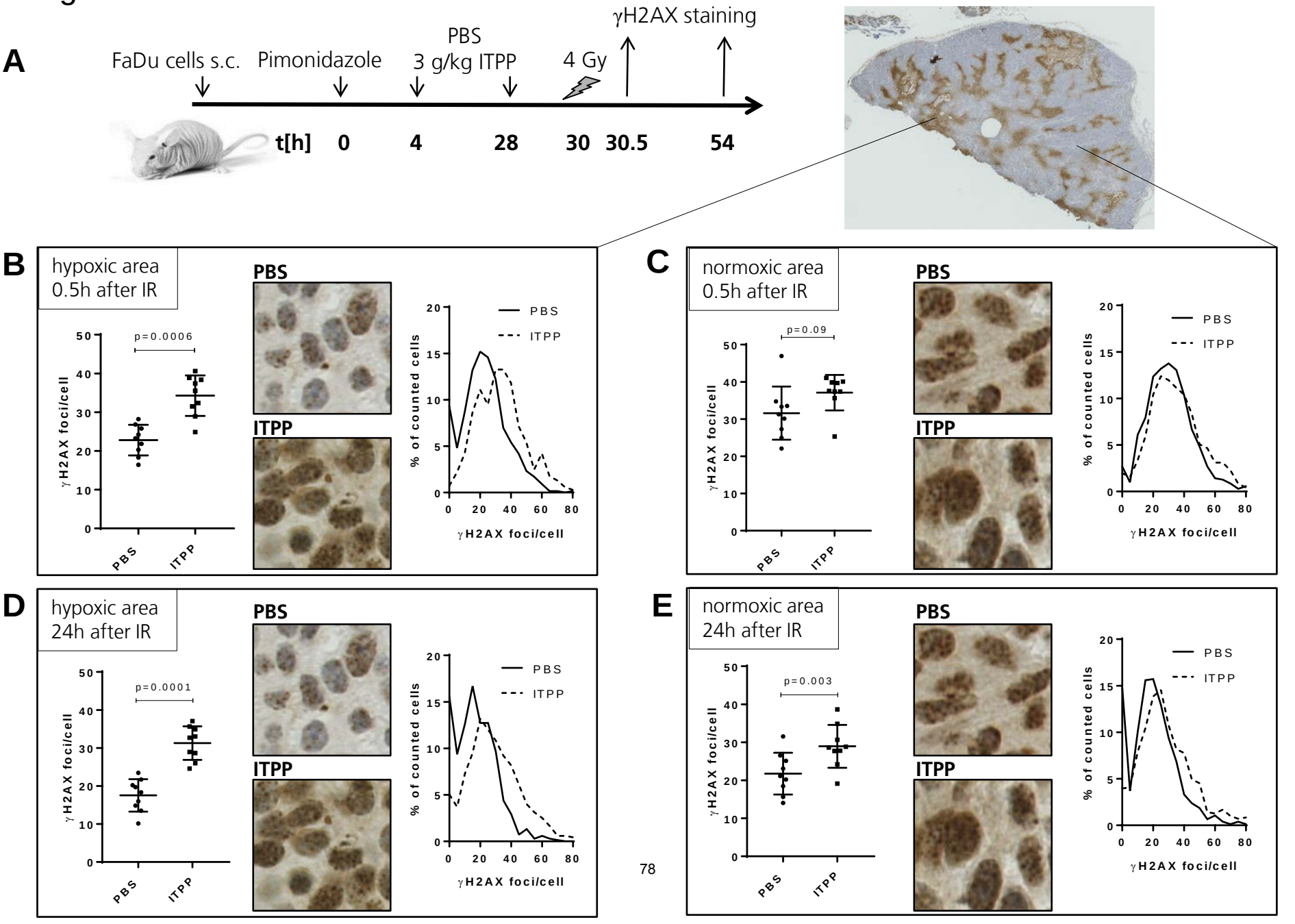
A
FaDu cells s.c.
Pimonidazole
PBS
3 g/kg ITPP
4 Gy
γH2AX staining
t[h]
0
4
28
30
30.5
54
B
hypoxic area
0.5h after IR
PBS
ITPP
p=0.0006
γH2AX foci/cell
% of counted cells
C
normoxic area
0.5h after IR
p=0.09
D
hypoxic area
24h after IR
p=0.0001
E
normoxic area
24h after IR
p=0.003

Fig.5

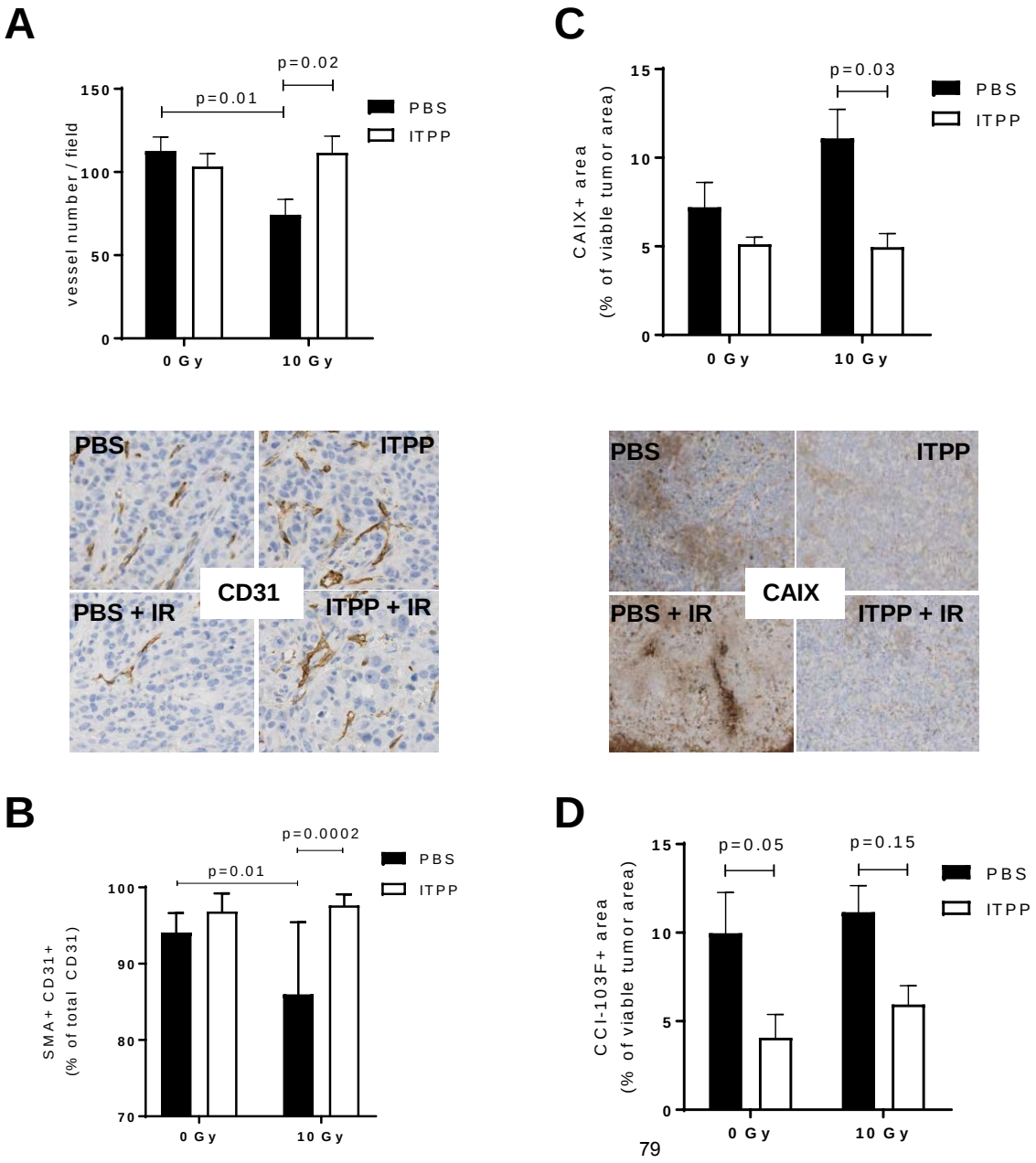
A
p=0.02
p=0.01
PBS
ITPP
vessel number / field
150
100
50
0
0 Gy
10 Gy
C
p=0.03
PBS
ITPP
CAIX+ area
(% of viable tumor area)
15
10
5
0
0 Gy
10 Gy
PBS
ITPP
CD31
PBS + IR
ITPP + IR
PBS
ITPP
CAIX
PBS + IR
ITPP + IR
B
p=0.0002
p=0.01
PBS
ITPP
SMA+ CD31+
(% of total CD31)
100
90
80
70
0 Gy
10 Gy
D
p=0.05
p=0.15
PBS
ITPP
CCI-103F+ area
(% of viable tumor area)
15
10
5
0
0 Gy
10 Gy

Fig.6

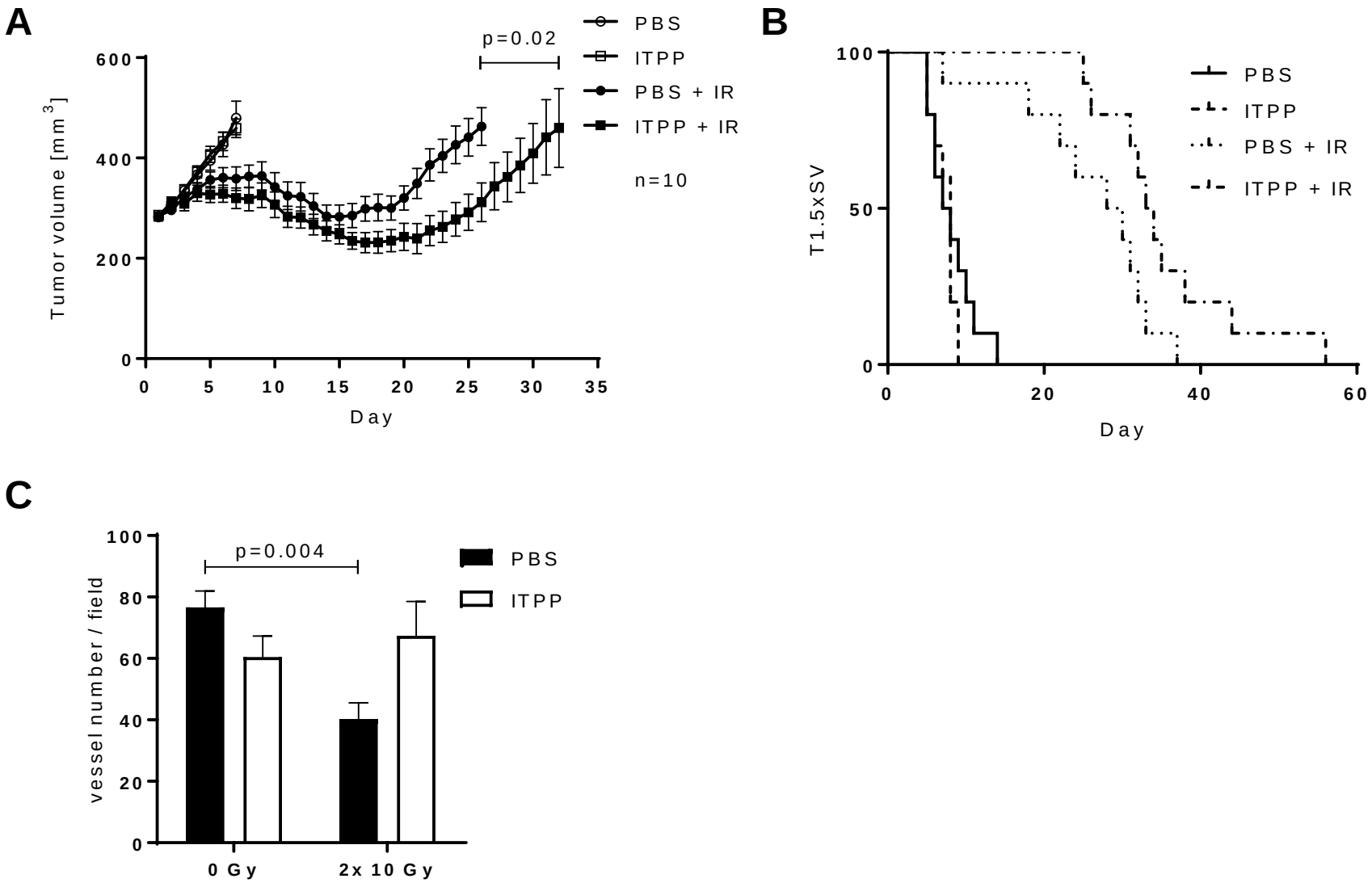
A
p=0.02
PBS
ITPP
PBS + IR
ITPP + IR
n=10
Tumor volume [mm3]
600
400
200
0
0
5
10
15
20
25
30
35
Day
B
100
50
0
T1.5xSV
0
20
40
60
Day
PBS
ITPP
PBS + IR
ITPP + IR
C
p=0.004
PBS
ITPP
vessel number / field
100
80
60
40
20
0
0 Gy
2x 10 Gy

Supplementary Fig. S1

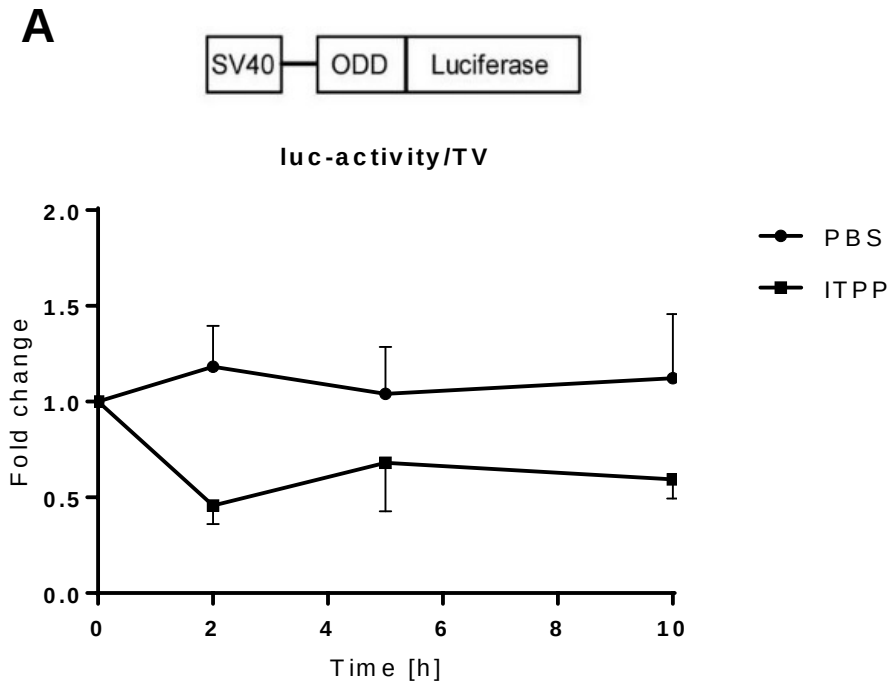

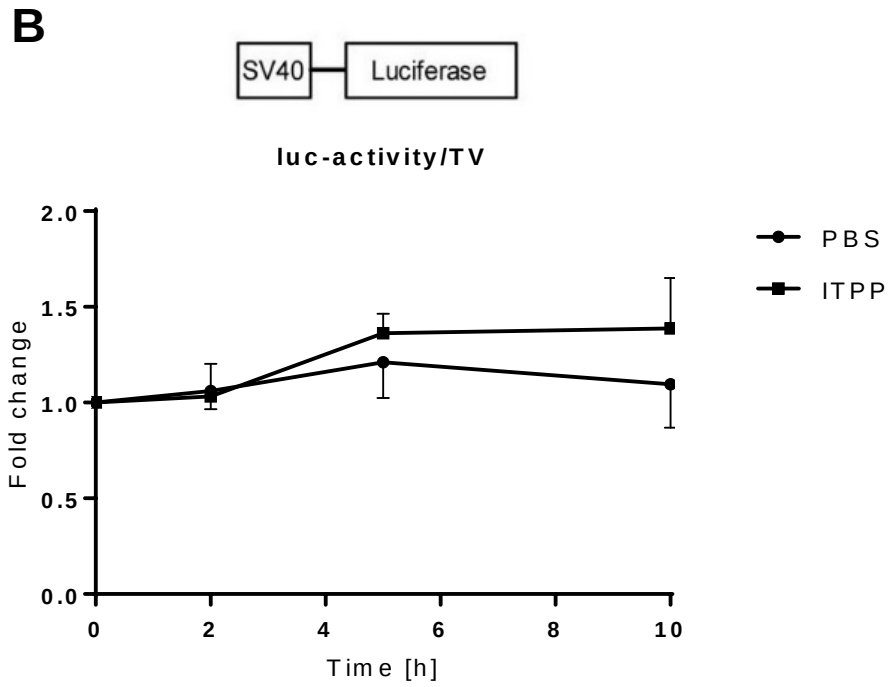

Supplementary Fig. S2

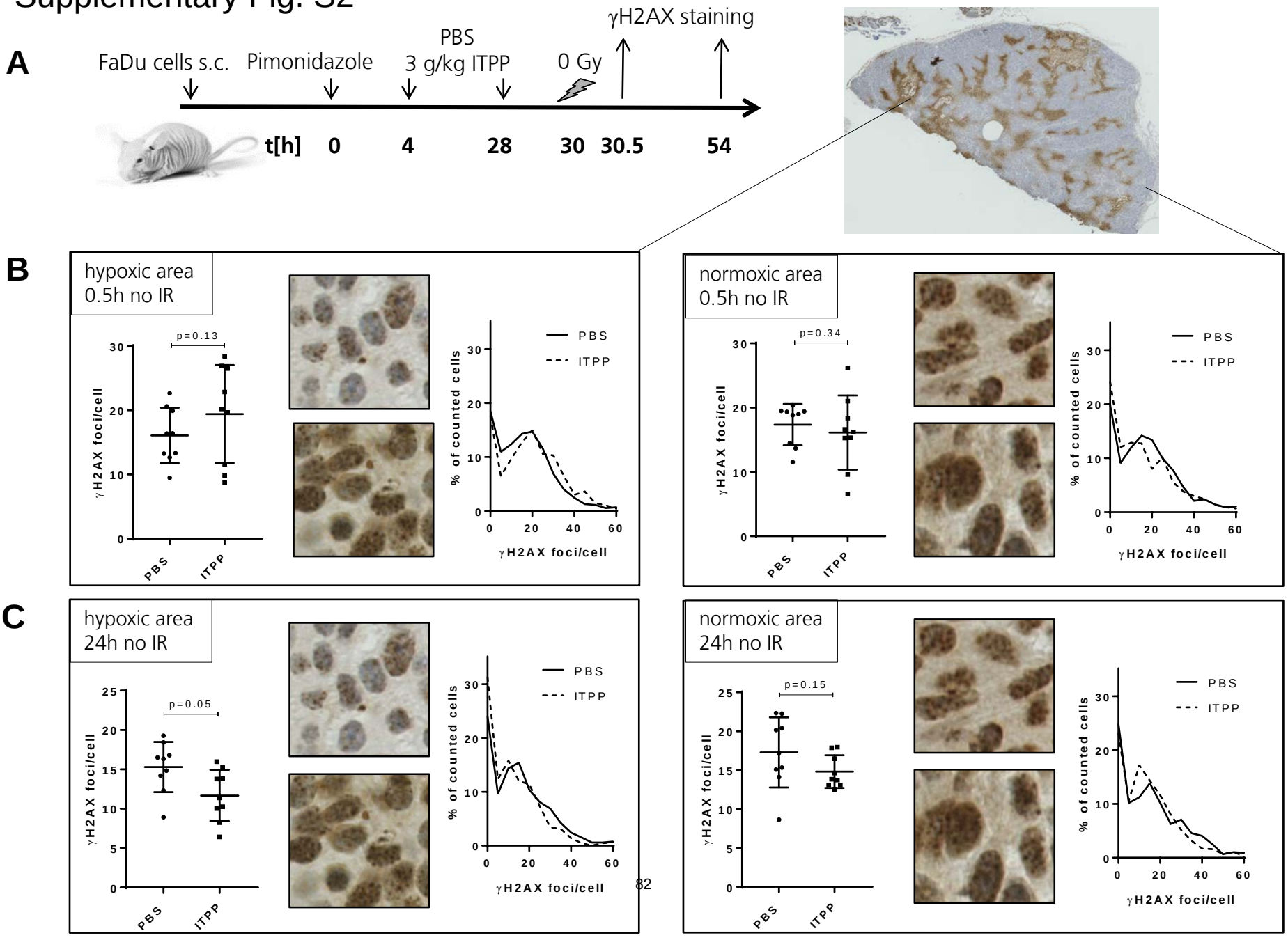

Supplementary Fig. S3

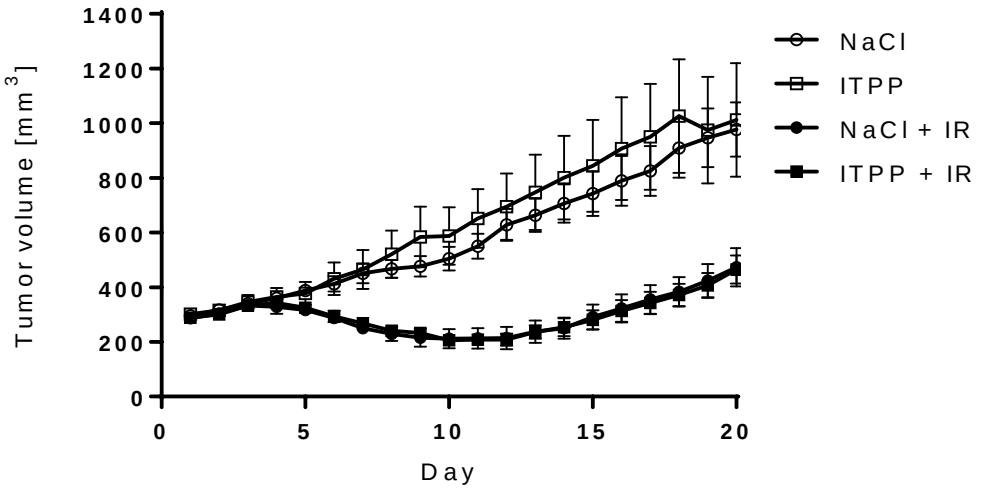

3.3 Image-guided radiotherapy of murine colorectal liver metastases

Nathalie Borgeaud[1*], Ivo Grgic[2*], Jérôme Krayenbühl[2], Matthias Guckenberger[2], P.A. Clavien[1], Rolf Graf[1], Martin Pruschy[2]

* contributed equally

[1]Laboratory of the Swiss-Hepato-Pancreatico-biliary (HPB) Centre, Dept. of Visceral Surgery, University Hospital Zurich, University Zurich

[2]Laboratory for Applied Radiobiology, Dept. Radiation Oncology University Hospital Zurich, University Zurich

Status of the manuscript: In preparation for submission

Author contribution I. Grgic:

- Planning, data acquisition, analysis and interpretation of the experiments
- Fig.2 – all
- Fig.3 – all
- Fig.5 – a
- Writing of the manuscript

Image-guided radiotherapy of murine colorectal liver metastases

Nathalie Borgeaud[1*], Ivo Grgic[2*], Jérôme Krayenbühl[2], Matthias Guckenberger[2], P.A. Clavien[1], Martin Pruschy[2], Rolf Graf[1]

* contributed equally

[1]Laboratory of the Swiss-Hepato-Pancreatico-biliary (HPB) Centre, Dept. of Visceral Surgery, University Hospital Zurich, University Zurich

[2]Laboratory for Applied Radiobiology, Dept. Radiation Oncology University Hospital Zurich, University Zurich

Corresponding Author: Prof. Dr. Rolf Graf

Key words: colorectal liver metastases, small animal image guided radiotherapy, MRI

Word count: 2892

Abstract word count: 199

Pages: 8

Abstract

Background and purpose: The treatment of colorectal liver metastases by SBRT is currently under clinical investigation. Remarkably, this exact treatment approach has not yet been reported on the preclinical level. Here, we developed an irradiation strategy for murine colorectal liver metastases that enables to study combined treatment modalities and thereby improve the treatment options in the clinical situation.

Materials and methods: We generated an animal model for colorectal liver metastases, affecting exclusively the right liver lobe by selective portal vein injection of murine MC-38 colon carcinoma cells. The metastasized liver lobe was visualized by contrast-enhanced cone beam CT imaging and irradiated with an image-guided small animal radiotherapy platform. MRI was applied to follow volumetric changes in colorectal liver metastases after SBRT.

Results: Selective intraportal injection of colorectal cancer cells yields a high rate in liver metastasis formation. Targeted irradiation of the right liver lobe with single fractions of 10 and 15 Gy is effective in reducing the growth of metastatic lesions without causing radiation-induced toxicities.

Conclusion: We present a robust and reproducible preclinical colorectal liver metastases model and image-guided irradiation strategy to study combined treatment approaches *in vivo* with the perspective to translate the results from bench to bedside.

Introduction

Colorectal cancer (CRC) is the third most common cancer worldwide and ranked fourth in cancer mortality. It shows higher incidence rates in developed countries and in the male population [1]. CRC cells metastasize to different organs. Caused by the portal circulation, the liver is the most frequent organ acquiring colorectal metastases (CLM) and accounts for 70 % of the metastatic lesions in CRC patients [2]. Surgical resection is the most effective treatment option for colorectal liver metastases, but depending on location, size and number of metastases, only a minority of patients are eligible for surgery [3, 4]. Metastases that cannot be surgically resected are treated with systemic or local chemotherapy and if possible with radiofrequency ablation (RFA) [5, 6]. However, the success of these therapies often remains insufficient [7, 8]. Conventional radiotherapy of hepatic tumor lesions has only played a very limited role, as radiotoxicity in the non-tumorous liver tissue often leads to radiation-induced liver disease (RILD) [9]. However, with the development of stereotactic body radiation therapy (SBRT) it is nowadays possible to precisely deliver conformal high doses of ionizing radiation (IR) to the tumor without overly compromising the healthy surrounding tissue [10]. A prospective phase II clinical trial, investigating SBRT of patients with inoperable colorectal liver metastases demonstrated optimal local control and promising overall survival rates without causing RILD or other severe radiation-induced complications [11]. To further understand and improve SBRT of colorectal liver metastases, preclinical animal models that accurately represent the clinical situation have to be investigated. Numerous rodent models wherein cancer cells are injected to the cecal wall and thereby resemble primary colorectal tumors in patients have been described. Unfortunately, only few of the models succeed to specifically metastasize to the liver or have an unpractically low penetrance rate and long incubation time [12, 13]. Other routes of CRC cell injections include the spleen, portal vein or the hepatic parenchyma [14-16]. As opposed to intrasplenic or hepatic injection, the portal route mimics vascular spread and limits the risk of tumor growth at other intra-abdominal organs than the liver [17]. In recent years, the field of small-animal image-guided radiotherapy has made tremendous progress. CT-based treatment planning with Monte Carlo dose calculation, followed by static or dynamic irradiation enables to precisely treat very small structures in animal models [18].

In this study, we generated an animal model to study the orthotopic irradiation of colorectal liver metastases with SBRT. Contrast-enhanced cone beam CT (CBCT) and histological characterization of IR-induced cellular damage were employed to achieve an optimal balance between tumor targeting and sparing of surrounding healthy organs. To follow volumetric changes in colorectal liver metastases after SBRT, we used MRI.

Material and Methods

Cell culture

The murine colorectal cancer cell line MC-38, a kind gift from Prof. B. Becher (Institute of Experimental Immunology, University of Zürich), was cultured in DMEM cell culture medium supplemented with L-glutamine (GlutaMAX, Life Technologies), 10% FBS and 1% penicillin-streptomycin at 37°C in 5% CO_2. MC-38 cells have been tested negative for mycoplasma (Mycoplasma Detection Kit, Lonza). Cell number and cell viability were determined using an automated cell counter (NucleoCounter® NC-200 ™, Chemometec).

Orthotopic colorectal liver metastases model

MC-38 cells were orthotopically transplanted to the liver of 8-week old, female C57BL/6 mice (Envigo). The surgical protocol was adapted from Limani et al. [19]. Before laparatomy, Buprenorphine (0.1 mg/kg, subcutaneous) was preoperatively administered and anesthesia was induced by isoflurane inhalation. The caudate liver lobe was detached from ligaments and completely resected and a microvascular clamp was applied to the portal triad, supplying the left and median liver lobes. For injection, exponentially growing MC-38 cells (2×10^5 cells/100 µL PBS) were injected in the portal vein (29G needle). Hemorrhagic control was performed using TachoSil and by compression with cotton swabs. The clamp was removed and the abdominal walls were closed by sutures. After surgery, animals were allowed to recover on a warming pad in a separate cage until completely conscious. For pain relief, buprenorphine was injected after surgery every 3-6 hours. All animals were maintained under specific pathogen-free conditions. All experiments were performed in accordance with Swiss Federal Animal Regulations and approved by the Veterinary Office of Zurich.

Image-guided radiotherapy

An image-guided small animal radiotherapy platform (Precision X-Ray, X-Rad SmART) 225 kV unit with a dose rate of 3 Gy/min, equipped with a cone beam CT (CBCT) scanner was used for mouse irradiation. Animals were kept under isoflurane anesthesia for imaging and irradiation. Fenestra LC or Fenestra VC (MediLumine ™) contrast-enhancing agent, specifically taken up by hepatocytes, was intraperitoneally (LC) or intravenously (VC) injected at a concentration of 8 ml/kg at least 2 hours prior to CBCT-imaging.

Blood serum analysis

Serum albumin, bilirubin, alanine aminotransferase (ALT) and aspartate aminotransferase (AST) levels were measured with a multiple biochemical analyzer (Fudji Dri-Chem 4000i).

MRI

MRI was conducted on a 4.7 T/16 cm Bruker PharmaScan small animal scanner (Bruker BioSpin) equipped with a transmit/receive 40 mm bird-cage resonator. After anatomical reference images were obtained in coronal, transversal and sagittal slice orientations (FLASH sequence, TR/TE 200/3 ms, image matrix size 128 x 128, FOV 60 x 60 mm^2, 5 slices) T2-weighted images were collected with a fat-suppressed RARE sequence (TEeff/TR 22/2950 ms, NA 4, RARE Factor 4, matrix size 256 x 256, FOV 30 x 30 mm^2) from 40 axial slices at a spatial resolution of 117x117x500 μm^3. During MRI, mice were placed in supine position onto a heated animal bed and maintained under isoflurane anesthesia. Image analysis was performed with the OsiriX DICOM viewer.

Immunohistochemistry

Immunohistological endpoints were analyzed on formalin-fixed paraffin-embedded (FFPE) 3 µm tissue sections for hematoxyline & eosine (H&E) and γH2AX (1:1000, Cell Signaling, 20E3). Images were taken on a wide-field Nikon Eclipse TI microscope.

Statistical analysis

The effects of IR on relative animal weight and colorectal liver metastases volume changes were analyzed by one-way ANOVA with Tukey post test. For the analysis of serum markers, values were first tested for normal distribution by the Shapiro-Wilk test and subsequently compared by t-test or Mann-Whitney test. Statistical analyses were performed using GraphPad Prism v7.

Results

Portal vein injection is a powerful tool to study colorectal liver metastases

MC-38 cells were orthotopically transplanted to the liver of female C57BL/6 mice via the portal vein. In 90% of the operated mice, colorectal liver metastases developed successfully in the right liver lobe. H&E staining could differentiate colorectal liver metastases from the healthy hepatic tissue (Fig. 1E). The most frequent complication was hemorrhagic bleeding after intraportal cell injection caused by increased portal pressure after clamping of the portal vein and removal of the caudate liver lobe. Portal bleeding provoked intraperitoneal carcinomatosis and approximately 10 % of the mice died after surgery.

Abdominal organs have approximately the same tissue density and discrimination of the liver from other organs by conventional CT-imaging is hampered (Fig. 2A). To overcome this challenge, two different liver-specific contrast agents were tested (Fenestra LC & VC). Intraperitoneal administration of the LC contrast agent distincted the liver from its surrounding organs already 80 minutes after injection (Fig. 2B) and remained active for up to 7 hours after

injection (Fig. 2C). The VC contrast agent was equally potent in distinguishing the liver from other organs at 7 hours after injection but was not active at 80 minutes after administration (data not shown). In addition, both contrast agents showed unspecific uptake in the spleen.
Since these contrast agents are only taken up by hepatocytes and not colorectal tumor-derived carcinoma cells, metastatic nodules should be distinguishable from the healthy liver. However, presumably caused by the low resolution of the CT scans, could not detect colorectal liver metastases in the tumor-bearing liver lobe. In some liver scans, we observed structures without contrast-enhancement but we could not reliably determine whether these are colorectal liver metastases or parts of the small intestine.
Overall, these results demonstrate that the contrast of the liver can be enhanced by Fenestra contrast agents in a time-dependent manner and thereby facilitate treatment planning. (Due to the favorable pharmacokinetics, we decided to perform the following experiments with the Fenestra LC contrast agent).

The right liver lobe can be targeted with acceptable healthy tissue involvement

In order to define a treatment plan with maximal tumor coverage and minimal normal tissue toxicity different irradiation approaches were designed. The entire tumor-bearing liver lobe was planned for irradiation, since single metastases were not accurately detectable by contrast-enhanced CT-imaging. Due to the lack of a multileaf collimator and the inability to control for breathing-related liver movements irradiation of the tumor-bearing liver lobe was performed with a rectangular collimator (8 x 12 mm).
Dose-volume histograms (DVHs) of different irradiation plans were calculated for the tumor-bearing liver lobe and the relevant organs at risk, which included the healthy liver, the right kidney and the stomach. The small intestine and the colon could not be included in the calculations, as their clear differentiation on a CT scan is impossible (Fig. 3A).
Maximal tumor coverage was achieved when two opposing beams (AP/PA) were planned. The directly adjacent right kidney thereby receives approximately the same dose as the tumor-bearing liver lobe. As this lobe corresponds to only approximately 20 % of the whole liver, the dose to the remaining healthy liver was relatively low. The angle of the two opposing beams could be positioned in a way to almost completely spare the stomach from ionizing radiation (Fig. 3B). More complex irradiation plans e.g. arc-beam therapy, wherein the respective liver lobe is targeted with a 360°-rotating radiation beam were inferior. In such a protocol, the median dose to the tumor was reduced by approximately 1.2 fold but at the same time the median dose to the healthy liver and to the stomach were strongly increased (9 and 20 fold, respectively). On the other hand, arc beam therapy favored the dose deposition to the kidney, by delivering a 1.4 fold lower dose.
Therefore, the AP/PA irradiation approach was used for tumor irradiation compromising best tumor coverage and healthy tissue sparing.

The *in silico* treatment plan successfully translates to the biological readout of DNA damage

In a test cohort of healthy mice, different liver segments were histologically analyzed one hour after irradiation for IR-induced γH2AX-foci formation as a marker for IR-induced DNA double strand breaks. Dense staining of γH2AX-foci was detectable in the right liver lobe (Fig. 4C). Staining intensity of γH2AX-foci in other liver segments further decreased proportionally to the distance from the treatment planning volume, e.g. an intermediately-intense staining was detectable in the middle liver lobe, which is anatomically in close proximity to the right lobe, whereas the left liver lobe was free from γH2AX-foci (Fig. 4A, B). Thereby, we demonstrated that we could precisely deliver ionizing radiation and its accompanying DNA damaging potential towards colorectal liver metastases.

Irradiation of the right liver lobe with doses above 20 Gy is hepatotoxic

In order to determine the maximally tolerated dose of IR and potential late-phase toxicities, e.g. RILD, the right liver in a cohort of metastases-free, healthy mice was irradiated with single fractions of either 0, 20 or 30 Gy. As a potent surrogate marker for animal well-being, body weights were regularly monitored after irradiation. While sham-irradiated mice gained in body weight, body weight drastically decreased in mice irradiated with a single dose of 20 or 30 Gy (0 Gy vs. 20 Gy: p= 0.003, 0 Gy vs. 30 Gy: p= 0.0006) (Fig. 5A). Furthermore, two out of four mice irradiated with 30 Gy were found dead at 44 and 48 days after irradiation respectively. To investigate liver functional parameters, the serum concentrations of alanine transaminase (ALT), aspartate transaminase (AST), bilirubin and albumin was determined in mice 50 days after irradiation. As compared to sham-irradiated mice, the AST levels were 2.5-fold (p= 0.01) and the ALT levels 1.3-fold (p= 0.11) increased in mice irradiated with 20 Gy, indicating hepatic inflammation (Fig. 5B, C). Whereas bilirubin levels were not affected, the concentration of serum albumin was 2-fold (p= 0.002) decreased after irradiation with 20 Gy (Fig. 5D, E). As albumin is produced and secreted by the liver, these results indicate liver impairment. Since only two mice remained in the group irradiated with 30 Gy at this time point, their values were excluded for the analysis. Overall, irradiation of the right liver lobe with s single fraction equal or higher than 20 Gy is hepatotoxic and potentially lethal for the female C57bl6 mouse model (see discussion below).

IR dose-dependently reduces the growth of colorectal liver metastases

An IR-dose-response tumor growth delay experiment was performed in metastases-bearing mice. Metastases could be detected in the right liver lobe by MRI 14 days after surgical implantation. At day 15, the right liver lobe of mice was irradiated with increasing single doses

from 0 to 15 Gy. Once weekly, the mice were scanned by MRI to monitor the cumulative change in tumor volume after irradiation (Fig. 6A). As determined by relative weight change, all doses were well tolerated throughout the course of the experiment (Fig. 6B). Irradiation of the right liver lobe successfully reduced the growth of colorectal liver metastases in a dose-dependent manner. While the cumulative metastasis-volume of unirradiated mice increased by 22-fold within 2 weeks, irradiation with 10 Gy increased the volume only by 4-fold ($p= 0.05$). Furthermore, irradiation with a single fraction of 15 Gy even decreased the volume by 1.2-fold ($p= 0.02$) at the same time point (Fig. 6C, D).

Overall, our results demonstrate that stereotactic irradiation of colorectal liver metastases is feasible and effective also on the preclinical level. This approach enables to study combined treatment modalities against CLMs *in vivo,* to further decrease the radiation dose delivered to the radiosensitive liver thereby reducing normal tissue toxicities.

Discussion

Stereotactic radiotherapy is an emerging approach for the treatment of patients suffering from non-resectable colorectal liver metastases. Although it is already being investigated in clinical routine for over a decade, to our best understanding no studies have been performed on the preclinical level. Up to now, targeted irradiation to orthotopic CLMs in rodents was only applied by brachytherapy [20]. Owing to fundamental progress in small-animal image-guided radiotherapy, it is nowadays adequate to translate preclinical SBRT results into clinical practice.

In this study, we present a highly reproducible mouse model to study SBRT of CLMs. The liver is a comparably radiosensitive organ and application of high IR-doses often leads to RILD [21]. Our model restricts CLM formation to the right liver lobe, which enables selective ablation of a small liver fraction (approximately 20 % of the total liver) and thereby decreases hepatotoxicity in the remaining healthy liver. In addition, removal of the caudate liver lobe prevents co-irradiation of the stomach, which is anatomically covering the caudate liver lobe. Contrast-enhanced CT imaging, clearly delineating the metastatic liver lobe, further reduced unnecessary involvement of healthy liver tissue. Furthermore, it strongly facilitated the recognition of other abdominal organs and allowed to generate a DVH of the relevant organs at risk. We ascertained selective liver lobe irradiation by Monte-Carlo based dose calculations and by immunohistochemical analyisis of DNA DSBs in different liver lobes.

Wu et al. aimed to define the exact doses that result in hepatotoxicity in healthy mice and observed significant changes in RILD parameters when the whole liver was irradiated with single fractions of 25 Gy or higher [22]. Based on these results we designed a dose-escalation study in our CLM model. Interestingly and considering that we only irradiated 20 % of the liver, significant weight loss and RILD signs were already determined at single doses of 20 Gy. This

discrepancy in radiation tolerance could be due to several reasons. RILD is a time-dependent phenomenon, and whereas Wu et al. assessed RILD parameters at 3 weeks after irradiation, we sacrificed the irradiated mice after 7 weeks. Furthermore, their experiments were performed in male mice, while our mice had another genetic background and were female. Other researchers demonstrated that female mice are more sensitive to liver irradiation [23]. Most importantly, we cannot exclude the involvement of other abdominal organs to the observed toxicity. As compared to the study of Wu et al., our irradiation approach delivered a substantially higher dose to the right kidney. Contribution of renal radiotoxicity to animal weight loss is however rather unlikely, as Ahmad et al. have shown that even bilateral kidney irradiation with a total dose of 14 Gy is not lethal for the course of at least 11 weeks [24]. Even though we did not observe any of the typical signs for gastrointestinal radiotoxicity, including pain, diarrhea and rectal bleeding, we cannot entirely exclude an involvement between healthy tissue toxicity of the small intestine and the extended body weight loss after irradiation with 20 and 30 Gy, respectively [25].

Single fractions of 15 Gy were well tolerated and sufficiently high to induce a cytostatic effect in CLMs. We demonstrated significant delay in tumor growth upon right liver lobe irradiation with single fractions of 10 or 15 Gy. Nonetheless, it will be of high importance to increase the maximally tolerated dose of IR towards the liver, since CLMs contain larger proportions of radioresistant hypoxic cells compared to other tumor types [26]. In addition, combined treatment modalities with hypoxia-targeting or immunomodulating compounds might even further extend the therapeutic window.

Here, we deliver a robust and reproducible preclinical CLM model and irradiation strategy to study such combined approaches with the perspective to translate the results from bench to bedside.

References

1. Torre, L.A., et al., *Global cancer statistics, 2012.* CA Cancer J Clin, 2015. **65**(2): p. 87-108.
2. Aranda, E., et al., *Treatment recommendations for metastatic colorectal cancer.* Clin Transl Oncol, 2011. **13**(3): p. 162-78.
3. Siegel, R., D. Naishadham, and A. Jemal, *Cancer statistics, 2012.* CA Cancer J Clin, 2012. **62**(1): p. 10-29.
4. Cummings, L.C., J.D. Payes, and G.S. Cooper, *Survival after hepatic resection in metastatic colorectal cancer: a population-based study.* Cancer, 2007. **109**(4): p. 718-26.
5. Adam, R., et al., *Managing synchronous liver metastases from colorectal cancer: a multidisciplinary international consensus.* Cancer Treat Rev, 2015. **41**(9): p. 729-41.
6. Cirocchi, R., et al., *Radiofrequency ablation in the treatment of liver metastases from colorectal cancer.* Cochrane Database Syst Rev, 2012(6): p. CD006317.
7. Folprecht, G., et al., *Survival of patients with initially unresectable colorectal liver metastases treated with FOLFOX/cetuximab or FOLFIRI/cetuximab in a multidisciplinary concept (CELIM study).* Ann Oncol, 2014. **25**(5): p. 1018-25.
8. Ruers, T., et al., *Radiofrequency ablation combined with systemic treatment versus systemic treatment alone in patients with non-resectable colorectal liver metastases: a randomized EORTC Intergroup phase II study (EORTC 40004).* Ann Oncol, 2012. **23**(10): p. 2619-26.
9. Kim, J. and Y. Jung, *Radiation-induced liver disease: current understanding and future perspectives.* Exp Mol Med, 2017. **49**(7): p. e359.
10. Videtic, G.M., *The role of stereotactic radiotherapy in the treatment of oligometastases.* Curr Oncol Rep, 2014. **16**(7): p. 391.
11. Scorsetti, M., et al., *Final results of a phase II trial for stereotactic body radiation therapy for patients with inoperable liver metastases from colorectal cancer.* J Cancer Res Clin Oncol, 2015. **141**(3): p. 543-53.
12. Bresalier, R.S., et al., *An animal model for colon cancer metastasis: establishment and characterization of murine cell lines with enhanced liver-metastasizing ability.* Cancer Res, 1987. **47**(5): p. 1398-406.
13. Boni, L., et al., *Injection of colorectal cancer cells in mesenteric and antimesenteric sides of the colon results in different patterns of metastatic diffusion: an experimental study in rats.* World J Surg Oncol, 2005. **3**: p. 69.
14. Casillas, S., et al., *Perfusion to colorectal cancer liver metastases is not uniform and depends on tumor location and feeding vessel.* J Surg Res, 1997. **67**(2): p. 179-85.
15. Shinozaki, K., O. Ebert, and S.L. Woo, *Treatment of multi-focal colorectal carcinoma metastatic to the liver of immune-competent and syngeneic rats by hepatic artery infusion of oncolytic vesicular stomatitis virus.* Int J Cancer, 2005. **114**(4): p. 659-64.
16. Rothbarth, J., et al., *Melphalan antitumor efficacy and hepatotoxicity: the effect of variable infusion duration in the hepatic artery.* J Pharmacol Exp Ther, 2003. **305**(3): p. 1098-103.
17. de Jong, G.M., et al., *Animal models for liver metastases of colorectal cancer: research review of preclinical studies in rodents.* J Surg Res, 2009. **154**(1): p. 167-76.
18. Butterworth, K.T., K.M. Prise, and F. Verhaegen, *Small animal image-guided radiotherapy: status, considerations and potential for translational impact.* Br J Radiol, 2015. **88**(1045): p. 20140634.
19. Limani, P., et al., *Selective portal vein injection for the design of syngeneic models of liver malignancy.* Am J Physiol Gastrointest Liver Physiol, 2016. **310**(9): p. G682-8.
20. de Jong, G., et al., *Adjuvant radioimmunotherapy after radiofrequency ablation of colorectal liver metastases in an experimental model.* Eur J Surg Oncol, 2011. **37**(3): p. 258-64.
21. Lawrence, T.S., et al., *Hepatic toxicity resulting from cancer treatment.* Int J Radiat Oncol Biol Phys, 1995. **31**(5): p. 1237-48.
22. Wu, Z.F., et al., *A mouse radiation-induced liver disease model for stereotactic body radiation therapy validated in patients with hepatocellular carcinoma.* Med Phys, 2016. **43**(7): p. 4349.
23. Wang, S., et al., *Hedgehog signaling influences gender-specific response of liver to radiation in mice.* Hepatol Int, 2013. **7**(4): p. 1065-74.
24. Ahmad, A., et al., *Sphingomyelinase-like phosphodiesterase 3b mediates radiation-induced damage of renal podocytes.* FASEB J, 2017. **31**(2): p. 771-780.
25. Stacey, R. and J.T. Green, *Radiation-induced small bowel disease: latest developments and clinical guidance.* Ther Adv Chronic Dis, 2014. **5**(1): p. 15-29.
26. van Laarhoven, H.W., et al., *Hypoxia in relation to vasculature and proliferation in liver metastases in patients with colorectal cancer.* Int J Radiat Oncol Biol Phys, 2006. **64**(2): p. 473-82.

Figure Legends

Fig.1 Surgical approach for the selective intraportal injection of colorectal cancer cells. (A) Schematic representation of a healthy murine liver prior to surgery. (B) The caudate liver lobe is surgically removed. (C) The portal vein is clamped above the right liver lobe and colorectal cancer cells are injected in the portal vein, resulting in metastases specifically in the right liver lobe. (D) The irradiation field is restricted to the right liver lobe with a rectangular collimator (E) H&E staining showing the border between a colorectal liver metastasis and the healthy liver.

Fig.2 Abdominal CT scans of a mouse with colorectal liver metastases. (A) CT scan without contrast enhancement. (B) CT scan at 80 minutes after intraperitoneal injection of the Fenestra LC contrast agent. (C) CT scan at 7 hours after intraperitoneal injection of the Fenestra LC contrast agent.

Fig.3 Treatment plan for the irradiation of colorectal liver metastases. (A) Contrast-enhanced CT scan with delineation of the target volume (cancerous liver) and organs at risk (total liver, healthy liver, right kidney and stomach). (B) Dose volume histogram of an AP/PA treatment plan. (C) Dose volume histogram of a 360° arc-beam treatment plan.

Fig.4 Histological characterization of DNA double strand breaks by γH2AX staining 1 hour after irradiation with 10 Gy. Staining was performed for the (A) middle (B) left and (C) right liver lobe. (D) Unirradiatet right liver lobe with colorectal liver metastasis as control.

Fig.5 Evaluation of radiation-induced toxicity after single fraction irradiation of the right liver lobe of healthy mice with 0, 20 or 30 Gy. (A) Relative weight change monitored for 6 weeks after radiotherapy. Dotted line = 0 Gy, full line = 20 Gy, dashed line = 30 Gy. Serum concentrations at 50 days after radiotherapy for (B) aspartate transaminase (C) alanine transaminase (D) bilirubin and (E) albumin.

Fig.6 Irradiation of mice with colorectal liver metastases with increasing single doses of IR. (A) Treatment schedule for surgery, irradiation and imaging of the mice. (B) Relative weight change at one and two weeks after irradiation. (C) Representative abdominal MRI scans at one day before and two weeks after irradiation with 0 and 10 Gy, respectively. (D) Dose-dependent change in relative, cumulative metastatic volume at one and two weeks after radiotherapy.

Fig.1

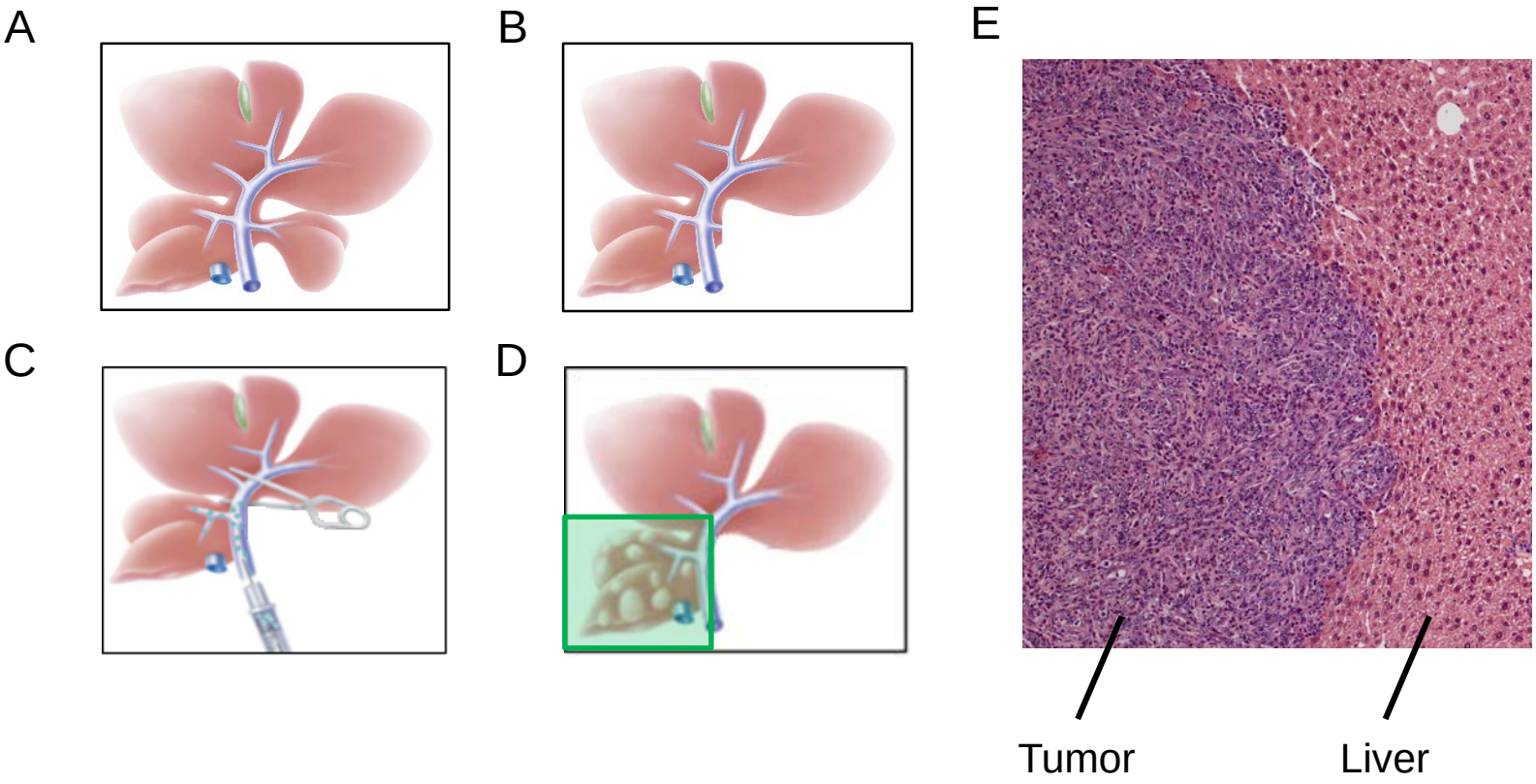

Fig.2

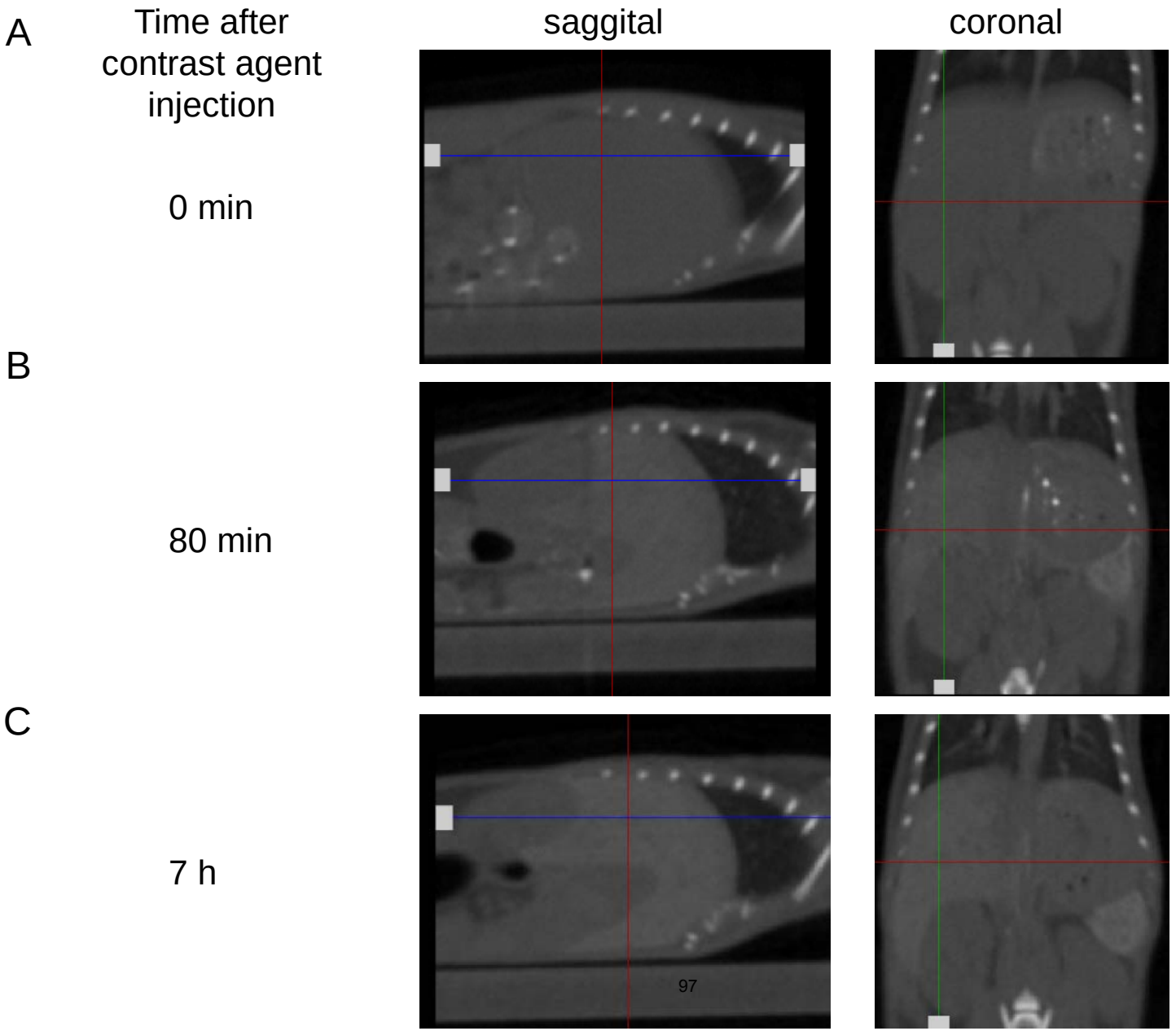
A
Time after contrast agent injection
saggital
coronal
0 min
B
80 min
C
7 h
97

Fig.3

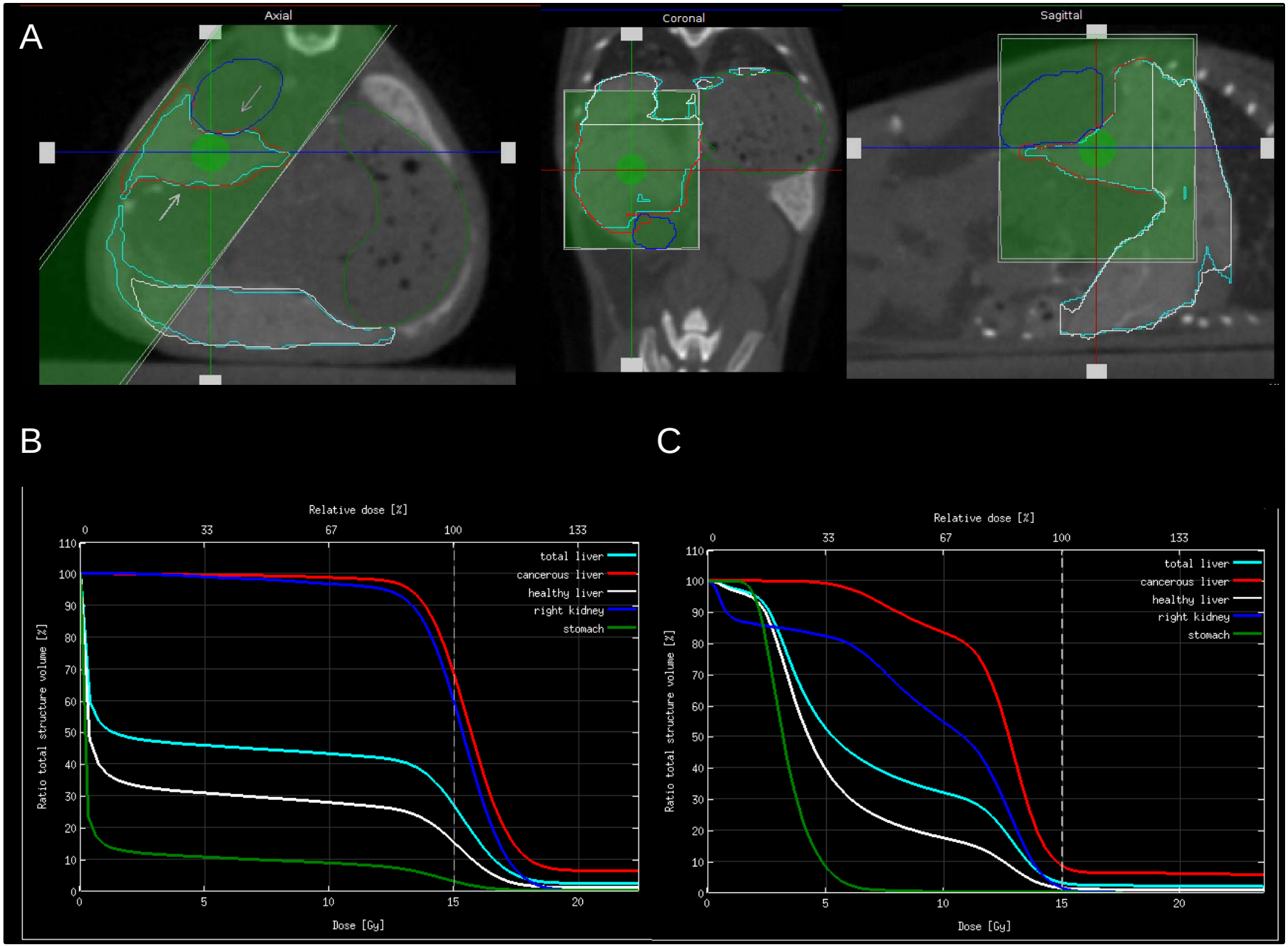
A
Axial
Coronal
Sagittal
B
Relative dose [%]
0
33
67
100
133
Ratio total structure volume [%]
Dose [Gy]
total liver
cancerous liver
healthy liver
right kidney
stomach
C
Relative dose [%]
Ratio total structure volume [%]
Dose [Gy]
total liver
cancerous liver
healthy liver
right kidney
stomach

Fig.4

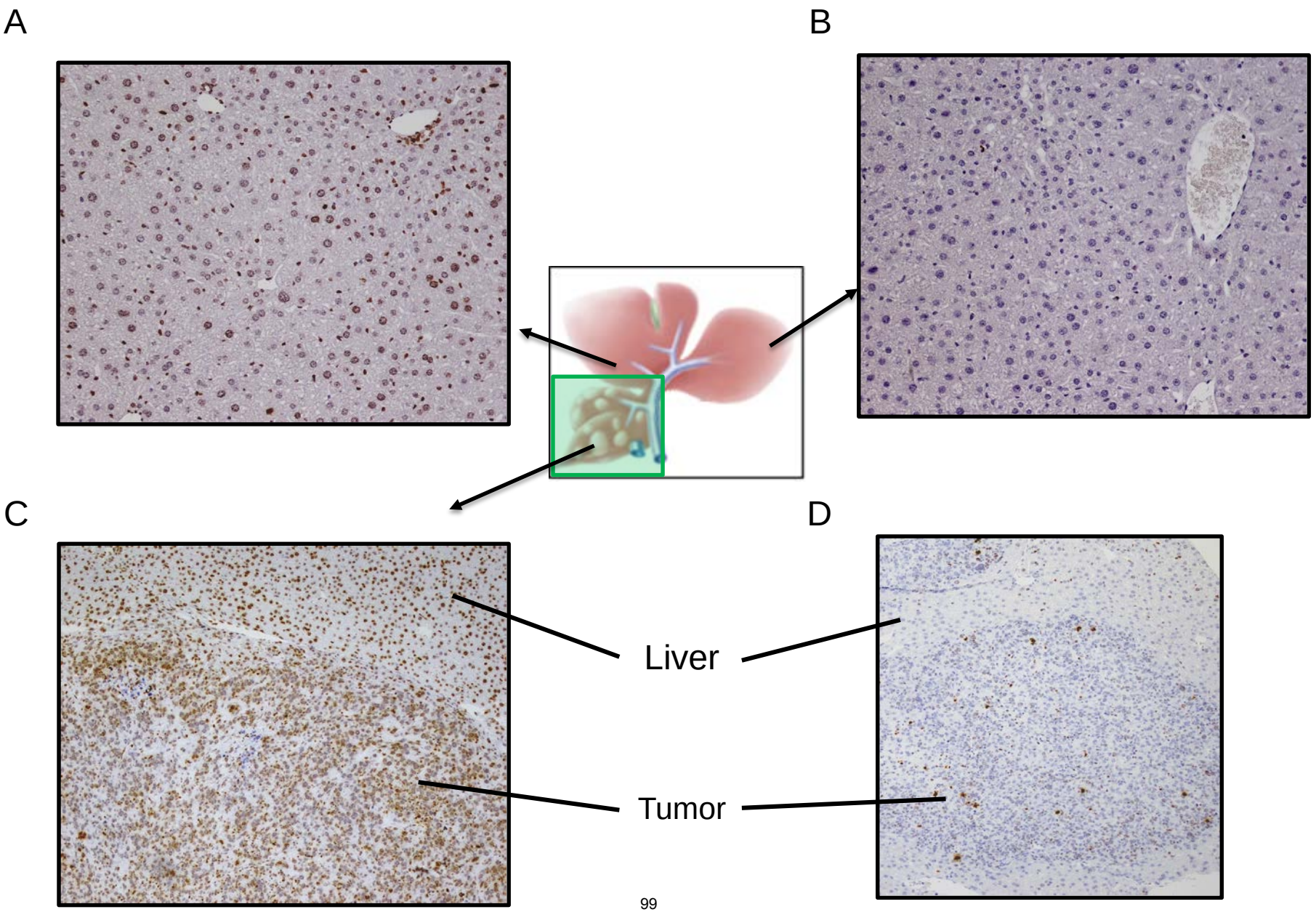

Fig.5

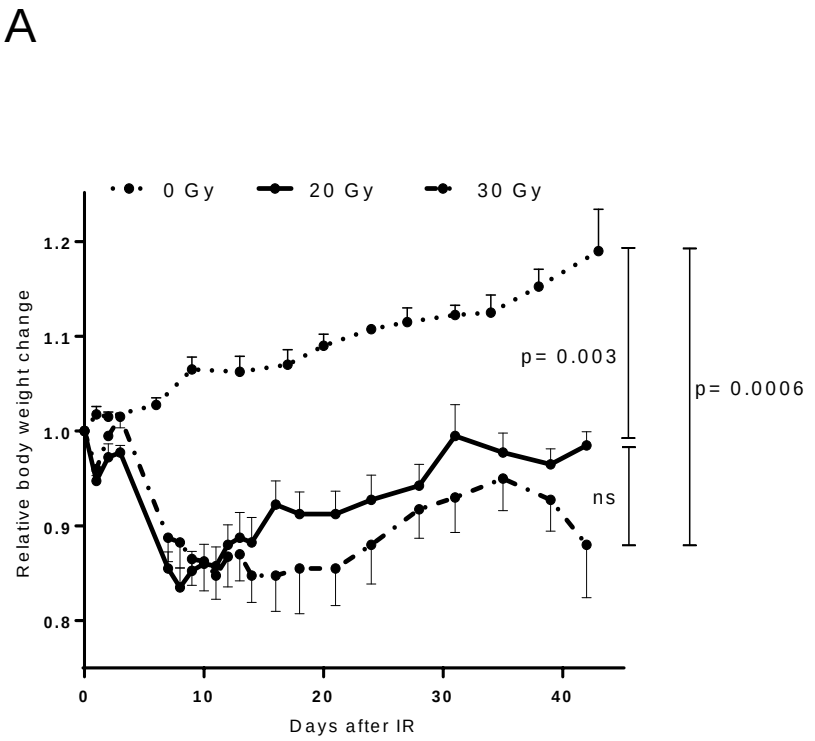
A
0 Gy
20 Gy
30 Gy
Relative body weight change
1.2
1.1
1.0
0.9
0.8
0
10
20
30
40
Days after IR
p= 0.003
ns
p= 0.0006

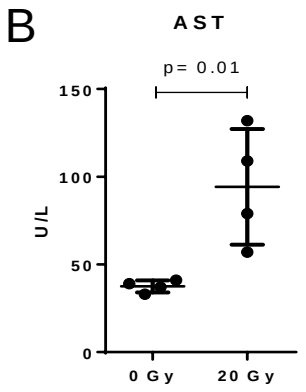
B
AST
p= 0.01
150
100
50
0
U/L
0 Gy
20 Gy

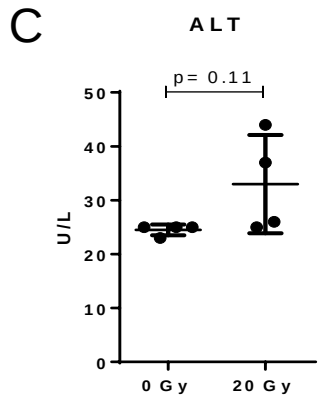
C
ALT
p= 0.11
50
40
30
20
10
0
U/L
0 Gy
20 Gy

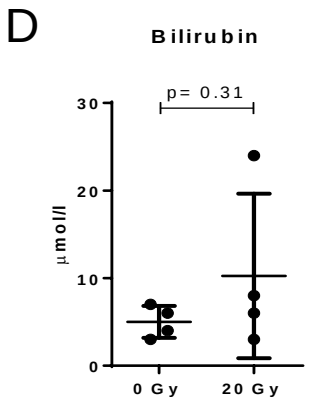
D
Bilirubin
p= 0.31
30
20
10
0
µmol/l
0 Gy
20 Gy

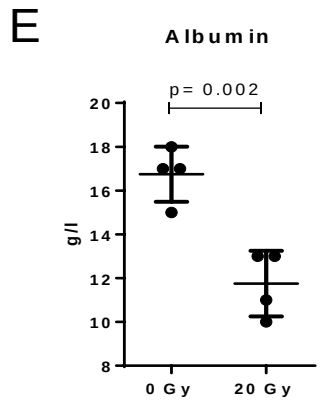
E
Albumin
p= 0.002
20
18
16
14
12
10
8
g/l
0 Gy
20 Gy

Fig.6

A

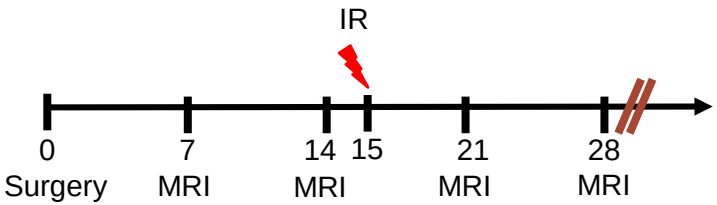
IR
0
Surgery
7
MRI
14
15
MRI
21
MRI
28
MRI

B

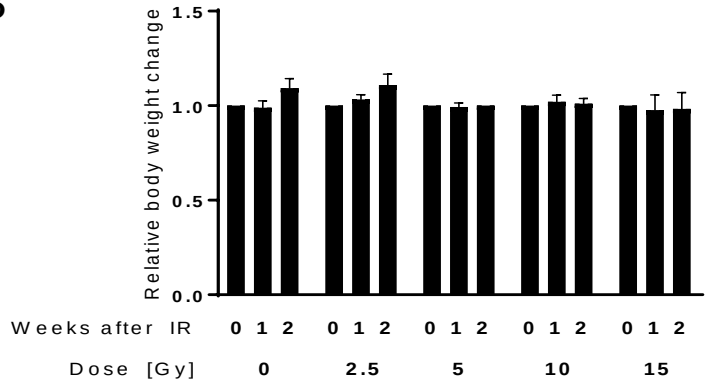
Relative body weight change
1.5
1.0
0.5
0.0
Weeks after IR
0 1 2 0 1 2 0 1 2 0 1 2 0 1 2
Dose [Gy]
0
2.5
5
10
15

C

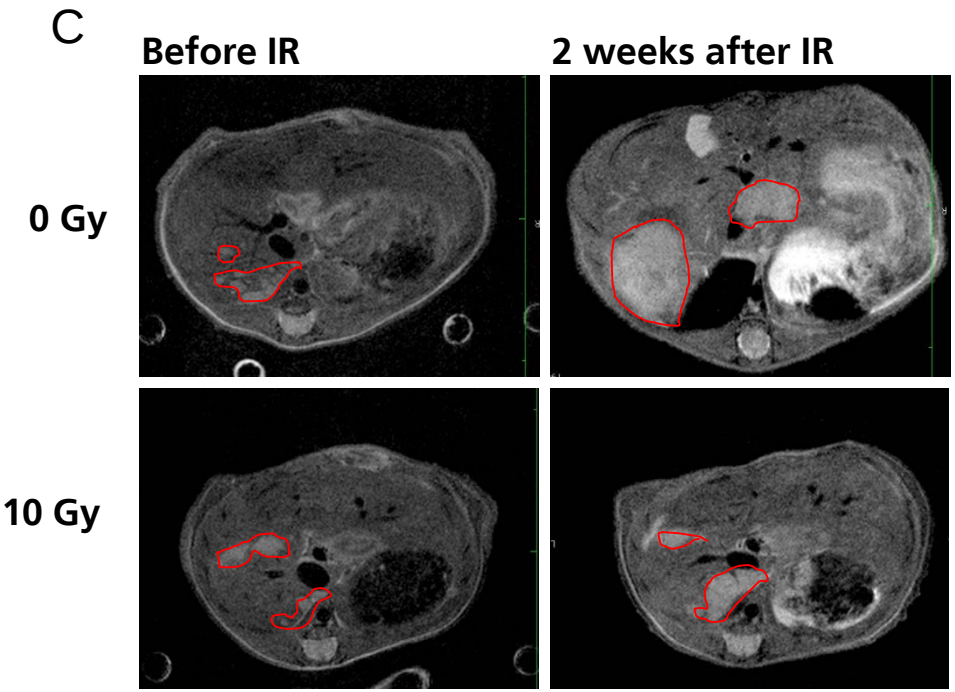
Before IR
2 weeks after IR
0 Gy
10 Gy

D

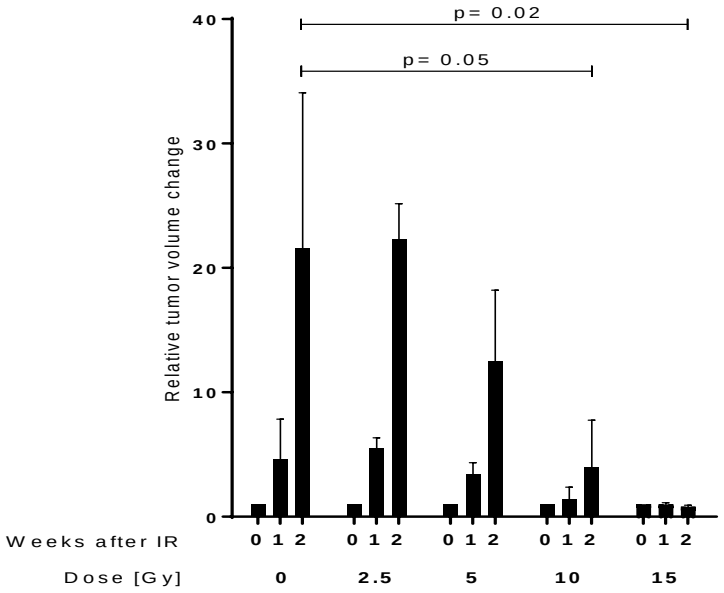
p= 0.02
p= 0.05
Relative tumor volume change
40
30
20
10
0
Weeks after IR
0 1 2 0 1 2 0 1 2 0 1 2 0 1 2
Dose [Gy]
0
2.5
5
10
15

4. Discussion

4.1 Current status of hypoxia modulation for radiotherapy

Tumor hypoxia occurs in almost all solid tumor entities [170]. On the one hand, hypoxia renders most solid tumors partly resistant to radiotherapy but on the other hand represents itself as promising target to overcome radioresistance. As such, an ideal radiosensitizer targeting tumor hypoxia should work independently of the genetic background and protein expression pattern of the respective cancer cells. The mechanisms and molecular aberrations leading to hypoxia in solid tumors are nowadays well known. In response to low oxygen concentrations, HIF-1α is stabilized in cancer cells and translocates to the nucleus where it promotes the expression of target genes that aim to restore the oxygen levels in the affected hypoxic cells [49]. Owing to the high proliferation rate of cancer cells, the cellular oxygen restoration process is usually unsuccessful in solid tumors. In fact, overproduction of VEGF results in a leaky and chaotic tumor vasculature and promotes a vicious cycle of angiogenesis and hypoxia [205]. The molecular hypoxia response process offers a handful of druggable targets that may prevent hypoxia progression and its associated negative consequences. As previously discussed in the introduction of my thesis, selective HIF-1α inhibition was associated with toxicity and did not result in therapeutic efficacy. It is important to note that HIF-1α inhibition increases the expression of the compensatory subunit HIF-2α and results in a more aggressive and invasive tumor phenotype [206]. Moreover, the exact function and relation of the third subunit HIF-3α, which was found to be a negative regulator of HIF-1α and HIF-2α remains to be fully elucidated [207]. Therapeutic efficacy of HIF-inhibition may be enhanced by developing inhibitors selectively targeting HIF-2α or both HIF-α subtypes simultaneously and by unravelling the role of HIF-3α.

Recent attempts to target the hypoxia response pathway have focussed on the tumor metabolism. Cancer cells reprogram their metabolism from oxidative phosphorylation to glycolysis in response to HIF-1α expression. Glycolysis and increased expression of the glucose transporter GLUT-1 - as detected in various tumor entities - is associated with radioresistance [208-211]. Molecular targeting of GLUT-1 and its downstream effectors may represent an effective way to improve the outcome of radiotherapy [212]. Selective GLUT-1 inhibitors have recently been developed and tested in preclinical tumor animal models in combination with radiotherapy. The GLUT-1 inhibitor WZB117 sensitizes radioresistant breast cancer cells to radiotherapy and novel compounds with improved selectivity against other GLUT isoforms e.g. BAY-876 are currently being tested on the preclinical level [213, 214].

As mentioned earlier, an ideal radiosensitzer should be active in a wide variety of tumor entities, independent of deregulated signalling pathways. Therefore, multitudes of pharmaceutical agents targeting the physiological consequences of tumor hypoxia have been developed in the past decades. Some of the treatment regimens including Carbogen and nitroimidazoles were briefly described in the introduction. Although Carbogen treatment slightly improves the outcome of radiotherapy, the practical limitations accompanying its use result in minimal clinical impact [215]. Metronidazole and Misonidazole were associated with frequent side effects and lack of efficacy. They were replaced with third generation nitroimidazoles like Etanidazole and Nimorazole, which were expected to yield a more potent radiosensitization together with decreased toxicity [195, 216]. Jens Overgaard summarized the clinical significance of hypoxia modifiers for radiotherapy (Carbogen & nitroimidazoles) in a meta-analysis reviewing 4805 HNSCC patients treated in 32 randomized clinical trials. Unfortunately, hypoxia modifications did not result in significant benefits in both loco-regional control and survival. Nevertheless, two individual trials showed a significant improvement in loco-regional control. Interestingly, these two studies investigating

Misonidazole and Nimorazole were among the few trials with a sufficiently large number of patients, indicating the importance of patient selection and cohort size for statistical power [217]. The aim of this PhD thesis is to overcome radioresistance by targeting tumor hypoxia with novel pharmacological approaches. As such, we have investigated two different classes of anti-hypoxia compounds exploiting the physiological abnormalities associated with tumor hypoxia. The first approach involved a hypoxia-activated prodrug that selectively kills hypoxic tumor cells, while in the second approach we restored the oxygen levels in hypoxic cells.

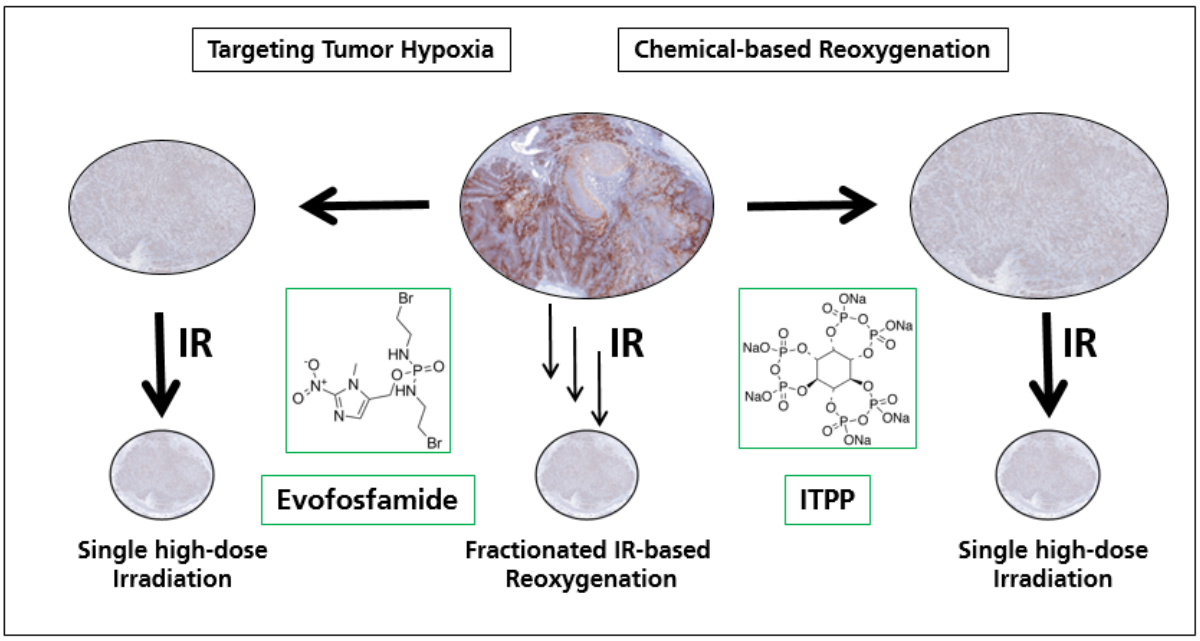

Figure 8 Tumor hypoxia is a major factor contributing to radioresistance. Hypoxia especially limits the efficacy of hypofractionated irradiation as it does not exploit the process of tumor reoxygenation that partly occurs between single IR-fractions in fractionated radiotherapy. The aim of this PhD thesis is to overcome hypoxia-mediated radioresistance by distinct pharmacological approaches. On the one hand we have investigated the effect of the hypoxia-activated prodrug **evofosfamide** that selectively kills hypoxic tumor cells and on the other hand we restored the hypoxic tumor fraction with myo-inostiol trispyrophosphate (**ITPP**). We demonstrate that both compounds act synergistically with high-dose radiotherapy and significantly delay the growth of tumors when compared to high-dose radiotherapy alone.

4.2 Hypoxia activated prodrugs and their implications in clinical oncology

Hypoxia-activated prodrugs are specifically activated under low oxygen concentrations to their active, DNA-alkylating state. The rationale behind HAPs was to develop compounds that act independently of the genetic tumor background and solely rely on hypoxia for their activation. However, recent preclinical investigations however revealed that also expression of prodrug-activating oxidoreductases and intrinsic sensitivity of cancer cells to the cytotoxic effector determine the efficacy of HAPs [218].

In this PhD project, we evaluated the radiosensitizing potential of evofosfamide (Th-302) with fractionated and hypofractionated radiotherapy. We identified a synergistic effect of evofosfamide in combination with radiotherapy in a NSCLC model, while evofosfamide on its own was inactive in a HNSCC model. Interestingly, both tumor models were hypoxic to the same extent as determined by pimonidazole staining, thereby eliminating physiological hypoxia levels as resistance mechanism. Using genome-scale shRNA screens, Hunter at al. have previously identified

the P450 Oxidoreductase (POR) as a major determinant of sensitivity to HAPs *in vitro* [219]. We demonstrated high expression of POR in the evofosfamide-responding NSCLC tumor xenografts, whereas the resistant HNSCC tumors were found to be negative for POR expression by immunohistochemistry. SiRNA-mediated knockdown of POR in the responding NSCLC cell line completely abrogated the activity of evofosfamide *in vitro*. Considering the recent failure of two clinical trials with the preclinically potent HAPs tirapazamine and evofosfamide it will be important to include predictive biomarkers of HAP-activity to select patients [200, 220].
Assessment of tumor hypoxia would be a straightforward approach to select for patients expected to benefit from HAP treatment. A retrospective analysis of HNSCC patients treated with radiotherapy and either tirapazamine or cisplatin/5-FU revealed that patients with baseline tumor hypoxia had improved loco-regional control and failure free survival upon tirapazamine treatment [221]. Despite these clinical observations, the baseline tumor hypoxia was not determined in patients selected for the evofosfamide trial, but instead respective treatment groups were assigned randomly. As such, therapeutic failure of evofosfamide as compared to doxorubicin in patients suffering from soft tissue sarcoma has to be regarded carefully. Soft tissue sarcomas are not amongst the most hypoxic tumor entities and the distribution of tumor hypoxia across different patients is relatively high [222, 223]. Moreover, patients were not screened for POR expression prior to treatment. Definition of predictive biomarkers for HAP activity (e.g. Hypoxia or POR expression) and their incorporation into patient stratification will be of high importance for the success of future clinical trials. An effective but invasive solution would be histological staining of tumor biopsies for POR expression and a hypoxia marker, e.g. CAIX. Unfortunately, based on the negative outcome of evofosfamide in the pivotal phase III clinical trial its registration and other ongoing clinical trials were discontinued without considering the lack of patient selection. A number of novel HAPs with higher potency are currently being tested in preclinical trials [224-227]. To translate the increased potency of these compounds into improved tumor control in patients, it will be crucial to include predictive patient selection criteria.

4.3 Overcoming radioresistance by tumor reoxygenation with myo-inositol trispyrophosphate

In this PhD project, we demonstrate that neoadjuvant myo-inositol trispyrophosphate (ITPP) administration synergistically enhances the cytotoxic effect of ionizing radiation. Pharmacokinetic monitoring of tumor reoxygenation with a non-invasive luciferase-based hypoxia reporter construct revealed rapid tumor reoxygenation already 2 hours after ITPP injection. Tumor oxygen levels steadily decrease to the baseline level over a course of 24 hours post ITPP administration. Given these aspects, it is crucial to synchronize the irradiation time with the maximal tumor oxygenation state, which is reached 2 hours after intraperitoneal ITPP injection. Furthermore, the synergistic radiosensitization is dependent on the injected dose of ITPP. The maximal tolerated dose (MTD) was determined as an intraperitoneal bolus of 3 g/kg. Doses of 1.5 g/kg and lower failed to induce tumor reoxygenation and consequently did not result in radiosensitization as determined by tumor growth delay experiments. Doses of 4 g/kg and higher were associated with acute toxicities that resulted in sudden death in approximately 20 % of the mice. Post mortem examinations by experienced veterinarians could not determine the exact cause of death. Considering the molecular structure of ITPP that contains six sodium ions per molecule (myo-inositol trispyrophosphate hexasodium salt) and additionally requires 0.04 equimolar sodium hydroxide for pH neutralization, the observed acute toxicities are presumably caused by hypernatremia. This hypothesis is further supported by the apathetic behaviour and thirst of animals immediately after injection, both associated with hypernatremia in humans [228]. Since

the lower doses of 3 g/kg did not result in toxicities and at the same time substantially induced tumor reoxygenation we did not investigate the described side effects.
The exact mechanism by which ITPP leads to tumor reoxygenation is yet to be elucidated. It was shown that ITPP is actively taken up by erythrocytes via the anion transporter band3 [203]. The according implications are unclear but it is hypothesized that ITPP influx lowers the intracellular pH in erythrocytes, thereby decreasing the binding affinity between hemoglobin and oxygen. Consequently, oxygen liberation from hemoglobin facilitated oxygenation of tissues upon demand. Oxygen is unevenly distributed in tissues, forming pO_2 gradients along the small blood capillaries from the arterial to the venous ends [42]. The physiological oxygen levels in the human body are regulated by an equilibrium between oxygen availability and oxygen demand and range between 110 mmHg in lung alveolar cells to 8 mmHg in superficial skin cells [229]. Increased oxygen availability upon ITPP treatment is unlikely to hyperoxygenate tissues with a physiological pO_2 but will rather instantaneously reoxygenate tissues residing in a hypoxic state, e.g. solid tumors. Raykov et al. could confirm this hypothesis by invasively measuring pO_2 levels of pancreatic carcinoma xenografts and healthy muscle upon ITPP injection. ITPP drastically reoxygenated the hypoxic tumor xenografts whereas the physiological pO_2 in the muscle was not increased [41].
As such, ITPP does not directly act on cancer cells but rather indirectly affects their tumor microenvironment. We could confirm this fact by demonstrating a lack of radiosensitization in cell culture experiments. By targeting hemoglobin, ITPP is capable of reoxygenating hypoxic tumors irrespectively of their anatomic and genetic background. Therefore, the radiosensitization is dependent on the physicochemical extent of reoxygenation. We could demonstrate that the synergistic effect of ITPP and IR was higher in a tumor model with a high hypoxic fraction (A549 NSCLC) as compared to a tumor model with a low hypoxic fraction (FaDu HNSCC). Apart from rapidly induced physicochemical tumor reoxygenation, we further identified a protective effect of ITPP on the tumor microvasculature. High-dose fractions of IR lead to endothelial cell death and subsequent reduction of the tumor micro vessel density as reported by other groups [230]. Neoadjuvant ITPP administration however completely abrogates IR-mediated vascular depletion. Our *in vitro* data shows increased PTEN and decreased pAKT levels in cancer cell lysates and HUVEC endothelial cells upon ITPP treatment. In line with our results, Kieda et al. could demonstrate PTEN activation specifically in tumor endothelial cells after ITPP treatment [231]. Activation of PTEN in endothelial cells could promote a radioprotective effect in the vasculature, since it was recently demonstrated that stromal PTEN loss is associated with decreased DNA repair and genomic instability in the associated epithelium [232]. Further evidence for radioprotection could be observed in our orthotopic colorectal liver metastases mouse model. Ablation of the right liver lobe of healthy mice with a single IR fraction of 20 Gy resulted in a profound weight loss and irradiation with 30 Gy was even lethal for 50 % of the animals tested. In agreement with this deteriorating progression, blood serum analysis indicated an impaired liver function 7 weeks after irradiation, as determined by increased AST and decreased serum albumin levels. Neoadjuvant ITPP administration remarkably diminished the radiation-induced weight loss and none of the irradiated animals died over the course of the experiment. As these mice had no tumors, ITPP exerted its effect on the healthy liver tissue.
We confirmed that increased IR-induced DNA damage following tumor reoxygenation is the underlying mechanism of the synergistic effect of ITPP and IR. Neoadjuvant ITPP treatment selectively increased the number of DNA DSBs in initially hypoxic tumor areas and did not elevate the amount of DNA damage in the normoxic tumor regions. This further supports the hypothesis of selective radiosensitization of hypoxic tissues and inactivity in tissues with a physiological pO_2. Further experiments will be necessary to unravel the promising role of ITPP on radioprotection of healthy tissue.

Additional experiments investigating the effect of multimodal ITPP and IR treatment in immunocompetent mice bearing MC-38 colorectal carcinoma allografts determined a secondary effect of ITPP. Even though these tumors only manifest with intermediate tumor hypoxia, they had the strongest growth delay upon combined ITPP and IR treatment amongst all evaluated tumor models. We could confirm that the radioprotection in the tumor vasculature was accompanied with improved immune cell infiltration. The emerging use of SBRT relies on distinct radiobiological features compared to classical fractionated radiotherapy, including enhanced release of tumor antigens and vascular depletion [139]. Depletion of the tumor vasculature is mutually regarded as a positive asset of SBRT as it indirectly induces cell death by starving tumors from nutrients [230, 233]. However, thoracic and abdominal SBRT is often associated with toxicities, especially when combined with anti-VEGF therapy [234-236]. A combined treatment modality of ITPP and SBRT could prevent vascular depletion while maintaining enhanced tumor antigen secretion. Thereby activated immune cells could augment tumor control by improved accessibility of cancer cells to the intact tumor vasculature. Preservation of the tumor vasculature would consequently impede tumor hypoxia and its associated malignant transformations resulting in treatment resistance.
In conclusion, we demonstrate that ITPP sensitizes hypoxic tumors to radiotherapy, irrespective of their anatomic and genetic background. Selective sensitization of hypoxic tissues manifests in low off-target toxicity and even poses the hypothesis of radioprotection by presently unclear mechanisms. Our results provide a strong rationale to evaluate the clinical efficacy of neoadjuvant ITPP treatment combined with SBRT in clinical trials.

4.4 Implementation of image-guided small animal radiotherapy in Zurich

Radiotherapy is a fundamental treatment approach to combat cancer. Unlike in the field of chemotherapy or immunotherapy, the translation of data obtained from preclinical radiotherapy studies to the clinical setting is aggravated by the lack of clinically comparable beam-delivery platforms. To bridge the gap between preclinical and clinical radiotherapy, we implemented an image-guided small animal radiotherapy platform in this PhD project.
Historically, targeted tumor irradiation in small animals was achieved by shielding the healthy tissue with lead and exposing the tissue to be irradiated to the photon beam. Nowadays, CT-based treatment planning together with dynamic beam-delivery systems allow us to apply clinically relevant irradiation protocols to small animals. To further investigate our promising results obtained with ITPP treatment of subcutaneous tumors, we generated an orthotopic colorectal liver metastases (CLM) model. CLMs manifest in a high unmet need for novel treatment strategies, as the golden standard - surgical resection - is not always applicable [237]. A recent phase II clinical trial demonstrated optimal local control and promising overall survival rates in CLM patients treated with SBRT [238]. The rationale for combining ITPP and SBRT for this indication is given by the high hypoxic fractions found in CLMs [239-241]. Moreover, our collaborators could demonstrate a combined effect of ITPP and chemotherapy in the same CLM model [242, 243].
Our own results demonstrate the feasibility of highly selective irradiation of the right liver lobe with acceptable healthy tissue involvement. In contrast to the results obtained by Wu et al. after total liver irradiation, we observed signs of hepatotoxicity at lower doses despite irradiating only a fifth of the liver volume [244]. The presumably reasons for this observation, including differences in tissue sampling, mouse model and gender were adequately discussed in our manuscript. Nonetheless, CLM irradiation with single doses of 15 Gy and lower was well tolerated and resulted in dose-dependent tumor growth kinetics. Preliminary multimodal treatments with ITPP indicated a radioprotective effect on the healthy liver as previously discussed. Moreover, a pronounced

tumor reoxygenation occurred in orthotopic CLMs after ITPP treatment as determined by pimonidazole staining. In the next step, we will assess the combined treatment of ITPP and image-guided radiotherapy in orthotopic CLMs.
In conclusion and to our best knowledge, we could show for the first time that small animal image-guided radiotherapy of CLMs is feasible, accurate and effective. Even though we observed a tumor growth arrest at two weeks after a single fraction of 15 Gy, further radiosensitization will be necessary to ameliorate tumor control over a longer period and to translate novel treatment protocols to the clinical stage.

4.5 Translational relevance

The major goal of this PhD project was to investigate novel treatment strategies to overcome radioresistance in cancer patients. Tumor hypoxia is a highly complex phenomenon driven by a dysregulated tumor microenvironment including the vasculature, tumor stroma and immune cells. As such, *in vivo* experiments were crucial to simultaneously incorporate all contributing factors associated with tumor hypoxia in order to generate clinically relevant data.
Our results demonstrate that evofosfamide is a potent radiosensitizer for hypoxic cancer cells expressing POR. Other groups observing synergistic effects in different tumor entities support our findings [245, 246]. Nevertheless, the registrational clinical trial investigating evofosfamide in soft tissue sarcoma patients failed due to inefficacy [200]. Inadequately translational preclinical tumor animal models and major differences between murine and human carcinogenesis are often used to explain clinical failure of novel compounds. However, in this case it is legitimate to question the design of the clinical trial. Redundant results from Hunter et al. and our group strongly support the importance of POR expression for the bioreductive activation of evofosfamide [219]. Based on these findings, the lack of patient stratification according to tumor hypoxia and POR-expression is likely to be the reason for the failure of this phase III clinical trial. Discontinuation of other clinical trials involving evofosfamide without regarding the aspect of patient stratification scrutinizes the attempts of preclinical researchers to conduct translational research by identifying biomarkers predictive for treatment outcome [198].
Resistance to novel anti-cancer compounds is frequently caused by selection of pre-existing cancer cells that are intrinsically resistant or by mutational adaptations that impede drug efficacy. Intrinsic or acquired resistance to ITPP on the other hand is rather unlikely, as ITPP does not directly interfere with cancer cells. The indirect effect of ITPP on cancer cells is physicochemical and does not require binding sites, cellular transport, activation or other features that are relevant for conventional anti-cancer drugs. ITPP is presumably transported into red blood cells by the anion exchanger band 3 that is exclusively expressed on erythrocytes (10^6 copies per cell) and on a subset of kidney cells. Band 3 mutations across the population are rare and often hereditary [247-250]. Moreover, there are minimal species-specific differences between murine and human band 3 that should not impede the translation of preclinical results [251]. In line with these facts, we and other groups have demonstrated synergism of ITPP with chemo- and radiotherapy across a multitude of tumor entities [41, 242, 252, 253]. ITPP is currently being investigated in clinical trials under the name OXY111A. A Phase I single ascending dose clinical trial in healthy volunteers was completed without any safety findings and demonstrated a dose-dependent pharmacokinetic activity profile (unpublished data on NormOxys website). Our collaborators are conducting a prospective Phase Ib/IIa trial investigating the safety and efficacy of OXY111A in combination with standard chemotherapy in patients suffering from non-resectable primary and secondary tumors of the liver, pancreas and biliary tract. One of the major limitations of ITPP treatment is the requirement of high doses for preclinical and clinical efficacy. In the current clinical trial the administration of weekly doses up to 43'500 mg/m^2 ITPP are planned, which requires intravenous drug infusion over

several hours [254]. Therefore, future clinical trials investigating ITPP in combination with radiotherapy will be complicated due to the tight treatment schedule that aims to irradiate tumors at their maximal state of reoxygenation.
Hemoglobin-mediated treatment mechanisms are rare and thereby impede the forecast of clinical ITPP-efficacy. The only other compound with a comparable mode of action is efaproxiral, which also reduces the hemoglobin-oxygen binding affinity resulting in enhanced tissue oxygenation [255]. Efaproxiral in combination with chemo- or radiotherapy modestly improved overall survival and quality of life in patients suffering from NSCLC or brain metastases but was not approved by the FDA thereafter [256-258]. The translational relevance of our proposed combination therapy consisting of ITPP and IR will be further strengthened by examinations in orthotopic tumor models. In the long term, image-guided radiotherapy of orthotopically growing tumors can be used to improve patient irradiation.

4.6 Design of multimodal treatment strategies to overcome radioresistance

Over the past few decades, the understanding of disease mechanisms has resulted in the increasing discovery of putative targets to prevent or reverse malignant progressions. Together with high-throughput based technologies to screen drug libraries against newly discovered disease targets it has led to the discovery of a plethora of clinically effective anti-cancer compounds. However, driven by intrinsic and acquired resistance against these agents it became evident that the likelihood to discover a "magic bullet" that entirely cures cancer is unrealistic. Therefore, using combination therapy to overcome intrinsic and prevent acquired resistance is particularly important in oncology. A meta-analysis of clinical trials conducted between 2008 and 2013 revealed a higher prevalence of combination therapies in oncology (25.6%) in comparison with all other indications (6.9%). Moreover, it was noted that combinatorial treatments are often conducted as part of investigator-initiated clinical trials (e.g. by the NIH) rather than by pharmaceutical companies that are primarily focussed to market their own novel single agent products [259]. Future preclinical research and clinical trials should follow rationale-based drug combinations, preferably by repurposing approved drugs from other indications for the field of oncology. This would drastically reduce the costs and duration of clinical trials in favour of cancer patients and healthcare systems. Numerous approved compounds including some blockbuster-drugs (e.g. Aspirin or Methotrexate) are promising candidates for drug repurposing in oncology [260]. Radiotherapy is an attractive combination partner as it acts locally and thereby prevents systemic toxicity. Consequently, it can be combined with systemic treatments that are associated with higher toxicity profiles to optimally utilize the therapeutic window.
The novel findings of this PhD project can be used to overcome hypoxia as a major limiting factor of radiotherapy and combination therapies involving IR. Recent advances in cancer research are now shifting the focus to the field of immuno-oncology. Despite showing only modest improvements in overall patient survival, immune checkpoint inhibitors are being praised as new milestones in cancer therapeutics [120, 121, 190]. This class of molecules has undoubtedly the potential to perform better if certain limiting factors can be resolved. The combined treatment of SBRT and immune checkpoint inhibition is paradoxical since SBRT on the one hand improves antigen presentation but on the other hand leads to a depletion of the tumor vasculature. Consequently, activated lymphocytes cannot exert their cytotoxic effect since tumor infiltration is obstructed. We suggest a solution to overcome this controversy by pre-conditioning the TME with ITPP prior to combined radioimmunology treatments. ITPP-mediated vascular protection might preserve the integrity of tumor blood vessels and subsequently improve lymphocyte infiltration after SBRT. Moreover, tumor reoxygenation upon ITPP administration will enhance the cytotoxicity

of IR in hypoxic tumor cells. The release of tumor antigens from initially hypoxic cancer cells after combined ITPP and SBRT treatment will further enhance the diversity and activation of anti-tumorigenic lymphocytes and improve tumor control when combined with immune checkpoint blockade. Such multimodal treatments modulating tumor hypoxia and immune cell activation for improved SBRT require further investigation of therapeutic dosing and scheduling.

5. Outlook

Tumor hypoxia is a negative prognostic factor for the efficacy of radiotherapy. An attempt to overcome this limitation is the use of pharmaceutical agents that modulate hypoxic tumor fractions prior to radiotherapy. In this PhD thesis, we demonstrate a synergistic efficacy of evofosfamide and myo-inositol trispyrophosphate when combined with radiotherapy. We show the biological mechanism of these synergies and present predictive biomarkers for therapeutic success.

We and other groups demonstrated that evofosfamide is a potent radiosensitizer. We showed that evofosfamide requires the cellular presence of POR for bioreductive activation irrespective of tumor hypoxia. Based on the therapeutic failure of a registrational phase III clinical trial the patent holder Merck decided to discontinue further development of evofosfamide. Strong evidence suggests that therapeutic inefficacy was caused by a poor study design that did not consider patient stratification according to tumor hypoxia or POR expression. Further preclinical and clinical investigations with evofosfamide are therefore not expected.

Neoadjuvant ITPP treatment significantly enhances the cytotoxicity of IR and leads to delayed tumor growth when compared to radiotherapy alone. This radiosensitizing effect is independent of the genetic cancer cell background and tumor entity. Based on that, additional efficacy-oriented experiments in other tumor entities will not be required. However, it will be of high importance to evaluate the efficacy of ITPP and image-guided SBRT in orthotopic tumors to closer mimic a patient irradiation setting. Preliminary experiments conducted in orthotopically growing colorectal liver metastases showed tumor reoxygenation upon ITPP treatment and further efficacy-oriented investigations with the combined treatment of ITPP and SBRT are planned. Our current experiments can be categorized as Proof of Concept (PoC) studies exploring whether ITPP-mediated tumor reoxygenation leads to radiosensitization. As we successfully confirmed this hypothesis, future experiments could be conducted with a curative intent. It will be interesting to evaluate the relevance of serial ITPP treatment in combination with fractionated radiotherapy or concurrent chemotherapy for tumor control and vascular protection. Furthermore, our mechanistic evidence strongly suggests adding an immune-checkpoint inhibitor to our treatment protocol as ITPP-mediated vascular protection combined with SBRT might improve the tumor controlling properties of immune-checkpoint blockade.

The future development and relevance of ITPP is currently unclear as there is intriguing information about the patent situation. Nevertheless, we are looking forward to the outcome of the ongoing Phase Ia/IIb clinical trial that will decide about the future relevance of ITPP.

In conclusion, the present PhD work illustrates tumor hypoxia as an attractive target to overcome radiotherapy. Pharmacological reduction or exploitation of tumor hypoxia significantly increases the efficacy of radiotherapy. Together with the implementation of a small-animal image-guided radiotherapy platform, we generated powerful data for the translation to future clinical trials.

References

1. Bianconi, E., et al., *An estimation of the number of cells in the human body.* Ann Hum Biol, 2013. **40**(6): p. 463-71.
2. Alberts B., J.A., Lewis J., Raff M., Roberts K., Walter P., *Molecular Biology of the Cell. 5th ed.* Garland Science, 2007.
3. Wood, L.D., et al., *The genomic landscapes of human breast and colorectal cancers.* Science, 2007. **318**(5853): p. 1108-13.
4. Kandoth, C., et al., *Mutational landscape and significance across 12 major cancer types.* Nature, 2013. **502**(7471): p. 333-339.
5. Morris, L.G. and T.A. Chan, *Therapeutic targeting of tumor suppressor genes.* Cancer, 2015. **121**(9): p. 1357-68.
6. Nagarajan, A., P. Malvi, and N. Wajapeyee, *Oncogene-directed alterations in cancer cell metabolism.* Trends Cancer, 2016. **2**(7): p. 365-377.
7. Anand, P., et al., *Cancer is a preventable disease that requires major lifestyle changes.* Pharm Res, 2008. **25**(9): p. 2097-116.
8. Lozano, R., et al., *Global and regional mortality from 235 causes of death for 20 age groups in 1990 and 2010: a systematic analysis for the Global Burden of Disease Study 2010.* Lancet, 2012. **380**(9859): p. 2095-128.
9. Torre, L.A., et al., *Global cancer statistics, 2012.* CA Cancer J Clin, 2015. **65**(2): p. 87-108.
10. Hanahan, D. and R.A. Weinberg, *The hallmarks of cancer.* Cell, 2000. **100**(1): p. 57-70.
11. Hanahan, D. and R.A. Weinberg, *Hallmarks of cancer: the next generation.* Cell, 2011. **144**(5): p. 646-74.
12. Quail, D.F. and J.A. Joyce, *Microenvironmental regulation of tumor progression and metastasis.* Nat Med, 2013. **19**(11): p. 1423-37.
13. Wang, M., et al., *Role of tumor microenvironment in tumorigenesis.* J Cancer, 2017. **8**(5): p. 761-773.
14. Landskron, G., et al., *Chronic inflammation and cytokines in the tumor microenvironment.* J Immunol Res, 2014. **2014**: p. 149185.
15. Nagarsheth, N., M.S. Wicha, and W. Zou, *Chemokines in the cancer microenvironment and their relevance in cancer immunotherapy.* Nat Rev Immunol, 2017. **17**(9): p. 559-572.
16. Sato, E., et al., *Intraepithelial CD8+ tumor-infiltrating lymphocytes and a high CD8+/regulatory T cell ratio are associated with favorable prognosis in ovarian cancer.* Proc Natl Acad Sci U S A, 2005. **102**(51): p. 18538-43.
17. Curiel, T.J., et al., *Specific recruitment of regulatory T cells in ovarian carcinoma fosters immune privilege and predicts reduced survival.* Nat Med, 2004. **10**(9): p. 942-9.
18. Fang, W.B., et al., *CCL2/CCR2 chemokine signaling coordinates survival and motility of breast cancer cells through Smad3 protein- and p42/44 mitogen-activated protein kinase (MAPK)-dependent mechanisms.* J Biol Chem, 2012. **287**(43): p. 36593-608.
19. Sukkurwala, A.Q., et al., *Immunogenic calreticulin exposure occurs through a phylogenetically conserved stress pathway involving the chemokine CXCL8.* Cell Death Differ, 2014. **21**(1): p. 59-68.
20. Shiga, K., et al., *Cancer-Associated Fibroblasts: Their Characteristics and Their Roles in Tumor Growth.* Cancers (Basel), 2015. **7**(4): p. 2443-58.
21. Mitra, A.K., et al., *MicroRNAs reprogram normal fibroblasts into cancer-associated fibroblasts in ovarian cancer.* Cancer Discov, 2012. **2**(12): p. 1100-8.
22. Wiseman, B.S. and Z. Werb, *Stromal effects on mammary gland development and breast cancer.* Science, 2002. **296**(5570): p. 1046-9.
23. Kalluri, R. and M. Zeisberg, *Fibroblasts in cancer.* Nat Rev Cancer, 2006. **6**(5): p. 392-401.
24. Gout, S. and J. Huot, *Role of cancer microenvironment in metastasis: focus on colon cancer.* Cancer Microenviron, 2008. **1**(1): p. 69-83.
25. Kharaishvili, G., et al., *The role of cancer-associated fibroblasts, solid stress and other microenvironmental factors in tumor progression and therapy resistance.* Cancer Cell Int, 2014. **14**: p. 41.
26. Ohlund, D., E. Elyada, and D. Tuveson, *Fibroblast heterogeneity in the cancer wound.* J Exp Med, 2014. **211**(8): p. 1503-23.
27. Paulsson, J. and P. Micke, *Prognostic relevance of cancer-associated fibroblasts in human cancer.* Semin Cancer Biol, 2014. **25**: p. 61-8.
28. Thorsson, V., et al., *The Immune Landscape of Cancer.* Immunity, 2018. **48**(4): p. 812-830 e14.
29. Connolly, D.T., et al., *Tumor vascular permeability factor stimulates endothelial cell growth and angiogenesis.* J Clin Invest, 1989. **84**(5): p. 1470-8.

30. Risau, W., *Angiogenic growth factors.* Prog Growth Factor Res, 1990. **2**(1): p. 71-9.
31. Carmeliet, P. and R.K. Jain, *Angiogenesis in cancer and other diseases.* Nature, 2000. **407**(6801): p. 249-57.
32. Krishna Priya, S., et al., *Tumour angiogenesis-Origin of blood vessels.* Int J Cancer, 2016. **139**(4): p. 729-35.
33. Jain, R.K., *Normalization of tumor vasculature: an emerging concept in antiangiogenic therapy.* Science, 2005. **307**(5706): p. 58-62.
34. Fukumura, D., et al., *Tumor microvasculature and microenvironment: novel insights through intravital imaging in pre-clinical models.* Microcirculation, 2010. **17**(3): p. 206-25.
35. Jain, R.K., *Determinants of tumor blood flow: a review.* Cancer Res, 1988. **48**(10): p. 2641-58.
36. Carmeliet, P. and R.K. Jain, *Principles and mechanisms of vessel normalization for cancer and other angiogenic diseases.* Nat Rev Drug Discov, 2011. **10**(6): p. 417-27.
37. Dvorak, H.F., *Vascular permeability factor/vascular endothelial growth factor: a critical cytokine in tumor angiogenesis and a potential target for diagnosis and therapy.* J Clin Oncol, 2002. **20**(21): p. 4368-80.
38. Motzer, R.J., et al., *Sunitinib versus interferon alfa in metastatic renal-cell carcinoma.* N Engl J Med, 2007. **356**(2): p. 115-24.
39. Ellis, L.M. and D.J. Hicklin, *VEGF-targeted therapy: mechanisms of anti-tumour activity.* Nat Rev Cancer, 2008. **8**(8): p. 579-91.
40. Maes, H., et al., *Tumor vessel normalization by chloroquine independent of autophagy.* Cancer Cell, 2014. **26**(2): p. 190-206.
41. Raykov, Z., et al., *Myo-inositol trispyrophosphate-mediated hypoxia reversion controls pancreatic cancer in rodents and enhances gemcitabine efficacy.* Int J Cancer, 2014. **134**(11): p. 2572-82.
42. Wenger, R.H., et al., *Frequently asked questions in hypoxia research.* Hypoxia (Auckl), 2015. **3**: p. 35-43.
43. Muz, B., et al., *The role of hypoxia in cancer progression, angiogenesis, metastasis, and resistance to therapy.* Hypoxia (Auckl), 2015. **3**: p. 83-92.
44. Bayer, C., et al., *Acute versus chronic hypoxia: why a simplified classification is simply not enough.* Int J Radiat Oncol Biol Phys, 2011. **80**(4): p. 965-8.
45. Chaudary, N. and R.P. Hill, *Hypoxia and metastasis.* Clin Cancer Res, 2007. **13**(7): p. 1947-9.
46. Hammond, E.M., et al., *The meaning, measurement and modification of hypoxia in the laboratory and the clinic.* Clin Oncol (R Coll Radiol), 2014. **26**(5): p. 277-88.
47. Brahimi-Horn, M.C. and J. Pouyssegur, *HIF at a glance.* J Cell Sci, 2009. **122**(Pt 8): p. 1055-7.
48. Wang, G.L., et al., *Hypoxia-inducible factor 1 is a basic-helix-loop-helix-PAS heterodimer regulated by cellular O2 tension.* Proc Natl Acad Sci U S A, 1995. **92**(12): p. 5510-4.
49. Schofield, C.J. and P.J. Ratcliffe, *Oxygen sensing by HIF hydroxylases.* Nat Rev Mol Cell Biol, 2004. **5**(5): p. 343-54.
50. Kallio, P.J., et al., *Signal transduction in hypoxic cells: inducible nuclear translocation and recruitment of the CBP/p300 coactivator by the hypoxia-inducible factor-1alpha.* EMBO J, 1998. **17**(22): p. 6573-86.
51. Semenza, G.L., *Targeting HIF-1 for cancer therapy.* Nat Rev Cancer, 2003. **3**(10): p. 721-32.
52. Pires, I.M., et al., *Effects of acute versus chronic hypoxia on DNA damage responses and genomic instability.* Cancer Res, 2010. **70**(3): p. 925-35.
53. Kumareswaran, R., et al., *Chronic hypoxia compromises repair of DNA double-strand breaks to drive genetic instability.* J Cell Sci, 2012. **125**(Pt 1): p. 189-99.
54. Bristow, R.G. and R.P. Hill, *Hypoxia and metabolism. Hypoxia, DNA repair and genetic instability.* Nat Rev Cancer, 2008. **8**(3): p. 180-92.
55. Yun, Z. and Q. Lin, *Hypoxia and regulation of cancer cell stemness.* Adv Exp Med Biol, 2014. **772**: p. 41-53.
56. Carnero, A. and M. Lleonart, *The hypoxic microenvironment: A determinant of cancer stem cell evolution.* Bioessays, 2016. **38 Suppl 1**: p. S65-74.
57. Kim, H., et al., *The hypoxic tumor microenvironment in vivo selects the cancer stem cell fate of breast cancer cells.* Breast Cancer Res, 2018. **20**(1): p. 16.
58. Rankin, E.B. and A.J. Giaccia, *Hypoxic control of metastasis.* Science, 2016. **352**(6282): p. 175-80.
59. Shin, D.H., et al., *Regulation of MMP-1 expression in response to hypoxia is dependent on the intracellular redox status of metastatic bladder cancer cells.* Biochim Biophys Acta, 2015. **1852**(12): p. 2593-602.
60. Cox, T.R., et al., *LOX-mediated collagen crosslinking is responsible for fibrosis-enhanced metastasis.* Cancer Res, 2013. **73**(6): p. 1721-32.

61. Erler, J.T., et al., *Lysyl oxidase is essential for hypoxia-induced metastasis.* Nature, 2006. **440**(7088): p. 1222-6.
62. Ramachandran, S., et al., *Epigenetic Therapy for Solid Tumors: Highlighting the Impact of Tumor Hypoxia.* Genes (Basel), 2015. **6**(4): p. 935-56.
63. Wan, L., K. Pantel, and Y. Kang, *Tumor metastasis: moving new biological insights into the clinic.* Nat Med, 2013. **19**(11): p. 1450-64.
64. Azab, A.K., et al., *Hypoxia promotes dissemination of multiple myeloma through acquisition of epithelial to mesenchymal transition-like features.* Blood, 2012. **119**(24): p. 5782-94.
65. Thiery, J.P., et al., *Epithelial-mesenchymal transitions in development and disease.* Cell, 2009. **139**(5): p. 871-90.
66. Katsuno, Y., S. Lamouille, and R. Derynck, *TGF-beta signaling and epithelial-mesenchymal transition in cancer progression.* Curr Opin Oncol, 2013. **25**(1): p. 76-84.
67. Lamouille, S., J. Xu, and R. Derynck, *Molecular mechanisms of epithelial-mesenchymal transition.* Nat Rev Mol Cell Biol, 2014. **15**(3): p. 178-96.
68. Kessenbrock, K., V. Plaks, and Z. Werb, *Matrix metalloproteinases: regulators of the tumor microenvironment.* Cell, 2010. **141**(1): p. 52-67.
69. Valastyan, S. and R.A. Weinberg, *Tumor metastasis: molecular insights and evolving paradigms.* Cell, 2011. **147**(2): p. 275-92.
70. Chambers, A.F., A.C. Groom, and I.C. MacDonald, *Dissemination and growth of cancer cells in metastatic sites.* Nat Rev Cancer, 2002. **2**(8): p. 563-72.
71. Palumbo, J.S., et al., *Platelets and fibrin(ogen) increase metastatic potential by impeding natural killer cell-mediated elimination of tumor cells.* Blood, 2005. **105**(1): p. 178-85.
72. Gay, L.J. and B. Felding-Habermann, *Contribution of platelets to tumour metastasis.* Nat Rev Cancer, 2011. **11**(2): p. 123-34.
73. Psaila, B. and D. Lyden, *The metastatic niche: adapting the foreign soil.* Nat Rev Cancer, 2009. **9**(4): p. 285-93.
74. Chen, Q., X.H. Zhang, and J. Massague, *Macrophage binding to receptor VCAM-1 transmits survival signals in breast cancer cells that invade the lungs.* Cancer Cell, 2011. **20**(4): p. 538-49.
75. Lyden, D., et al., *Impaired recruitment of bone-marrow-derived endothelial and hematopoietic precursor cells blocks tumor angiogenesis and growth.* Nat Med, 2001. **7**(11): p. 1194-201.
76. Gao, D., et al., *Endothelial progenitor cells control the angiogenic switch in mouse lung metastasis.* Science, 2008. **319**(5860): p. 195-8.
77. Aguirre-Ghiso, J.A., *Models, mechanisms and clinical evidence for cancer dormancy.* Nat Rev Cancer, 2007. **7**(11): p. 834-46.
78. Gao, D., et al., *Myeloid progenitor cells in the premetastatic lung promote metastases by inducing mesenchymal to epithelial transition.* Cancer Res, 2012. **72**(6): p. 1384-94.
79. Klein, C.A., *Parallel progression of primary tumours and metastases.* Nat Rev Cancer, 2009. **9**(4): p. 302-12.
80. Gupta, G.P. and J. Massague, *Cancer metastasis: building a framework.* Cell, 2006. **127**(4): p. 679-95.
81. Fidler, I.J., *The pathogenesis of cancer metastasis: the 'seed and soil' hypothesis revisited.* Nat Rev Cancer, 2003. **3**(6): p. 453-8.
82. Pinsky, P.F., *Principles of Cancer Screening.* Surg Clin North Am, 2015. **95**(5): p. 953-66.
83. Buder, A., C. Tomuta, and M. Filipits, *The potential of liquid biopsies.* Curr Opin Oncol, 2016. **28**(2): p. 130-4.
84. Spiegel, P.K., *The first clinical X-ray made in America--100 years.* AJR Am J Roentgenol, 1995. **164**(1): p. 241-3.
85. Kim, H.J., et al., *Dosimetric effect of CT contrast agent in CyberKnife treatment plans.* Radiat Oncol, 2013. **8**: p. 244.
86. McRobbie, D.W., *MRI from picture to proton.* Cambridge, UK; New York: Cambridge University Press., 2007.
87. Cheng, W., et al., *Magnetic resonance imaging (MRI) contrast agents for tumor diagnosis.* J Healthc Eng, 2013. **4**(1): p. 23-45.
88. Xiao, Y.D., et al., *MRI contrast agents: Classification and application (Review).* Int J Mol Med, 2016. **38**(5): p. 1319-1326.
89. Pagani, E., et al., *Basic concepts of advanced MRI techniques.* Neurol Sci, 2008. **29 Suppl 3**: p. 290-5.
90. Krause, B.J., S. Schwarzenbock, and M. Souvatzoglou, *FDG PET and PET/CT.* Recent Results Cancer Res, 2013. **187**: p. 351-69.

91. Novikov, S.N., et al., *Axillary lymph node staging in breast cancer: clinical value of single photon emission computed tomography-computed tomography (SPECT-CT) with 99mTc-methoxyisobutylisonitrile.* Ann Nucl Med, 2015. **29**(2): p. 177-83.
92. Delbeke, D., et al., *Hybrid imaging (SPECT/CT and PET/CT): improving therapeutic decisions.* Semin Nucl Med, 2009. **39**(5): p. 308-40.
93. Zegers, C.M., et al., *Repeatability of hypoxia PET imaging using [(1)(8)F]HX4 in lung and head and neck cancer patients: a prospective multicenter trial.* Eur J Nucl Med Mol Imaging, 2015. **42**(12): p. 1840-9.
94. Lindenberg, L., et al., *Safety and biodistribution of 111In-amatuximab in patients with mesothelin expressing cancers using single photon emission computed tomography-computed tomography (SPECT-CT) imaging.* Oncotarget, 2015. **6**(6): p. 4496-504.
95. Nordsmark, M., et al., *Prognostic value of tumor oxygenation in 397 head and neck tumors after primary radiation therapy. An international multi-center study.* Radiother Oncol, 2005. **77**(1): p. 18-24.
96. Evans, C.E., et al., *Techniques of assessing hypoxia at the bench and bedside.* Angiogenesis, 2011. **14**(2): p. 119-24.
97. Aquino-Parsons, C., A. Green, and A.I. Minchinton, *Oxygen tension in primary gynaecological tumours: the influence of carbon dioxide concentration.* Radiother Oncol, 2000. **57**(1): p. 45-51.
98. Rademakers, S.E., et al., *Metabolic markers in relation to hypoxia; staining patterns and colocalization of pimonidazole, HIF-1alpha, CAIX, LDH-5, GLUT-1, MCT1 and MCT4.* BMC Cancer, 2011. **11**: p. 167.
99. Rosenberger, C., et al., *Pimonidazole adduct immunohistochemistry in the rat kidney: detection of tissue hypoxia.* Methods Mol Biol, 2009. **466**: p. 161-74.
100. Toustrup, K., et al., *Development of a hypoxia gene expression classifier with predictive impact for hypoxic modification of radiotherapy in head and neck cancer.* Cancer Res, 2011. **71**(17): p. 5923-31.
101. Eustace, A., et al., *A 26-gene hypoxia signature predicts benefit from hypoxia-modifying therapy in laryngeal cancer but not bladder cancer.* Clin Cancer Res, 2013. **19**(17): p. 4879-88.
102. Fleming, I.N., et al., *Imaging tumour hypoxia with positron emission tomography.* Br J Cancer, 2015. **112**(2): p. 238-50.
103. Baudelet, C. and B. Gallez, *How does blood oxygen level-dependent (BOLD) contrast correlate with oxygen partial pressure (pO2) inside tumors?* Magn Reson Med, 2002. **48**(6): p. 980-6.
104. Taylor, N.J., et al., *BOLD MRI of human tumor oxygenation during carbogen breathing.* J Magn Reson Imaging, 2001. **14**(2): p. 156-63.
105. Bernstein, J.M., J.J. Homer, and C.M. West, *Dynamic contrast-enhanced magnetic resonance imaging biomarkers in head and neck cancer: potential to guide treatment? A systematic review.* Oral Oncol, 2014. **50**(10): p. 963-70.
106. Mendichovszky, I. and A. Jackson, *Imaging hypoxia in gliomas.* Br J Radiol, 2011. **84 Spec No 2**: p. S145-58.
107. Krishna, M.C., et al., *Electron paramagnetic resonance imaging of tumor pO(2).* Radiat Res, 2012. **177**(4): p. 376-86.
108. Bishayee, A. and K. Block, *A broad-spectrum integrative design for cancer prevention and therapy: The challenge ahead.* Semin Cancer Biol, 2015. **35 Suppl**: p. S1-S4.
109. Wyld, L., R.A. Audisio, and G.J. Poston, *The evolution of cancer surgery and future perspectives.* Nat Rev Clin Oncol, 2015. **12**(2): p. 115-24.
110. Puyo, S., D. Montaudon, and P. Pourquier, *From old alkylating agents to new minor groove binders.* Crit Rev Oncol Hematol, 2014. **89**(1): p. 43-61.
111. Shewach, D.S. and T.S. Lawrence, *Antimetabolite radiosensitizers.* J Clin Oncol, 2007. **25**(26): p. 4043-50.
112. Komlodi-Pasztor, E., et al., *Mitosis is not a key target of microtubule agents in patient tumors.* Nat Rev Clin Oncol, 2011. **8**(4): p. 244-50.
113. Pommier, Y., *Drugging topoisomerases: lessons and challenges.* ACS Chem Biol, 2013. **8**(1): p. 82-95.
114. Joo, W.D., I. Visintin, and G. Mor, *Targeted cancer therapy--are the days of systemic chemotherapy numbered?* Maturitas, 2013. **76**(4): p. 308-14.
115. Huang, M., et al., *Molecularly targeted cancer therapy: some lessons from the past decade.* Trends Pharmacol Sci, 2014. **35**(1): p. 41-50.
116. Yang, Y., *Cancer immunotherapy: harnessing the immune system to battle cancer.* J Clin Invest, 2015. **125**(9): p. 3335-7.
117. Schreiber, R.D., L.J. Old, and M.J. Smyth, *Cancer immunoediting: integrating immunity's roles in cancer suppression and promotion.* Science, 2011. **331**(6024): p. 1565-70.

118. Lesterhuis, W.J., J.B. Haanen, and C.J. Punt, *Cancer immunotherapy--revisited.* Nat Rev Drug Discov, 2011. **10**(8): p. 591-600.
119. Buchbinder, E.I. and A. Desai, *CTLA-4 and PD-1 Pathways: Similarities, Differences, and Implications of Their Inhibition.* Am J Clin Oncol, 2016. **39**(1): p. 98-106.
120. Hodi, F.S., et al., *Improved survival with ipilimumab in patients with metastatic melanoma.* N Engl J Med, 2010. **363**(8): p. 711-23.
121. Garon, E.B., et al., *Pembrolizumab for the treatment of non-small-cell lung cancer.* N Engl J Med, 2015. **372**(21): p. 2018-28.
122. Borghaei, H., et al., *Nivolumab versus Docetaxel in Advanced Nonsquamous Non-Small-Cell Lung Cancer.* N Engl J Med, 2015. **373**(17): p. 1627-39.
123. Cheadle, E.J., et al., *CAR T cells: driving the road from the laboratory to the clinic.* Immunol Rev, 2014. **257**(1): p. 91-106.
124. Turtle, C.J., et al., *CD19 CAR-T cells of defined CD4+:CD8+ composition in adult B cell ALL patients.* J Clin Invest, 2016. **126**(6): p. 2123-38.
125. Baskar, R., et al., *Biological response of cancer cells to radiation treatment.* Front Mol Biosci, 2014. **1**: p. 24.
126. Barcellos-Hoff, M.H., C. Park, and E.G. Wright, *Radiation and the microenvironment - tumorigenesis and therapy.* Nat Rev Cancer, 2005. **5**(11): p. 867-75.
127. Videtic, G.M., *The role of stereotactic radiotherapy in the treatment of oligometastases.* Curr Oncol Rep, 2014. **16**(7): p. 391.
128. Amaldi, U. and G. Kraft, *European developments in radiotherapy with beams of large radiobiological effectiveness.* J Radiat Res, 2007. **48 Suppl A**: p. A27-41.
129. Sharma, S., L. Hertan, and J. Jones, *Palliative radiotherapy: current status and future directions.* Semin Oncol, 2014. **41**(6): p. 751-63.
130. Good, J.S. and K.J. Harrington, *The hallmarks of cancer and the radiation oncologist: updating the 5Rs of radiobiology.* Clin Oncol (R Coll Radiol), 2013. **25**(10): p. 569-77.
131. Steel, G.G., T.J. McMillan, and J.H. Peacock, *The 5Rs of radiobiology.* Int J Radiat Biol, 1989. **56**(6): p. 1045-8.
132. Guedea, F., *Perspectives of brachytherapy: patterns of care, new technologies, and "new biology".* Cancer Radiother, 2014. **18**(5-6): p. 434-6.
133. Guedea, F., et al., *Patterns of care for brachytherapy in Europe: updated results.* Radiother Oncol, 2010. **97**(3): p. 514-20.
134. Strohmaier, S. and G. Zwierzchowski, *Comparison of (60)Co and (192)Ir sources in HDR brachytherapy.* J Contemp Brachytherapy, 2011. **3**(4): p. 199-208.
135. Goitein, M., *Radiation Oncology: A Physicist's-Eye View.* Springer, 2008.
136. Marcu, L.G., *Altered fractionation in radiotherapy: from radiobiological rationale to therapeutic gain.* Cancer Treat Rev, 2010. **36**(8): p. 606-14.
137. Bourhis, J., et al., *Hyperfractionated or accelerated radiotherapy in head and neck cancer: a meta-analysis.* Lancet, 2006. **368**(9538): p. 843-54.
138. Jang, W.I., et al., *High-dose stereotactic body radiotherapy correlates increased local control and overall survival in patients with inoperable hepatocellular carcinoma.* Radiat Oncol, 2013. **8**: p. 250.
139. Song, C.W., et al., *Radiobiological basis of SBRT and SRS.* Int J Clin Oncol, 2014. **19**(4): p. 570-8.
140. Abuodeh, Y., P. Venkat, and S. Kim, *Systematic review of case reports on the abscopal effect.* Curr Probl Cancer, 2016. **40**(1): p. 25-37.
141. Reynders, K., et al., *The abscopal effect of local radiotherapy: using immunotherapy to make a rare event clinically relevant.* Cancer Treat Rev, 2015. **41**(6): p. 503-10.
142. Butterworth, K.T., K.M. Prise, and F. Verhaegen, *Small animal image-guided radiotherapy: status, considerations and potential for translational impact.* Br J Radiol, 2015. **88**(1045): p. 20140634.
143. Ramos, P. and M. Bentires-Alj, *Mechanism-based cancer therapy: resistance to therapy, therapy for resistance.* Oncogene, 2015. **34**(28): p. 3617-26.
144. Coco, S., et al., *Next generation sequencing in non-small cell lung cancer: new avenues toward the personalized medicine.* Curr Drug Targets, 2015. **16**(1): p. 47-59.
145. Hamilton, G. and B. Rath, *A short update on cancer chemoresistance.* Wien Med Wochenschr, 2014. **164**(21-22): p. 456-60.
146. Huang, L. and L. Fu, *Mechanisms of resistance to EGFR tyrosine kinase inhibitors.* Acta Pharm Sin B, 2015. **5**(5): p. 390-401.

147. Vadlapatla, R.K., et al., *Mechanisms of drug resistance in cancer chemotherapy: coordinated role and regulation of efflux transporters and metabolizing enzymes.* Curr Pharm Des, 2013. **19**(40): p. 7126-40.
148. Sharom, F.J., *ABC multidrug transporters: structure, function and role in chemoresistance.* Pharmacogenomics, 2008. **9**(1): p. 105-27.
149. Zanger, U.M. and M. Schwab, *Cytochrome P450 enzymes in drug metabolism: regulation of gene expression, enzyme activities, and impact of genetic variation.* Pharmacol Ther, 2013. **138**(1): p. 103-41.
150. Perri, F., et al., *Radioresistance in head and neck squamous cell carcinoma: Biological bases and therapeutic implications.* Head Neck, 2015. **37**(5): p. 763-70.
151. Nijkamp, M.M., et al., *Interaction of EGFR with the tumour microenvironment: implications for radiation treatment.* Radiother Oncol, 2013. **108**(1): p. 17-23.
152. Li, J., et al., *Prognostic significance of epidermal growth factor receptor expression in glioma patients.* Onco Targets Ther, 2018. **11**: p. 731-742.
153. Bossi, P., et al., *Prognostic and predictive value of EGFR in head and neck squamous cell carcinoma.* Oncotarget, 2016. **7**(45): p. 74362-74379.
154. Bristow, R.G., S. Benchimol, and R.P. Hill, *The p53 gene as a modifier of intrinsic radiosensitivity: implications for radiotherapy.* Radiother Oncol, 1996. **40**(3): p. 197-223.
155. Santivasi, W.L. and F. Xia, *Ionizing radiation-induced DNA damage, response, and repair.* Antioxid Redox Signal, 2014. **21**(2): p. 251-9.
156. Kastan, M.B., et al., *Participation of p53 protein in the cellular response to DNA damage.* Cancer Res, 1991. **51**(23 Pt 1): p. 6304-11.
157. O'Connell, M.J. and K.A. Cimprich, *G2 damage checkpoints: what is the turn-on?* J Cell Sci, 2005. **118**(Pt 1): p. 1-6.
158. Hein, A.L., M.M. Ouellette, and Y. Yan, *Radiation-induced signaling pathways that promote cancer cell survival (review).* Int J Oncol, 2014. **45**(5): p. 1813-9.
159. Chen, T., et al., *Targeting the S and G2 checkpoint to treat cancer.* Drug Discov Today, 2012. **17**(5-6): p. 194-202.
160. Sancar, A., et al., *Molecular mechanisms of mammalian DNA repair and the DNA damage checkpoints.* Annu Rev Biochem, 2004. **73**: p. 39-85.
161. Mao, Z., et al., *Comparison of nonhomologous end joining and homologous recombination in human cells.* DNA Repair (Amst), 2008. **7**(10): p. 1765-71.
162. Kamochi, N., et al., *Irradiated fibroblast-induced bystander effects on invasive growth of squamous cell carcinoma under cancer-stromal cell interaction.* Cancer Sci, 2008. **99**(12): p. 2417-27.
163. Zhou, Y.C., et al., *Ionizing radiation promotes migration and invasion of cancer cells through transforming growth factor-beta-mediated epithelial-mesenchymal transition.* Int J Radiat Oncol Biol Phys, 2011. **81**(5): p. 1530-7.
164. Kirshner, J., et al., *Inhibition of transforming growth factor-beta1 signaling attenuates ataxia telangiectasia mutated activity in response to genotoxic stress.* Cancer Res, 2006. **66**(22): p. 10861-9.
165. Zhang, S., et al., *TGFbeta1-induced activation of ATM and p53 mediates apoptosis in a Smad7-dependent manner.* Cell Cycle, 2006. **5**(23): p. 2787-95.
166. Chargari, C., et al., *Understanding the functions of tumor stroma in resistance to ionizing radiation: emerging targets for pharmacological modulation.* Drug Resist Updat, 2013. **16**(1-2): p. 10-21.
167. Ahn, G.O. and J.M. Brown, *Matrix metalloproteinase-9 is required for tumor vasculogenesis but not for angiogenesis: role of bone marrow-derived myelomonocytic cells.* Cancer Cell, 2008. **13**(3): p. 193-205.
168. Rycaj, K. and D.G. Tang, *Cancer stem cells and radioresistance.* Int J Radiat Biol, 2014. **90**(8): p. 615-21.
169. Riley, P.A., *Free radicals in biology: oxidative stress and the effects of ionizing radiation.* Int J Radiat Biol, 1994. **65**(1): p. 27-33.
170. Brown, J.M. and W.R. Wilson, *Exploiting tumour hypoxia in cancer treatment.* Nat Rev Cancer, 2004. **4**(6): p. 437-47.
171. Brizel, D.M., et al., *Oxygenation of head and neck cancer: changes during radiotherapy and impact on treatment outcome.* Radiother Oncol, 1999. **53**(2): p. 113-7.
172. Ruan, K., G. Song, and G. Ouyang, *Role of hypoxia in the hallmarks of human cancer.* J Cell Biochem, 2009. **107**(6): p. 1053-62.
173. Zhong, J.T. and S.H. Zhou, *Warburg effect, hexokinase-II, and radioresistance of laryngeal carcinoma.* Oncotarget, 2017. **8**(8): p. 14133-14146.

174. Bhatt, A.N., et al., *Transient elevation of glycolysis confers radio-resistance by facilitating DNA repair in cells.* BMC Cancer, 2015. **15**: p. 335.
175. Denekamp, J., *Vascular endothelium as the vulnerable element in tumours.* Acta Radiol Oncol, 1984. **23**(4): p. 217-25.
176. Barker, H.E., et al., *The tumour microenvironment after radiotherapy: mechanisms of resistance and recurrence.* Nat Rev Cancer, 2015. **15**(7): p. 409-25.
177. Bonner, J.A., et al., *Radiotherapy plus cetuximab for squamous-cell carcinoma of the head and neck.* N Engl J Med, 2006. **354**(6): p. 567-78.
178. Bonner, J.A., et al., *Radiotherapy plus cetuximab for locoregionally advanced head and neck cancer: 5-year survival data from a phase 3 randomised trial, and relation between cetuximab-induced rash and survival.* Lancet Oncol, 2010. **11**(1): p. 21-8.
179. Madoz-Gurpide, J., et al., *Activation of MET pathway predicts poor outcome to cetuximab in patients with recurrent or metastatic head and neck cancer.* J Transl Med, 2015. **13**: p. 282.
180. Massacesi, C., et al., *PI3K inhibitors as new cancer therapeutics: implications for clinical trial design.* Onco Targets Ther, 2016. **9**: p. 203-10.
181. O'Connor, M.J., *Targeting the DNA Damage Response in Cancer.* Mol Cell, 2015. **60**(4): p. 547-60.
182. Dungey, F.A., D.A. Loser, and A.J. Chalmers, *Replication-dependent radiosensitization of human glioma cells by inhibition of poly(ADP-Ribose) polymerase: mechanisms and therapeutic potential.* Int J Radiat Oncol Biol Phys, 2008. **72**(4): p. 1188-97.
183. Gani, C., et al., *In vivo studies of the PARP inhibitor, AZD-2281, in combination with fractionated radiotherapy: An exploration of the therapeutic ratio.* Radiother Oncol, 2015. **116**(3): p. 486-94.
184. Hirai, T., et al., *Radiosensitization by PARP inhibition to proton beam irradiation in cancer cells.* Biochem Biophys Res Commun, 2016. **478**(1): p. 234-240.
185. Rohrer Bley, C., et al., *Microtubule stabilising agents and ionising radiation: multiple exploitable mechanisms for combined treatment.* Eur J Cancer, 2013. **49**(1): p. 245-53.
186. Talbot, D.C., et al., *Phase II study of vinflunine in malignant pleural mesothelioma.* J Clin Oncol, 2007. **25**(30): p. 4751-6.
187. Chinot, O.L., et al., *Bevacizumab plus radiotherapy-temozolomide for newly diagnosed glioblastoma.* N Engl J Med, 2014. **370**(8): p. 709-22.
188. Chen, S.W., et al., *Phase 2 study of combined sorafenib and radiation therapy in patients with advanced hepatocellular carcinoma.* Int J Radiat Oncol Biol Phys, 2014. **88**(5): p. 1041-7.
189. Balana, C., et al., *Sunitinib administered prior to radiotherapy in patients with non-resectable glioblastoma: results of a phase II study.* Target Oncol, 2014. **9**(4): p. 321-9.
190. Kwon, E.D., et al., *Ipilimumab versus placebo after radiotherapy in patients with metastatic castration-resistant prostate cancer that had progressed after docetaxel chemotherapy (CA184-043): a multicentre, randomised, double-blind, phase 3 trial.* Lancet Oncol, 2014. **15**(7): p. 700-12.
191. Esposito, A., C. Criscitiello, and G. Curigliano, *Immune checkpoint inhibitors with radiotherapy and locoregional treatment: synergism and potential clinical implications.* Curr Opin Oncol, 2015. **27**(6): p. 445-51.
192. Sundahl, N., et al., *A phase I/II trial of fixed-dose stereotactic body radiotherapy with sequential or concurrent pembrolizumab in metastatic urothelial carcinoma: evaluation of safety and clinical and immunologic response.* J Transl Med, 2017. **15**(1): p. 150.
193. Yu, T., B. Tang, and X. Sun, *Development of Inhibitors Targeting Hypoxia-Inducible Factor 1 and 2 for Cancer Therapy.* Yonsei Med J, 2017. **58**(3): p. 489-496.
194. Overgaard, J., et al., *Misonidazole combined with split-course radiotherapy in the treatment of invasive carcinoma of larynx and pharynx: report from the DAHANCA 2 study.* Int J Radiat Oncol Biol Phys, 1989. **16**(4): p. 1065-8.
195. Overgaard, J., et al., *A randomized double-blind phase III study of nimorazole as a hypoxic radiosensitizer of primary radiotherapy in supraglottic larynx and pharynx carcinoma. Results of the Danish Head and Neck Cancer Study (DAHANCA) Protocol 5-85.* Radiother Oncol, 1998. **46**(2): p. 135-46.
196. Lunt, S.J., et al., *Tirapazamine administered as a neoadjuvant to radiotherapy reduces metastatic dissemination.* Clin Cancer Res, 2005. **11**(11): p. 4212-6.
197. Nytko, K.J., et al., *The hypoxia-activated prodrug evofosfamide in combination with multiple regimens of radiotherapy.* Oncotarget, 2017. **8**(14): p. 23702-23712.
198. Larue, R.T., et al., *A phase 1 'window-of-opportunity' trial testing evofosfamide (TH-302), a tumour-selective hypoxia-activated cytotoxic prodrug, with preoperative chemoradiotherapy in oesophageal adenocarcinoma patients.* BMC Cancer, 2016. **16**: p. 644.

199. Borad, M.J., et al., *Randomized Phase II Trial of Gemcitabine Plus TH-302 Versus Gemcitabine in Patients With Advanced Pancreatic Cancer.* J Clin Oncol, 2015. **33**(13): p. 1475-81.
200. Tap, W.D., et al., *Doxorubicin plus evofosfamide versus doxorubicin alone in locally advanced, unresectable or metastatic soft-tissue sarcoma (TH CR-406/SARC021): an international, multicentre, open-label, randomised phase 3 trial.* Lancet Oncol, 2017. **18**(8): p. 1089-1103.
201. Shenouda, G., et al., *Long-term results of radiation therapy oncology group 9903: a randomized phase 3 trial to assess the effect of erythropoietin on local-regional control in anemic patients treated with radiation therapy for squamous cell carcinoma of the head and neck.* Int J Radiat Oncol Biol Phys, 2015. **91**(5): p. 907-15.
202. Janssens, G.O., et al., *Accelerated radiotherapy with carbogen and nicotinamide for laryngeal cancer: results of a phase III randomized trial.* J Clin Oncol, 2012. **30**(15): p. 1777-83.
203. Duarte, C.D., et al., *myo-Inositol trispyrophosphate: a novel allosteric effector of hemoglobin with high permeation selectivity across the red blood cell plasma membrane.* Chembiochem, 2010. **11**(18): p. 2543-8.
204. Fylaktakidou, K.C., et al., *Inositol tripyrophosphate: a new membrane permeant allosteric effector of haemoglobin.* Bioorg Med Chem Lett, 2005. **15**(6): p. 1605-8.
205. Nagy, J.A., et al., *Why are tumour blood vessels abnormal and why is it important to know?* Br J Cancer, 2009. **100**(6): p. 865-9.
206. Koh, M.Y., et al., *The hypoxia-associated factor switches cells from HIF-1alpha- to HIF-2alpha-dependent signaling promoting stem cell characteristics, aggressive tumor growth and invasion.* Cancer Res, 2011. **71**(11): p. 4015-27.
207. Yang, S.L., et al., *Progress on hypoxia-inducible factor-3: Its structure, gene regulation and biological function (Review).* Mol Med Rep, 2015. **12**(2): p. 2411-6.
208. Sadlecki, P., et al., *The role of Hypoxia-inducible factor-1 alpha , glucose transporter-1, (GLUT-1) and carbon anhydrase IX in endometrial cancer patients.* Biomed Res Int, 2014. **2014**: p. 616850.
209. Xiong, Y., Y.Y. Xiong, and Y.F. Zhou, *Expression and significance of beta-catenin, Glut-1 and PTEN in proliferative endometrium, endometrial intraepithelial neoplasia and endometrioid adenocarcinoma.* Eur J Gynaecol Oncol, 2010. **31**(2): p. 160-4.
210. Sattler, U.G., et al., *Glycolytic metabolism and tumour response to fractionated irradiation.* Radiother Oncol, 2010. **94**(1): p. 102-9.
211. Shimura, T., et al., *AKT-mediated enhanced aerobic glycolysis causes acquired radioresistance by human tumor cells.* Radiother Oncol, 2014. **112**(2): p. 302-7.
212. Tang, L., et al., *Role of metabolism in cancer cell radioresistance and radiosensitization methods.* J Exp Clin Cancer Res, 2018. **37**(1): p. 87.
213. Zhao, F., et al., *Inhibition of Glut1 by WZB117 sensitizes radioresistant breast cancer cells to irradiation.* Cancer Chemother Pharmacol, 2016. **77**(5): p. 963-72.
214. Siebeneicher, H., et al., *Identification and Optimization of the First Highly Selective GLUT1 Inhibitor BAY-876.* ChemMedChem, 2016. **11**(20): p. 2261-2271.
215. Hoskin, P.J., et al., *Radiotherapy with concurrent carbogen and nicotinamide in bladder carcinoma.* J Clin Oncol, 2010. **28**(33): p. 4912-8.
216. Lee, D.J., et al., *Results of an RTOG phase III trial (RTOG 85-27) comparing radiotherapy plus etanidazole with radiotherapy alone for locally advanced head and neck carcinomas.* Int J Radiat Oncol Biol Phys, 1995. **32**(3): p. 567-76.
217. Overgaard, J., *Hypoxic modification of radiotherapy in squamous cell carcinoma of the head and neck--a systematic review and meta-analysis.* Radiother Oncol, 2011. **100**(1): p. 22-32.
218. Hunter, F.W., B.G. Wouters, and W.R. Wilson, *Hypoxia-activated prodrugs: paths forward in the era of personalised medicine.* Br J Cancer, 2016. **114**(10): p. 1071-7.
219. Hunter, F.W., et al., *Identification of P450 Oxidoreductase as a Major Determinant of Sensitivity to Hypoxia-Activated Prodrugs.* Cancer Res, 2015. **75**(19): p. 4211-23.
220. Rischin, D., et al., *Tirapazamine, cisplatin, and radiation versus cisplatin and radiation for advanced squamous cell carcinoma of the head and neck (TROG 02.02, HeadSTART): a phase III trial of the Trans-Tasman Radiation Oncology Group.* J Clin Oncol, 2010. **28**(18): p. 2989-95.
221. Trinkaus, M.E., et al., *Correlation of p16 status, hypoxic imaging using [18F]-misonidazole positron emission tomography and outcome in patients with loco-regionally advanced head and neck cancer.* J Med Imaging Radiat Oncol, 2014. **58**(1): p. 89-97.
222. Nordsmark, M., et al., *Hypoxia in human soft tissue sarcomas: adverse impact on survival and no association with p53 mutations.* Br J Cancer, 2001. **84**(8): p. 1070-5.
223. Aggerholm-Pedersen, N., et al., *A prognostic profile of hypoxia-induced genes for localised high-grade soft tissue sarcoma.* Br J Cancer, 2016. **115**(9): p. 1096-1104.

224. Dragovich, P.S., et al., *Design, synthesis, and biological evaluation of pyrrolobenzodiazepine-containing hypoxia-activated prodrugs.* Bioorg Med Chem Lett, 2017. **27**(23): p. 5300-5304.
225. Jin, C., Q. Zhang, and W. Lu, *Synthesis and biological evaluation of hypoxia-activated prodrugs of SN-38.* Eur J Med Chem, 2017. **132**: p. 135-141.
226. Nesbitt, H., et al., *The unidirectional hypoxia-activated prodrug OCT1002 inhibits growth and vascular development in castrate-resistant prostate tumors.* Prostate, 2017. **77**(15): p. 1539-1547.
227. O'Connor, L.J., et al., *Design, synthesis and evaluation of molecularly targeted hypoxia-activated prodrugs.* Nat Protoc, 2016. **11**(4): p. 781-94.
228. Sam, R. and I. Feizi, *Understanding hypernatremia.* Am J Nephrol, 2012. **36**(1): p. 97-104.
229. Carreau, A., et al., *Why is the partial oxygen pressure of human tissues a crucial parameter? Small molecules and hypoxia.* J Cell Mol Med, 2011. **15**(6): p. 1239-53.
230. Park, H.J., et al., *Radiation-induced vascular damage in tumors: implications of vascular damage in ablative hypofractionated radiotherapy (SBRT and SRS).* Radiat Res, 2012. **177**(3): p. 311-27.
231. Kieda, C., et al., *Stable tumor vessel normalization with pO(2) increase and endothelial PTEN activation by inositol trispyrophosphate brings novel tumor treatment.* J Mol Med (Berl), 2013. **91**(7): p. 883-99.
232. Sizemore, G.M., et al., *Stromal PTEN determines mammary epithelial response to radiotherapy.* Nat Commun, 2018. **9**(1): p. 2783.
233. Kim, M.S., et al., *Radiobiological mechanisms of stereotactic body radiation therapy and stereotactic radiation surgery.* Radiat Oncol J, 2015. **33**(4): p. 265-75.
234. Stephans, K.L., et al., *Prediction of chest wall toxicity from lung stereotactic body radiotherapy (SBRT).* Int J Radiat Oncol Biol Phys, 2012. **82**(2): p. 974-80.
235. Barney, B.M., et al., *Increased bowel toxicity in patients treated with a vascular endothelial growth factor inhibitor (VEGFI) after stereotactic body radiation therapy (SBRT).* Int J Radiat Oncol Biol Phys, 2013. **87**(1): p. 73-80.
236. Haseltine, J.M., et al., *Fatal complications after stereotactic body radiation therapy for central lung tumors abutting the proximal bronchial tree.* Pract Radiat Oncol, 2016. **6**(2): p. e27-33.
237. Cummings, L.C., J.D. Payes, and G.S. Cooper, *Survival after hepatic resection in metastatic colorectal cancer: a population-based study.* Cancer, 2007. **109**(4): p. 718-26.
238. Scorsetti, M., et al., *Final results of a phase II trial for stereotactic body radiation therapy for patients with inoperable liver metastases from colorectal cancer.* J Cancer Res Clin Oncol, 2015. **141**(3): p. 543-53.
239. van Laarhoven, H.W., et al., *Hypoxia in relation to vasculature and proliferation in liver metastases in patients with colorectal cancer.* Int J Radiat Oncol Biol Phys, 2006. **64**(2): p. 473-82.
240. Van den Eynden, G.G., et al., *The histological growth pattern of colorectal cancer liver metastases has prognostic value.* Clin Exp Metastasis, 2012. **29**(6): p. 541-9.
241. Siriwardana, P.N., et al., *Biological and Prognostic Significance of the Morphological Types and Vascular Patterns in Colorectal Liver Metastases (CRLM): Looking Beyond the Tumor Margin.* Medicine (Baltimore), 2016. **95**(8): p. e2924.
242. Limani, P., et al., *Antihypoxic Potentiation of Standard Therapy for Experimental Colorectal Liver Metastasis through Myo-Inositol Trispyrophosphate.* Clin Cancer Res, 2016. **22**(23): p. 5887-5897.
243. Limani, P., et al., *The Allosteric Hemoglobin Effector ITPP Inhibits Metastatic Colon Cancer in Mice.* Ann Surg, 2017. **266**(5): p. 746-753.
244. Wu, Z.F., et al., *A mouse radiation-induced liver disease model for stereotactic body radiation therapy validated in patients with hepatocellular carcinoma.* Med Phys, 2016. **43**(7): p. 4349.
245. Peeters, S.G., et al., *TH-302 in Combination with Radiotherapy Enhances the Therapeutic Outcome and Is Associated with Pretreatment [18F]HX4 Hypoxia PET Imaging.* Clin Cancer Res, 2015. **21**(13): p. 2984-92.
246. Yoon, C., et al., *Hypoxia-activated chemotherapeutic TH-302 enhances the effects of VEGF-A inhibition and radiation on sarcomas.* Br J Cancer, 2015. **113**(1): p. 46-56.
247. Bruce, L.J., et al., *Band 3 mutations, renal tubular acidosis and South-East Asian ovalocytosis in Malaysia and Papua New Guinea: loss of up to 95% band 3 transport in red cells.* Biochem J, 2000. **350 Pt 1**: p. 41-51.
248. Flatt, J.F. and L.J. Bruce, *The Molecular Basis for Altered Cation Permeability in Hereditary Stomatocytic Human Red Blood Cells.* Front Physiol, 2018. **9**: p. 367.
249. Bruce, L., *Mutations in band 3 and cation leaky red cells.* Blood Cells Mol Dis, 2006. **36**(3): p. 331-6.

250. Reithmeier, R.A., et al., *Band 3, the human red cell chloride/bicarbonate anion exchanger (AE1, SLC4A1), in a structural context.* Biochim Biophys Acta, 2016. **1858**(7 Pt A): p. 1507-32.
251. van den Akker, E., et al., *Band 3 multiprotein complexes in the red cell membrane; of mice and men.* Blood Cells Mol Dis, 2010. **45**(1): p. 1-8.
252. Aprahamian, M., et al., *Myo-InositolTrisPyroPhosphate treatment leads to HIF-1alpha suppression and eradication of early hepatoma tumors in rats.* Chembiochem, 2011. **12**(5): p. 777-83.
253. Derbal-Wolfrom, L., et al., *Increasing the oxygen load by treatment with myo-inositol trispyrophosphate reduces growth of colon cancer and modulates the intestine homeobox gene Cdx2.* Oncogene, 2013. **32**(36): p. 4313-8.
254. Limani, P., et al., *Development of OXY111A, a novel hypoxia-modifier as a potential antitumor agent in patients with hepato-pancreato-biliary neoplasms - Protocol of a first Ib/IIa clinical trial.* BMC Cancer, 2016. **16**(1): p. 812.
255. Srinivasan, A.J., et al., *Should modulation of p50 be a therapeutic target in the critically ill?* Expert Rev Hematol, 2017. **10**(5): p. 449-458.
256. Choy, H., et al., *Phase II multicenter study of induction chemotherapy followed by concurrent efaproxiral (RSR13) and thoracic radiotherapy for patients with locally advanced non-small-cell lung cancer.* J Clin Oncol, 2005. **23**(25): p. 5918-28.
257. Suh, J.H., et al., *Phase III study of efaproxiral as an adjunct to whole-brain radiation therapy for brain metastases.* J Clin Oncol, 2006. **24**(1): p. 106-14.
258. Scott, C., et al., *Improved survival, quality of life, and quality-adjusted survival in breast cancer patients treated with efaproxiral (Efaproxyn) plus whole-brain radiation therapy for brain metastases.* Am J Clin Oncol, 2007. **30**(6): p. 580-7.
259. Wu, M., et al., *Characteristics of drug combination therapy in oncology by analyzing clinical trial data on ClinicalTrials.gov.* Pac Symp Biocomput, 2015: p. 68-79.
260. Gupta, S.C., et al., *Cancer drug discovery by repurposing: teaching new tricks to old dogs.* Trends Pharmacol Sci, 2013. **34**(9): p. 508-17.

Acknowledgements

I would like to express my thanks to all the people I came across at the University Hospital, the University, the ETH and the Life Science Graduate School during my PhD period in Zürich. Without their help and company, the completion of this project would have been considerably more difficult.

My sincere thanks go to Prof. Dr. Martin Pruschy for giving me the opportunity to work on a highly translational research project. His flexibility and trust allowed me to perform research according to my own interests and ideas. I am very thankful for the opportunity to implement image-guided small-animal radiotherapy in Zürich as part of my PhD thesis. Martin has been a great source of motivation and inspiration.

Furthermore, I would like to thank my PhD thesis committee members Prof. Dr. Lubor Borsig, Prof. Dr. Rolf Graf, Prof. Dr. Roger Schibli and Prof. Dr. med. Matthias Guckenberger for their support, advice and positive influence on my project. Their help diversified and improved the outcome and translational importance of my PhD thesis.

I would like to thank all the members of the lab for accompanying me throughout these four years: Ashish Sharma, Sabine Bender, Andrea Fontana, Angela Broggini-Tenzer, Janosch Ott, Tamara Kazimova, Simon Deycmar, Fiona Frank, Philip Knobel, Danielle Villars and Verena Waller.

My special thanks go to Katarzyna Nytko-Karouzakis, who supervised and guided me in the beginning of my Pruschy-Lab experience. She was a great help to establish myself in the lab and to learn the standard assays and techniques in radiobiology.

I also would like to express special thanks to my Master students Fabienne Tschanz and Irma Telarovic. I was delighted to work with these highly motivated and competent researchers that not only positively contributed to the content of my thesis, but also improved the working atmosphere in the lab with their positive thinking mentality. Fabienne was an indispensable help in the ITPP-project and Irma strongly facilitated the implementation of the image-guided small-animal radiotherapy platform with her biomedical and physics knowledge.

Herewith, I would also like to thank the Department of Radiation Oncology for their interest and support in my project. Personally, I would like to thank Dr. Jérôme Krayenbühl and Prof. Dr. Jan Unkelbach for their collaboration and help in the physics aspects of radiotherapy.

I would like to thank the clinical research priority programs “Tumor Oxygenation” and “Medical Imaging Network Zürich” for their financial support. Additionally, I thank the companies Merck and NormOxys who also partly financed my PhD work.

Big thanks go to all my friends that mentally supported me as part of the “Fiirabigbier” during these years. These regular events were indispensable for a good work-life balance.

I express my sincere gratitude to my parents and my brother for personally and financially supporting me throughout my whole academic career.

Finally, my last thanks go to my girlfriend Veronika whom I met during my PhD studies in the USZ. Thank you for your love and support during the course of my PhD project. Moreover, I would like to thank you for proofreading and correcting my thesis.